Novel Methods for the Rheological Characterization of Polymers and Polymeric Biofilms

by

Leonid Pavlovsky

A dissertation submitted in partial fulfillment
of the requirements for the degree of
Doctor of Philosophy
(Chemical Engineering)
in the University of Michigan
2014

Doctoral Committee:

Professor Michael J. Solomon, Chair
Professor Mark A. Burns
Professor Ronald G. Larson
Professor John G. Younger

2014

DEDICATION

To my parents, Lev and Anastasia, for the many sacrifices you have made for me and your unconditional support.

ACKNOWLEDGEMENTS

My experience as a graduate student at the University of Michigan has had a profound effect on me as a person as well as a scientist. Throughout my thesis work, I encountered many obstacles. However, during times of struggle (of which there were many), there were always people who supported me and encouraged me to persevere. I would like to thank all of the people in my life, both near and far, who have made my achievement possible.

First of all, I would like to thank my advisor, Mike Solomon. Mike is an amazing scientist who constantly shows his dedication to his students and their education. Mike has trusted me to take ownership of my work, while pushing me to be scientifically rigorous in all that I do. In the process, he has helped me refine my critical thinking, while allowing me to have the creative freedom in my projects that I thrive on. Throughout my experience, Mike has been a great motivator and, on countless occasions, I left our meetings with a new-found enthusiasm to implement the various ideas that we had brainstormed. With every passing year, I have understood that I truly won the advisor lottery by working with him.

My co-advisor, John Younger, has been a pleasure to work with. As doctor of emergency medicine, he brought a point of view to my project that I did not expect to experience as a chemical engineer. Early on in my research, he took me to a gross anatomy laboratory to show me where catheters prone to bloodstream infections are placed. This experience was the most impactful experience of my Ph.D. career as it gave me a true realization of why we were studying bacterial biofilms. John takes a great deal of interest in his students' work and was

commonly in the labs, working side by side with us and always ready to help. The sessions we had throwing ideas back and forth were some of the most enjoyable times of my research.

I would also like to thank the other members of my committee: Ron Larson and Mark Burns. Ron and Mark are both great and extremely thorough scientists who have been a joy to work with. Ron has been extremely valuable for the work on my polymer stretching side project and brought many ideas to the future of my cavitation work. Mark has been a key source of knowledge in discussing the cavitation rheometry project and has been kind enough to lend some of his equipment for the work, without which this project would not have been possible.

The members of the Solomon and Younger lab groups were essential to my time at Michigan. Much of my work was enabled by the willingness of these group members, both past and present, to lend a helping hand and teach new techniques, while our group outings were some of the most memorable times I had. I would also like to thank members of the Burns, Larson, Linic, and Savage groups who helped along the way and I am very appreciative of the company and friendly atmosphere that made it a pleasure to be part of this department over the past five years. Additionally, Eric Viges, a former Solomon lab undergraduate-turned-film stretching expert, has been vital to my side project. I am grateful for everything he taught me, the work he put in, and his willingness to take on this project with me.

The NCRC and chemical engineering departmental staff is an amazing group of people who were instrumental in allowing us to operate as researchers and helping us to transition between our Dow and NCRC labs seamlessly. I would like to thank Susan Hamlin, Shelley Fellers, Kelly Raickovich, Rhonda Sweet, Mike Africa, Ruby Wicklund, Barbara Perry, Harald Eberhart, and Julie Gales for providing us with outstanding administrative and technical support. I would especially like to thank Kelly for making sure our group never went hungry!

I've also had many friends that have played a huge role in my years at Michigan. I would like to thank Thomas Yeh and Richmond Newman for always being willing to lend a hand in my work as well as taking my mind off of it in our various endeavors, such as biking, group dinners, ABC tastings, and especially homebrewing. Another big thank you goes to Thomas Noel, my departmental running buddy who I credit as being the biggest reason that I was able to achieve a life-long goal of qualifying for and running in the Boston Marathon. Mahesh has been a fountain of knowledge, a great friend, and a tireless collaborator. His help invaluable and advanced my research in ways I would have never imagined. Lilian, Youngri, and Ronak have also played an incredible role in helping me survive the Ph.D. process, especially in the final year when I have needed it most.

My family has been especially vital to my Ph.D. Thank you Grandpa Lazar for always quizzing me on my thesis projects whenever I visited and instilling in me the value of education. I also appreciated how well-informed you kept me on all of the goings-on of international soccer when we talked. Mom and Dad, thank you for everything that you have done over the years. You have sacrificed so much to ensure that I could succeed, whether it be the little things, like waking up to take me to 4:00 AM hockey practices, or the big things, such as relocating to a foreign country in order for me to have better opportunities. You have been a constant source of support and encouragement throughout my life and especially during my Ph.D., without which I would not have been able to accomplish what I have.

Finally, I would like to thank the two people without whom this thesis would not be possible: Tennessee and Michelle. Thank you for your constant love and support. No matter how difficult research was, seeing you would brighten my day. Michelle, you have done so much to enable and encourage me to achieve my dreams. I am lucky and thankful to have you in my life.

TABLE OF CONTENTS

LIST OF FIGURES

LIST OF TABLES

LIST OF APPENDICES

ABSTRACT

This dissertation reports that environmental conditions significantly impact the bulk mechanical properties of *Staphylococcus epidermidis* bacterial biofilms. Bacterial biofilms are commonly found as infections of implanted medical devices, which experience large shear forces within the bloodstream. The biofilm's ability to withstand these forces and host immune responses makes infections difficult to eliminate. We aim to reduce the disease burden of biofilms by understanding the mechanical properties that allow them to survive in the bloodstream. In this dissertation, we will discuss various methods of *in situ* characterization of these biofilms that allows them to be studied directly in their natural growth environments. Additionally, we present a technique to weaken the biofilm that may allow for easier removal of infections.

Our first challenge is to create a system capable of growing and analyzing the bacterial biofilm without the need for transplantation. We accomplish this by designing an *in situ* parallel plate bio-rheometer to mimic the native growth conditions of the biofilms. In this device, we are able to replicate the shear stress (0.1 Pa) and temperature (37°C) that *Staphylococcus epidermidis* would encounter in the bloodstream. We are then able to characterize the elastic modulus (G') and determine how biofilms respond to environmental conditions such as osmotic stresses and temperature. Through our osmotic stress study, we notice that the elastic modulus has a non-monotonic as a function of NaCl concentration, exhibiting a maximum elasticity at concentrations resembling human blood (135mM NaCl). Our temperature study showed an

irreversible decrease in G' after undergoing a heating cycle up to 60°C. Additionally, we were able to determine the biofilm yield stress (~20 Pa) and fit the linear creep behavior with the Kelvin-Voigt and Jeffreys viscoelastic models to determine the biofilm relaxation time (~750 s).

After observing decrease of elastic modulus following a heating cycle, we investigate the effect of heat treatment on biofilm on three different scales: the bacterial cells, the extracellular polymers, and the bulk biofilm. To accomplish this, we follow our previous *in situ* rheometric biofilm growth protocol with a one-hour exposure at 37°C, 45°C, and 60°C. These temperatures represent our control (body temperature), maximal treatment temperature, and high temperature observed to cause irreversible decrease of G', respectively. We find little difference between the lower temperatures, but significant decrease in cell viability (from ~90% to ~25%) and yield stress (from ~20 Pa to ~4 Pa) following a 60°C treatment.

Finally, we examine a technique, cavitation rheometry, which we believe can be used as a means of *in vivo* diagnostics for soft biological matter. Cavitation rheometry exploits the fundamental mechanics of cavitation in elastic materials in order to rapidly characterize their elastic modulus. Through experimentation, simulation, and theoretical analysis, we extend this technique to viscoelastic materials of as little as 1 microliter volumes, which is more comparable to what is typically encountered in clinical biofilm infections. Collectively, these results open the door for diagnostics of biological soft matter and bacterial biofilm infections based on the material elasticity.

CHAPTER I

Introduction

Bacterial biofilms are multicellular communities of bacteria that tend to grow in a matrix-enclosed formation and can adhere to a variety of water-rich surfaces.[1, 2] These biofilms have been present in nature for over three billion years, typically appearing in environments such as hydrothermal vents and river beds.[1, 3, 4] The bacteria synthesize an extracellular polymeric substance (EPS), which is known to serve a protective function for bacteria in hostile environments.[1, 2, 5, 6] This EPS is an integral part of the biofilm matrix that acts as a protective barrier from external stresses and is comprised of polysaccharides, proteins, and DNA.[2, 5, 6] Biofilms have adapted to grow in a variety of man-made environments, including industrial piping systems and medical devices within the human body.[2, 7]

A biofilm-forming species of particular interest to human health is *Staphylococcus epidermidis* (*S. epidermidis*).[2, 4-6] *S. epidermidis* is a biofilm-forming bacterium commonly found in the hospital environment. Out of all hospital admissions in the U.S., approximately 0.158 % of patients develop a bloodstream infection from *S. epidermidis*, making it one of the most frequent causes of bloodstream infections in the US.[8] This number is greatly increased in the intensive care unit as well as in patients receiving medical implants, as biofilms have an affinity for adhering and growing onto plastic surfaces such as catheters and prosthetic heart valves.[2, 8] Up to 70% of catheter related infections occur due to coagulase-negative staphylococci, of which *S. epidermidis* is the most commonly responsible.[9] Although not generally severe, *S. epidermidis*

infections can have mortality rates above 30% associated with immune-compromised patients.[8, 10]

The high mortality of hospital-acquired *S. epidermidis* infection is associated with systemic infection. The breakage and subsequent spreading and proliferation of the biofilms throughout the bloodstream can lead to sepsis, and ultimately death.[6, 7] In order to reduce the high mortality rates associated with *S. epidermidis*, it is vital to understand how bacterial colonies of the disease can deform, rupture and disseminate throughout the bloodstream, and thereby potentially lead to sepsis. We therefore aim to understand the deformation and rupture process of *S. epidermidis* bacterial biofilms by studying the mechanical properties of the biofilms through rheology.

Factors Influencing the Growth of *Staphylococcus epidermidis* Bacterial Biofilms

S. epidermidis is a Gram-positive bacteria that is also an opportunistic pathogen.[9-11] Although previously considered a harmless contaminant due to its ubiquitous presence on human skin, *S. epidermidis* is now considered one of the most common causes of nosocomial, or hospital acquired, infection.[9, 10] This may be due to *S. epidermidis* biofilm's polymeric matrix structure, which gives it the ability to adapt to various harsh environments.

Bacterial biofilms are complex, heterogeneous materials that, as they grow in the body, are exposed to certain conditions that dictate the structure they will take. First and foremost, the bacteria are exposed to shear forces, under which they preferentially form a biofilm.[2] The strength of the shear forces can dictate the morphology of the biofilm. For example, at low shear forces, the biofilms tend to form mounds, while at higher shear forces, they grow in configurations of long filamentous strands, or streamers.[4, 12] Within the bloodstream, these forces

are approximately 0.076-0.76 Pa.[13] Also, other factors in the growing environment of biofilm are the nutrients delivered through blood such as oxygen, carbohydrates such as sugars, and electrolytes such as sodium. Limits of oxygen and sugar directly correspond to reduced growth rates while surpluses account for high growth rates.[14, 15] However, altering sodium concentration can have interesting effects on the biofilm as well. It was found that by increasing the sodium chloride concentration present in a tryptic soy broth media, the resulting *S. epidermidis* displayed greater expression of its *ica* gene.[14, 16] This gene is responsible for the production of the polysaccharide that holds the individual bacterial cells together in the matrix.[10] Hence, higher expression of *ica* directly corresponds to increased polysaccharide production. Within human blood, the typical concentration of sodium ions is approximately 135mM.[17]

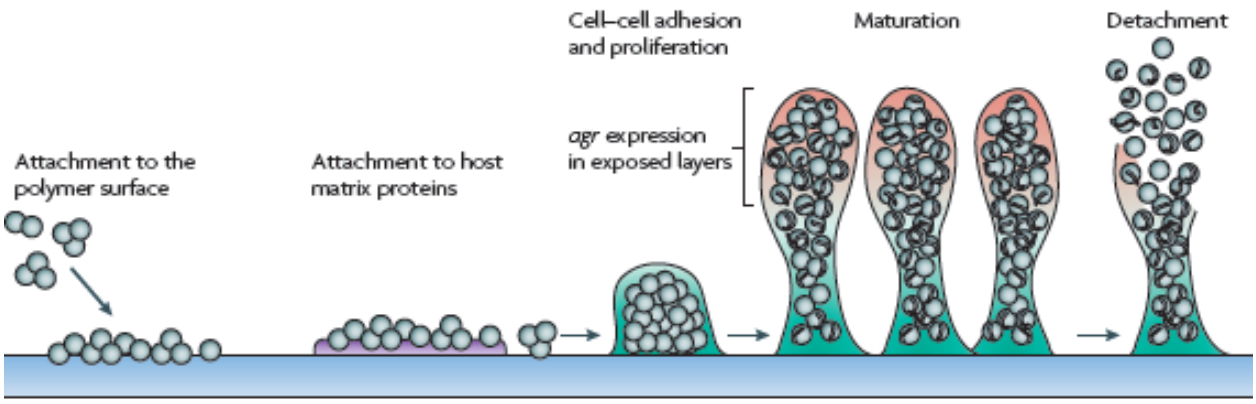

Figure 1.1. Growth process of *Staphyloccocus epidermidis* bacterial biofilm. This figure is replicated from Otto.[10]

When considering a common infection, the formation of a *S. epidermidis* biofilm at the infection site is believed to follow a simple process, as depicted in Figure 1.1.[10] First, individual bacterial cells attach to the polymer surface of the medical device. This attachment can be attributed to the surface hydrophobicity of the bacterial cells, due to a variety of surface proteins

present in *S. epidermidis*.[10] Cells begin to aggregate around this initial attachment area and form micro-colonies. Once enough cells have attached, as determined through quorum sensing, they begin to excrete a polysaccharide matrix.[10, 18] Quorum sensing is a density-dependent gene regulation system, termed *agr* in *S. epidermidis*, that controls the metabolism within the biofilm as well as bacterial virulence.[10, 19] The matrix further improves the biofilms' ability to undergo intercellular aggregation as the biofilm matures and grows through internal cell replication.[10, 20] Additionally, the polysaccharide matrix protects the bacteria cells from changes in applied stresses and from antibiotics.[1, 2, 5, 6, 10] In fact, biofilms are known to withstand short, transient changes in stress through reversible deformation as well as constant stresses over long times through irreversible deformation. This ability qualifies the biofilm as a viscoelastic material.[4]

After the biofilm has matured, eventually the structure will rupture and the bacterial cells will detach, releasing them into the bloodstream to potentially spread infection.[10] There are two mechanisms that govern the detachment process: quorum sensing and physical disruptive forces.[10, 19] As much is not known about the quorum sensing mechanisms and due to our interest in the material science aspect, we will only try to understand how these viscoelastic biofilms rupture through applied stresses, although we still recognize that these mechanical property changes may be mediated by signaling processing such as quorum sensing.

Biofilms as Viscoelastic Material

Biofilms can be considered as viscoelastic materials as they are able to deform both reversibly and irreversibly under applied stresses. A viscoelastic material is one that behaves as an elastic solid over short time scales and a viscous liquid over long time scales when experiencing an applied stress.[21] This can be seen in Figure 1.2 below.

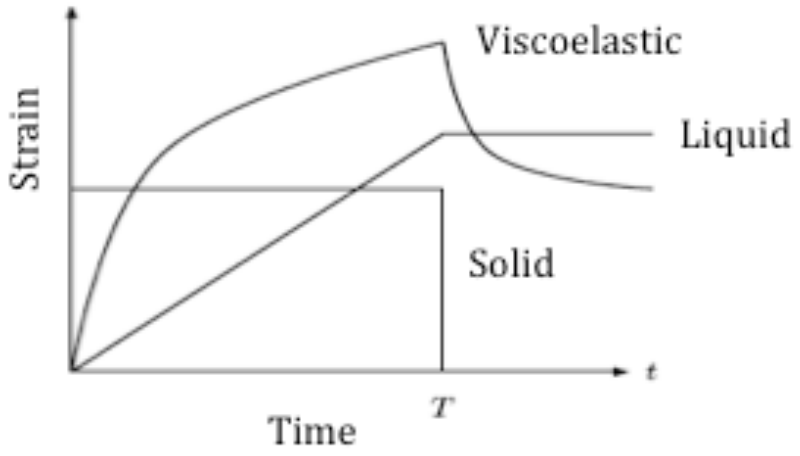

Figure 1.2. Response of an elastic solid, viscous fluid, and viscoelastic material to an applied stress. Constant stress applied from Time = 0 to Time = T, adapted from Shaw *et al.*[1]

In this diagram, when a constant stress is applied at time 0 and removed at time T, a solid exhibits an instantaneous strain step response to the application of a stress and subsequent return to its initial strain state upon removal of the stress. Thus, a solid has complete memory of its initial state during the period of deformation. Conversely, the strain experienced by a viscous liquid linearly increases with respect to the time of which the stress is applied and, upon removal of the stress, the liquid remains at its last known strain, thus losing memory of its state prior to application of the stress. Finally, a viscoelastic material is more complex and exhibits a combination of these two responses. The memory that a viscoelastic material can display is time dependent. At short time periods, provided the viscous element has not dominated the flow of the fluid, the substance would have almost complete memory of its initial state. However, after a sufficiently long time under stress, the substance will have essentially no memory of its initial state and will never be able to return. The simplest representation of such a material is the Maxwell model, which is a combination of a spring and dashpot to account for the elastic and viscous elements, respectively, of a viscoelastic fluid.[21]

However, the problem with a single mode Maxwell model being used to represent the biofilm is the limited applicable range of the model and the composite nature of the biofilm structure. The Maxwell model is only valid within the linear viscoelastic limit.[21, 22] Additionally, this model predicts perfectly elastic behavior with a frequency independent modulus at high frequencies identical to rubber, which is not realistic for many viscoelastic materials.[21] Hence, just to describe simple linear viscoelastic behavior, a more complex model will have to be implemented. A more effective means to accurately predict the behavior of a biofilm would be through a multi-mode Maxwell model with a generalization included to account for nonlinear as well as linear viscoelasticity. As most constitutive equations are constructed based upon molecular ideas about the materials they are describing, creating one to fit biofilms specifically may be difficult because not much is known about the polymer chain, colloidal, or molecular interactions at this time. However, the proper model should account for aggregation of bacterial cells and entanglements within the polymer chains of the polysaccharide matrix. Also, the contribution of the hard spherical cells to the biofilm elasticity should be included. A hierarchical approach may be the ideal way to characterize the mechanical response of biofilms due to individual cell-cell interactions, the damping caused by the polymer chains between the cells, and the dependence on each interaction within the complex network in deciding the overall viscoelastic response of the biofilm.

Unfortunately, with much information missing, current work has only been able to use simple models to describe the viscoelastic behavior of these biofilms.[23-26] Therefore, the next logical step would be to further explore the rheological properties of these biofilms in order to fill in knowledge gaps about the material that would allow for better models to be developed, such as the modulus of the biofilms, relaxation time of the polymer chains, and forces

responsible for biofilm fragmentation.

Rheometry

The viscoelasticity of biofilms can be interrogated through rheometry, which measures the mechanical properties of fluids as a function of their deformation rate.[27] Specifically for *S. epidermidis* biofilm, drag flow rheometry with a parallel plate is used. In this method, a moving surface, called the geometry, induces a shear on the fluid between itself and a fixed base.[21] This can be seen in Figure 1.3 below.

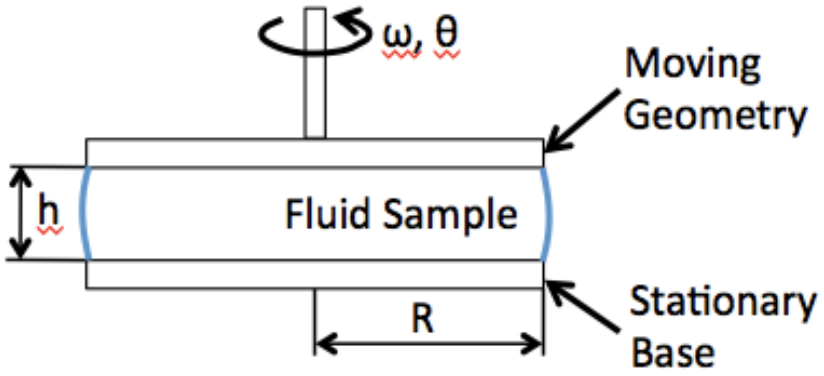

Figure 1.3. Illustration of parallel plate rheometry. This figure is adapted from Bird *et al.*[22]

Parallel plate rheometry is used, despite the non-homogenous flow produced under the geometry. Although the cone-and-plate geometry is ideal due to the uniform material strain that can be applied to the sample, the parallel plate is necessary as the goal is to grow the biofilm uniformly under the gap for analysis, which would be hard to accomplish with the finite gap size available with a cone. Also, the biofilm aggregates can potentially get stuck under the truncation gap of the cone geometry, causing inaccurate measurements. The flow state found in parallel plate rheology can be illustrated by the strain rate imposed on the fluid by the following equation:

$$\dot{\gamma}(r) = \frac{r\omega}{h}$$

where r is the radius from the center of the geometry at which the flow is being examined with a maximum radius of R, h is the height of the gap between the geometry and the base, and ω is the angular velocity at which the plate is rotating. This equation is vital in determining the angular velocity needed to grow biofilm under the desired shear stress.

In rheometry, the viscoelastic response of the biofilm is a bulk property quantified by the storage and loss moduli, G' and G'', respectively.[27] These moduli can be measured within the linear viscoelastic regime, where a small amplitude oscillatory shear (γ_0) is imposed onto the fluid so that its microstructure is not significantly deformed.[28] The sinusoidal shear stress from this oscillatory measurement can be related to the storage and loss moduli by the following equation:

$$\tau = G'\gamma_0 sin(\omega t) + G''\gamma_0 cos(\omega t)$$

where the storage modulus is the component of stress that is in-phase with the strain, while the loss modulus is the stress that is out-of-phase with the strain.[21, 27, 29] When the storage modulus is higher than the loss modulus, the material is more solid-like than liquid-like and vice versa. Constitutive models yield quantitative predictions of these linear viscoelastic moduli as a function of frequency.

Current State of the Field

There have been a variety of studies geared towards characterizing the viscoelastic properties of bacterial biofilms. Throughout literature many innovative techniques have been employed to accomplish this. However, many of these methods fail to take into account certain vital factors necessary to accurately analyze biofilms as they would be found in their natural

environments. Some of these shortcomings can be found in growth conditions, while others are due to transportation issues and the length scales of the analytical techniques used. Despite the shortcomings, these studies do provide us with interesting results that we can build on.

In order to find the relaxation time of a variety of biofilms, Shaw *et al.* conducted strain creep tests.[1] In these experiments, the stress on the biofilm was increased instantaneously to a value within the linear regime and held while the strain was recorded. The stress was then removed and the recoil of the strain was measured.[21] The extent to which the material is able to recover after being deformed is measured. A common relaxation time of roughly 18 minutes was determined for 44 different biofilms.[1]

However, methods used in these tests can affect the biofilm properties measured. Biofilms were scraped off of their growing environment in order to be analyzed. As biofilms are fragile enough that forces exerted to remove them from their source could cause deformation, any rheological tests done after this may be affected by this method of sample preparation. Therefore, it is vital to have the biofilms growing directly onto the analytical surfaces in order to obtain results that are clearly indicative of the conditions of their growth. Another problem was the non-uniform coverage of biofilms on the rheometer plate. As the instrument is highly sensitive to sample loading, any deviation from uniformity can greatly affect the results.

When conducting microrheological experiments with *S. epidermidis* biofilms, Hohne *et al.* found that the relaxation time was 13.8 seconds.[30] As this is multiple orders of magnitude shorter than the Shaw results, additional work should be done to determine a more precise timescale. Nevertheless, Hohne's system improved on other designs as the biofilms were allowed to adhere and grow directly onto the testing device. This eliminated the need to remove the biofilms from an intermediate surface and reduced the risk of deformation in the sample prior to

analysis.

In Towler *et al.*, an interesting strategy was used to grow a mixed culture of biofilms.[23] Rheometer plates were suspended into a tank and rotated with the use of a drive shaft at a known, constant rate. Growth media flowed continuously through the tank to ensure that there were proper amounts of nutrients in the system. An additional benefit from this setup was that, with such a small gap between the rheometer plates and the base, shear stress can be accurately calculated due to the one-dimensional nature of the system. This allows for reproducibility and greater control of the growing conditions of the biofilm.

Additionally, Towler used epifluorescence microscopy to determine the thickness of the biofilm in order to set the gap on the rheometer.[23] Knowing the thickness is important in order to generate sufficient contact between the biofilm and the parallel flat plates during analysis without causing additional stresses due to over-compression onto the analytical surface. Also, the strain applied is a direct function of the gap height. Therefore, an inaccurate gap height can greatly affect the measurements taken. The biofilms used were between 35-50 μm thick.[23] As flat plate rheology is typically performed with gaps between 250 μm and 1 mm, a larger biofilm thickness is desirable to ensure the error due to instrument sensitivity in the gap height is not significant.[9] Allowing a longer growth period or exposing the sample to higher nutrient concentrations would ensure that these samples are at a suitable thickness.

To determine the biofilm moduli, Jones *et al.* conducted rheometry on *S. epidermidis*.[24] Under many growth conditions, such as various salts and antibiotics being added, Jones found that the shear modulus of the biofilm was on the order of 0.5-15 kPa, which is consistent to that of Hohne (3.2 kPa), Di Stefano (0.5 kPa), and Aggarwal (0.1-6.5kPa).[24, 30-32] However, studies of mixed biofilms found them to be on the order of 0.3-45 Pa, with an overall hypothesis that the

relaxation time approximately constant.[1, 23, 33-35] Additionally, Jones *et al.* noticed that the presence of salt generally reduced the moduli. This is not necessarily in agreement with the works of the Rachid and Lim, as increases in NaCl concentrations actually showed an increase of biofilm production in *S. epidermidis* and *S. aureus.*[14, 16] Unfortunately, Rachid and Lim do not test biofilm mechanical properties and Jones only uses one concentration of NaCl; therefore no conclusions can be drawn about the trend. Another innovation that Jones used was individually adjusting the gaps for each biofilm based on the normal force response. However, all of the gap sizes used were well below the limit that is typically resolvable for mechanical rheometry. Additionally, these biofilms were not grown under the presence of shear stresses, which is known to greatly affect the material properties of the biofilms produced.[2, 4]

Finally, Jones, Towler, and others have used a Burger model to present their creep relaxation results.[23, 24] This model is an in-series combination of springs and dashpots from the Maxwell model (in-series) and the Kelvin model (in parallel). Although this multi-mode, four element model fits the relaxation data reasonably well, it is only valid for linear viscoelasticity and will be too primitive when large deformations and ruptures in the material are involved. Hence, material properties outside of the linear limits will need to be studied in order to determine a suitable model.

From the previous mechanical characterization work on *S. epidermidis* bacterial biofilms, the main aspect that requires further exploration is the effect of the environmental conditions, especially those that are physiologically relevant, on the biofilm's mechanical properties.

Research Objective

The objective of our research is to explore how the mechanical properties of *S.*

epidermidis biofilms can be measured under physiological conditions and how these properties change with various alterations in the biofilms' environment. Overall, our research objectives can be summarized in three sections:

1) Study the linear and non-linear rheological properties of biofilms in a natural state and investigate how these properties are affected by varying environmental conditions. We will quantify the linear elastic and viscous moduli, the yield stress, and relaxation time of the biofilm. Then, we will study how high salt concentration and increased temperatures induces stress on the organism, which is hypothesized to affect mechanical properties. The aim of this study is to understand standard *in situ* behavior of biofilms and develop a correlation between salt concentration and temperature with the biofilm properties.

2) Study possible strategies to treat biofilm infections while developing a physical and chemical understanding of what is happening to the biofilms during this treatment. Here, the focus is to further delve into the idea of using heat/temperature to treat biofilm infections with the aims of a) determining the effect of heat exposure on the yield stress of the biofilms b) investigating the cell morphology and viability after heat treatment and c) understanding the polymer interactions and changes occurring within the EPS. These results can be used to alter and improve the efficacy of current clinical treatment strategies for biofilm infections.

3) Study a method developed to rapidly characterize mechanical properties of large volumes of elastic solids and extend it to finite volumes of viscoelastic materials. Here, the focus

would be on using cavitation rheology to provide quick and robust measurements of the elastic modulus of the biofilms. The aim of this project is to show that this cavitation technique can be used to probe limited volumes of biofilm on various complex and clinically relevant geometries. By proving the accuracy of this method, various biofilm species and strains within a clinical setting can be studied to diagnose specific infections in vivo. Also, this method may become equally as vital for use in other applications such as high-throughput polymer rheology and tissue diagnostics.

References

1. T. Shaw, M. Winston, C. J. Rupp, I. Klapper and P. Stoodley, *Physical Review Letters*, 2004, **93**, 4.

2. R. M. Donlan and J. W. Costerton, *Clinical Microbiology Reviews*, 2002, **15**, 167-193.

3. B. Rasmussen, *Nature*, 2000, **405**, 676-679.

4. L. Hall-Stoodley, J. W. Costerton and P. Stoodley, *Nature Reviews Microbiology*, 2004, **2**, 95-108.

5. K. K. Jefferson, *Fems Microbiology Letters*, 2004, **236**, 163-173.

6. J. W. Costerton, P. S. Stewart and E. P. Greenberg, *Science*, 1999, **284**, 1318-1322.

7. M. J. Solomon, D. M. Bortz, R. Sureshkumar and J. G. Younger, ed. NSF, Editon edn., 2009.

8. H. M. Chung, M. M. Cartwright, D. M. Bortz, T. L. Jackson and J. G. Younger, *Shock*, 2008, **30**, 518-526.

9. J. P. O'Gara and H. Humphreys, *Journal of Medical Microbiology*, 2001, **50**, 582-587.

10. M. Otto, *Nature Reviews Microbiology*, 2009, **7**, 555-567.

11. F. Gotz, *Molecular Microbiology*, 2002, **43**, 1367-1378.

12. A. Valiei, A. Kumar, P. P. Mukherjee, Y. Liu and T. Thundat, *Lab on a Chip*, 2012, **12**, 5133-5137.

13. J. Loscalzo and A. I. Schafer, *Thrombosis and hemorrhage*, Williams & Wilkins, Baltimore, 1998.

14. Y. Lim, M. Jana, T. T. Luong and C. Y. Lee, *Journal of Bacteriology*, 2004, **186**, 722-729.

15. M. C. Walters, F. Roe, A. Bugnicourt, M. J. Franklin and P. S. Stewart, *Antimicrobial Agents and Chemotherapy*, 2003, **47**, 317-323.

16. S. Rachid, K. Ohlsen, W. Witte, J. Hacker and W. Ziebuhr, *Antimicrobial Agents and Chemotherapy*, 2000, **44**, 3357-3363.

17. R. L. Fournier, *Basic Transport Phenomena in Biomedical Engineering*, Second edn., Taylor & Francis Group, New York, 2007.

18. S. S. Branda, A. Vik, L. Friedman and R. Kolter, *Trends in Microbiology*, 2005, **13**, 20-26.

19. C. Vuong, C. Gerke, G. A. Somerville, E. R. Fischer and M. Otto, *Journal of Infectious Diseases*, 2003, **188**, 706-718.

20. J. W. Costerton, K. J. Cheng, G. G. Geesey, T. I. Ladd, J. C. Nickel, M. Dasgupta and T. J. Marrie, *Annual Review of Microbiology*, 1987, **41**, 435-464.

21. C. W. Macosko, *Rheology: Prinicples, Measurements, and Applications*, Wiley-VCH, New York, 1994.

22. R. B. Bird, R. C. Armstrong and O. Hassager, *Dynamics of Polymeric Liquids*, John Wiley & Sons, New York, 1987.

23. B. W. Towler, C. J. Rupp, A. B. Cunningham and P. Stoodley, *Biofouling*, 2003, **19**, 279-285.

24. W. L. Jones, M. P. Sutton, L. McKittrick and P. S. Stewart, *Biofouling*, 2011, **27**, 207-215.

25. A. M. Vinogradov, M. Winston, C. J. Rupp and P. Stoodley, *Biofilms*, 2004, **1**, 49-56.

26. V. Vadillo-Rodriguez and J. R. Dutcher, *Soft Matter*, 2011, **7**, 4101-4110.

27. R. G. Larson, *Constitutive Equations for Polymer Melts and Solutions*, Butterworths, Boston, 1988.

28. R. G. Larson, *The Structure and Rheology of Complex Fluids*, Oxford University Press, New York, 1999.

29. J. D. Ferry, *Viscoelastic Properties of Polymers*, Third edn., John Wiley & Sons, New York, 1980.

30. D. N. Hohne, J. G. Younger and M. J. Solomon, *Langmuir*, 2009, **25**, 7743-7751.

31. S. Aggarwal, E. H. Poppele and R. M. Hozalski, *Biotechnology and Bioengineering*, 2010, **105**, 924-934.

32. A. Di Stefano, E. D'Aurizio, O. Trubiani, R. Grande, E. Di Campli, M. Di Giulio, S. Di Bartolomeo, P. Sozio, A. Iannitelli, A. Nostro and L. Cellini, *Microbial Biotechnology*, 2009, **2**, 634-641.

33. C. J. Rupp, C. A. Fux and P. Stoodley, *Applied and Environmental Microbiology*, 2005, **71**, 2175-2178.

34. P. Stoodley, Z. Lewandowski, J. D. Boyle and H. M. Lappin-Scott, *Biotechnology and Bioengineering*, 1999, **65**, 83-92.

35. M. Wloka, H. Rehage, H. C. Flemming and J. Wingender, *Colloid and Polymer Science*, 2004, **282**, 1067-1076.

CHAPTER II

In Situ Rheology of *Staphylococcus epidermidis* Bacterial Biofilms[*†]

Abstract

We developed a method to grow *Staphylococcus epidermidis* bacterial biofilms and characterize their rheological properties *in situ* in a continuously-fed bioreactor incorporated into a parallel plate rheometer. The temperature and shear rates of growth modeled bloodstream conditions, a common site of *S. epidermidis* infection. We measured the linear elastic (G') and viscous moduli (G") of the material using small-amplitude oscillatory rheology and the yield stress using non-linear creep rheology. We found that the elastic and viscous moduli of the *S. epidermidis* biofilm were 11 ± 3 Pa and 1.9 ± 0.5 Pa at a frequency of 1 Hz (6.283 rad/s) and that the yield stress was approximately 20 Pa. We modeled the linear creep response of the biofilm using a Jeffreys model and found that *S. epidermidis* has a characteristic relaxation time of approximately 750 seconds and a linear creep viscosity of 3000 Pa·s. The effects on the linear viscoelastic moduli of environmental stressors, such as NaCl concentration and extremes of temperature, were also studied. We found a non-monotonic relationship between moduli and NaCl concentrations, with the stiffest material properties found at human physiological concentrations (135 mM). Temperature dependent rheology showed hysteresis in the moduli when heated and cooled between 5°C and 60°C. Through these experiments, we demonstrated

[*] This work was previously published by L. Pavlovsky *et al.* in *Soft Matter.*[1]
[†] Biochemical assays were performed in part by Ashley E. Satorius.

that biofilms are rheologically complex materials that can be characterized by a combination of low modulus (~10 Pa), long relaxation time (~10^3 seconds), and a finite yield stress (20 Pa). This suggests that biofilms should be viewed as soft viscoelastic solids whose properties are determined in part by local environmental conditions. The *in situ* growth method introduced here can be adapted to a wide range of biofilm systems and applied over a broad spectrum of rheological and environmental conditions because the technique minimizes the risk of irreversible, non-linear deformation of the microbial specimen before analysis.

Introduction

Bacterial biofilms are matrix-enclosed multicellular communities of microorganisms that can colonize environmental and man-made surfaces of ecological, industrial, and medical significance.[2-5] In most bacterial biofilms, the matrix is comprised primarily of a bacterially synthesized extracellular polymeric substance (EPS) that acts as a protective barrier. The EPS improves bacterial fitness through a set of mechanisms that are thought to include resistance to the diffusion of antimicrobial agents, promotion of intercellular communication to induce more resilient patterns of gene expression, and reversible deformation to resist fragmentation due to applied stresses.[2, 3, 6, 7] The EPS is composed partially of protein and DNA, but predominantly of polysaccharides.[6, 8]

Biofilms are persistent in a variety of settings where knowledge of their mechanical properties would be useful to maintaining clean surfaces as well as preserving the efficiency and effectiveness of the fouled components. For example, biofilm species can grow on the hulls of ships, increasing drag and overall fuel consumption for transportation.[9] Similarly, a buildup of biofilm in industrial pipelines can cause a loss of hydrodynamic pressure, leading to

increased power consumption, decreased plant efficiency, as well as possible cooling failures.[10] Importantly, biofilms also colonize implanted medical devices in concentrated regions, which tend to fragment under the shear stresses of blood and disseminate bacteria through the bloodstream, causing infection.[3]

A biofilm-forming species of particular interest to human health is *Staphylococcus epidermidis*. *S. epidermidis* is a normal member of skin flora. Commonly, this organism infects patients by contaminating the surface of medical devices at the time of surgical implantation or subsequently during routine care of such devices.[11] Although not generally severe, *S. epidermidis* infections have a mortality rate above 30% in a population of immunocompromised patients.[11, 12] Much more commonly, *S. epidermidis* biofilm formation prompts surgical removal and replacement of the affected implanted device, with the associated costs and risks of that procedure.[7]

Many implanted devices susceptible to colonization by this organism are positioned in the bloodstream, such as intravenous and intraarterial catheters, dialysis catheters, and prosthetic heart valves. In this setting, *S. epidermidis* biofilm extent and structure reflects immunological and physical interactions with the host, including hydrodynamic forces imposed by flowing blood in particular.[13] Accordingly, reducing the disease burden associated with *S. epidermidis* may require better understanding of the mechanical features that allow it to persist in the bloodstream.

Biofilms must be cultivated prior to rheological characterization. As a result, rheological measurements typically follow one of two paths: In the first, a biofilm is cultivated in a bioreactor, and then physically transferred to the rheometer for characterization. In the second, the rheological evaluation is performed *in situ*, but perhaps limited or non-standard techniques

are used. Examples in literature of the former include samples scraped off of their growth environment by Shaw *et al.*, and samples grown on suspended rheometer plates connected to a drive shaft and then moved to the analytical device by Towler *et al.* An example of the latter includes observations of biofilms grown on a microfluidic device by Hohne *et al*.[2, 14, 15] Other biofilm rheology studies have been reviewed by Wilking *et al.*[16]

Evidence for divergent results from these two approaches can be found in the broad range of values for the linear elastic modulus that have been reported in the literature for *S. epidermidis* biofilms, which include those of Di Stefano *et al.* (0.5 kPa), Jones *et al.* (0.5-15 kPa), Hohne *et al.* (3.2 kPa), and Aggarwal *et al.* (0.1-8.0 kPa).[14, 17-20] There is little doubt that biofilm mechanics are dependent on the conditions under which they develop.[21] It appears that the challenges posed by evaluating biofilms *in situ* in current rheometric fixtures have produced considerable uncertainty in biofilm mechanical properties reported in the literature. Experimental measurements that address the challenge of *in situ* growth and evaluation can support the development of theoretical models for biofilm mechanics that are grounded in polysaccharide and polymer rheology. They can furthermore be applied to evaluate hypotheses about the interaction of biofilms with the hydrodynamic stresses generated in the circulatory system.

Here we address the need for an *in situ* rheological characterization method for cultured biofilms. The method uses a chamber for *in situ* growth of biofilms under the fixture of a standard rheometer. After an initial phase of growth, the biofilm is fused to the rheometer fixture, thereby allowing rheological characterization of the bacterial biofilms. This method, here applied to the particular case of *S. epidermidis* biofilms, transforms a parallel plate rheometer into a continuously-fed bacterial bioreactor, thereby allowing the *in situ* rheological characterization to proceed. By doing so, we were able to sequentially grow biofilms under defined shear forces and

then perform small-amplitude oscillatory rheology and non-linear creep rheology, without disrupting the test material from its original site of growth. With this method, we report the characterization of the viscoelastic properties of *S. epidermidis* biofilms. We explore the impact on mechanical behavior of a well-known metabolic stressor, osmotic stress, which is generated by growth under high salt conditions. Additionally, we observe the behavior of biofilm mechanical properties under a range of temperatures and find behavior that reveals that complex rheology of these multiphase materials.

Methods and Materials

Staphylococcus epidermidis

S. epidermidis of strain RP62A, a biofilm-forming clinical isolate was obtained from American Type Culture Collection (culture 35984) and grown in tryptic soy broth (TSB; Fluka Scientific) media supplemented with 1% d-(+)-glucose (Sigma Life Science, 86 mM NaCl, viscosity 0.88 Pa.s at 37^{o}C). For experiments probing the osmotic stress induced by sodium chloride, media were enriched to 135 mM NaCl – which is reflective of human blood stream salinity, or 770 mM NaCl – the conventional high-stress condition used in the literature.[22, 23] As the rheometer bioreactor is an open system and therefore prone to contamination, cycloheximide (90 μg/mL; Fluka Scientific) and kanamycin (50 μg/mL; Sigma-Aldrich) were used as an antifungal and general antibacterial, respectively.[24, 25] The impact of both was confirmed in preliminary experiments in which *S. epidermidis* was cultured on tryptic soy agar plates in which each compound had been dosed. Neither had any discernible effect on *S. epidermidis* growth by a count of colony-forming units.

Rheometry

A mechanical rheometer (TA Instruments AR-G2) was used to create a controlled-shear rate environment during growth and characterization of the biofilm. The geometry used was a 40 mm stainless steel parallel plate. We conducted growth and testing while the geometry was submerged in media at gap heights between 250 μm and 1 mm. The lower limit was chosen because it was the minimal gap height for instrument sensitivity, as determined through independent testing on aqueous solutions of poly(ethylene oxide). This configuration was made possible by the use of an immersion ring attached to the bottom Peltier plate of the rheometer, which acted to keep the parallel plate geometry submerged in TSB media (Figure 2.1). The novelty of this approach is that it allows the biofilm to grow under the rheometer fixture as the media is slowly convected over the growth area while, simultaneously, the level is controlled.

To sterilize the apparatus prior to experiments, we filled the immersion bath with ethanol, and allowed it to disinfect for approximately 30 minutes. Additionally, we used a custom-made plastic cover to reduce the opportunity for airborne contamination of the open reactor. Variable-flow peristaltic pumps (Fisher Scientific) were used to constantly replenish the media in a chemostat configuration at a rate of approximately 0.5 mL/min with a total fill volume of approximately 30 mL, giving a media turnover rate of approximately 1 $hour^{-1}$. After reaching fill volume, we inoculated the media within the immersion ring with 2 mL of the initial *S. epidermidis* culture by pipette.

The experimental protocol is divided into three phases: growth, attachment, and rheological characterization. All phases of the experiments were conducted at 37°C unless otherwise noted.

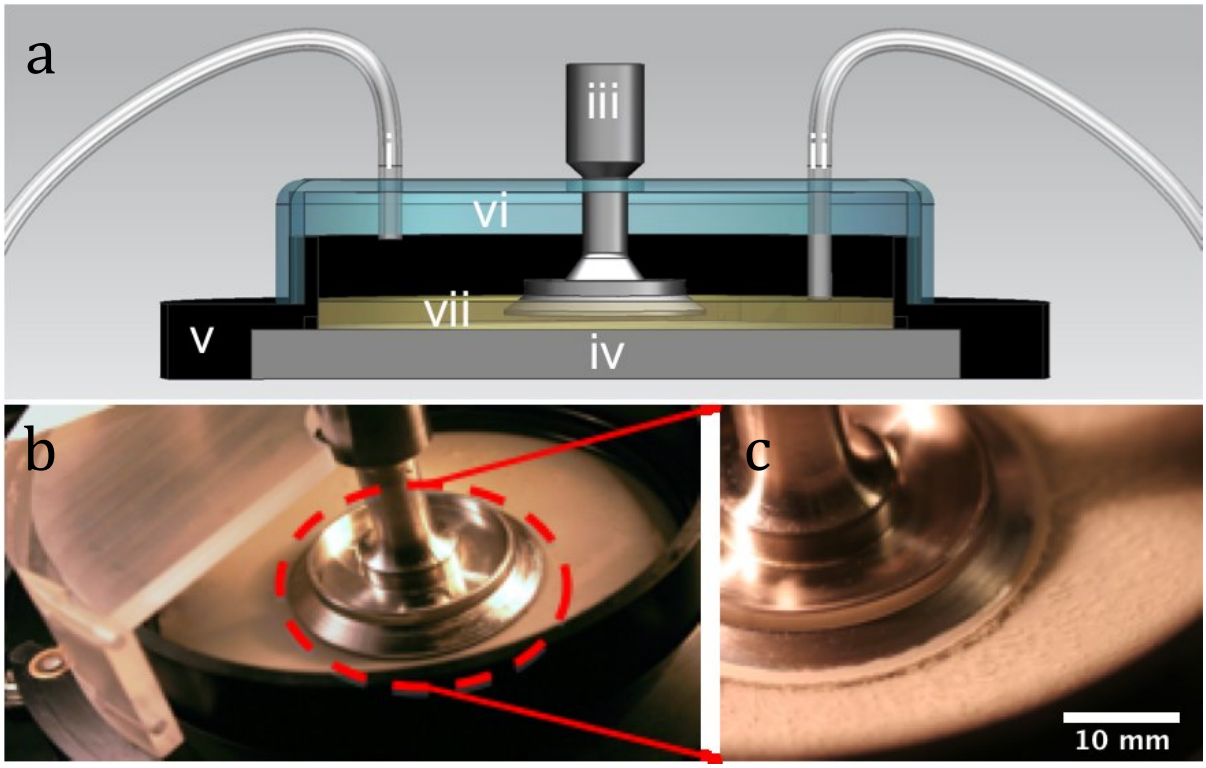

Figure 2.1. *In situ* biofilm rheometry setup. (a) Cross-sectional schematic of continuously-fed rheometer bacterial bioreactor where (i) is the growth media inlet, (ii) is its outlet, (iii) is the rheometer fixture, (iv) is the Peltier plate for temperature control, (v) is the immersion ring, (vi) is the cover, and (vii) is the liquid growth media, which is maintained at a fix level by the outlet suction. (b) Overhead view of the open rheometer bioreactor. (c) Close-up view of the rheometer geometry of the bioreactor with *Staphylococcus epidermidis* biofilms grown, post-analysis. Figure reproduced from Pavlovsky *et al.*[1]

Growth

During the growth phase, the rheometer parallel plate was positioned at a gap of 1.0 mm. Within the human circulatory system, which is a common contamination site for such biofilms, the shear rate can be in excess of 100 s^{-1} and the shear stress is in the range of 0.076 – 0.76 Pa.[22, 26] Therefore, we rotate the plate to generate an initial shear stress of 0.1 Pa, which corresponds to a shear rate of 113.6 s^{-1}. This shear rate is held fixed during the growth phase. Biochemical assessment of the reactor in the opening hours of the growth phase confirmed a transition from aerobic to micro-aerobic growth as oxygen and glucose consumption fell to steady-state values

within 7 hours. Altogether, growth was allowed to continue for 17 hours, after which the gap was reduced to 300 μm. This reduction in gap allowed the biofilm cultured on the base to come in contact with the upper plate. This timescale for growth was chosen due to the constraints of the organism and our interests in analysis, and could be varied to suit differences in organism and environment. At the conclusion of the growth phase, the biofilm has covered the rheometer Peltier plate completely, but has yet to connect to the upper plate.

Attachment

The attachment phase was a 7-hour period of linear oscillation of the geometry that allowed the biofilm to fuse from the rheometer Peltier plate to the upper plate. We accomplished this by reducing the parallel plate gap height to 300 μm and oscillating the plate at a strain of 0.016 for 7 hours. An oscillatory study at various gap heights was conducted to determine the maximum allowable gap height. The oscillatory strain of 0.016 was chosen such that it was within the linear viscoelastic regime of the biofilm to avoid altering the material before testing. We chose the 7-hour period because it provided for sufficient growth of the biofilm, as was discussed in the previous section.

We established a criterion to systematically determine whether a sample had attached to both the top and bottom of the parallel plate rheometer fixture, and thus was a good candidate for further rheological testing. During attachment, the linear elastic and viscous moduli, G' and G", respectively, were measured over time. Only biofilms whose moduli reached steady-state by the end of the 7-hour period were judged to have attached. The rate for successful attachment was approximately 70%. Examples of the time-dependent elastic modulus for attached and

unattached biofilms are shown in Figure 2.2; distinguishing between the two cases was straightforward because of the large rheological differences between the two states.

In addition to the attachment criterion, we performed three other studies to evaluate the quality of the rheological measurements on the biofilm. First, we evaluated the overall biofilm coverage. We removed the geometry fixture after rheological measurements were completed, stained the bacterial cells with Gram crystal violet (Becton, Dickinson and Company), and rinsed off the excess. In all attached samples, biofilm coverage was equal to or greater than 95% of the analytical surface area of the geometry. Second, we stained and imaged biofilm sampled from a number of regions of the rheometer with confocal laser scanning microscopy (CLSM) as per the methods of Hohne *et al*. and Dzul *et al*.[14, 27] These images showed that the biofilms displayed a uniform microscopic morphology over the testing surface. Representative images of the Gram staining and confocal microscopy are reported in Figure 2.3. Third, we evaluated the effect of parallel plate diameter on the rheology. In this testing, we applied the same growth and attachment procedures for a 60 mm parallel plate geometry. For the case of no added NaCl, the measured G' and G" did not show a significant difference between tests conducted with a 40 mm and 60 mm; measurements at all frequencies were within one standard deviation. This result demonstrates geometry independence of the material properties of the tested biofilms. A final issue was the selection between parallel plate fixtures and the cone and plate geometry for measurements. We opted for the former because of the nonhomogeneous nature of the biofilms, the need to assess the effect of multiple gap heights and pre- and post- compression testing, and because of the performance of temperature dependence rheology.

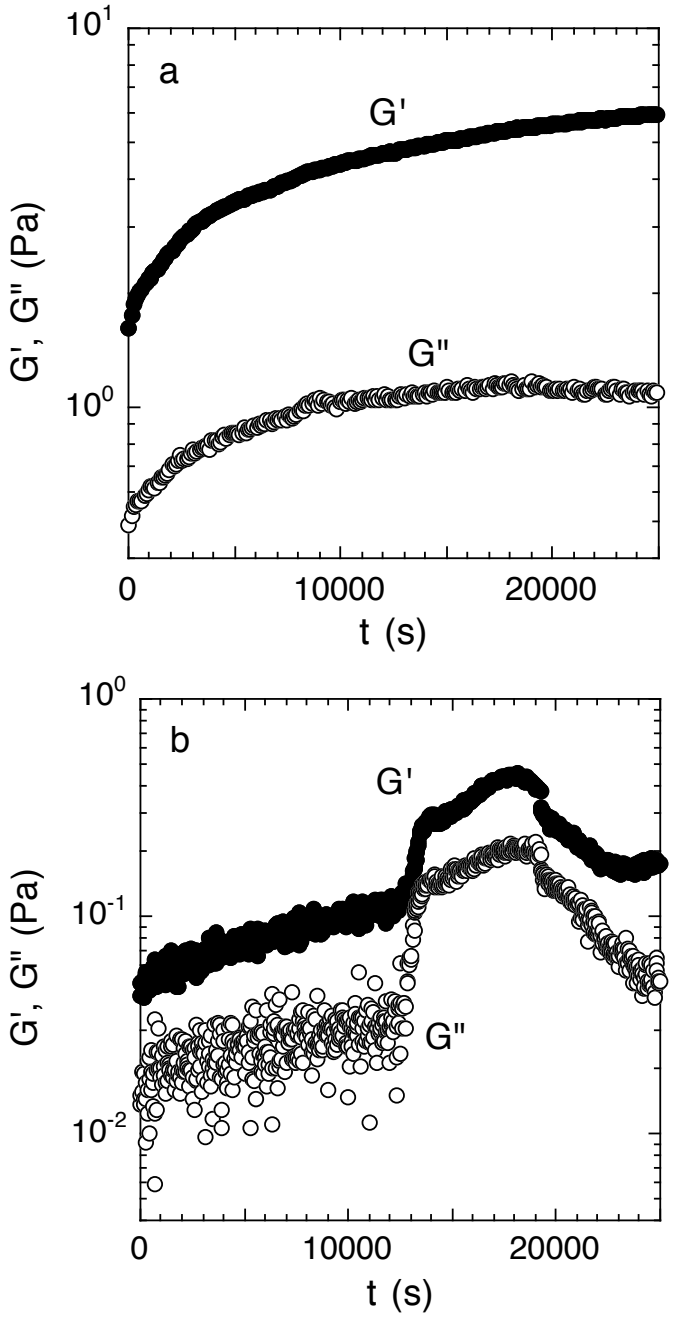

Figure 2.2. Criterion to determine biofilm attachment. (a) Accepted and (b) rejected attachment phase. Measured over 7 hours at 300 μm and a strain of 0.016 directly after the initial growth period. The moduli in accepted experiment have reached equilibrium while the rejected experiment has not. Examples of one experiment of each case are shown. Figure reproduced from Pavlovsky *et al.*[1]

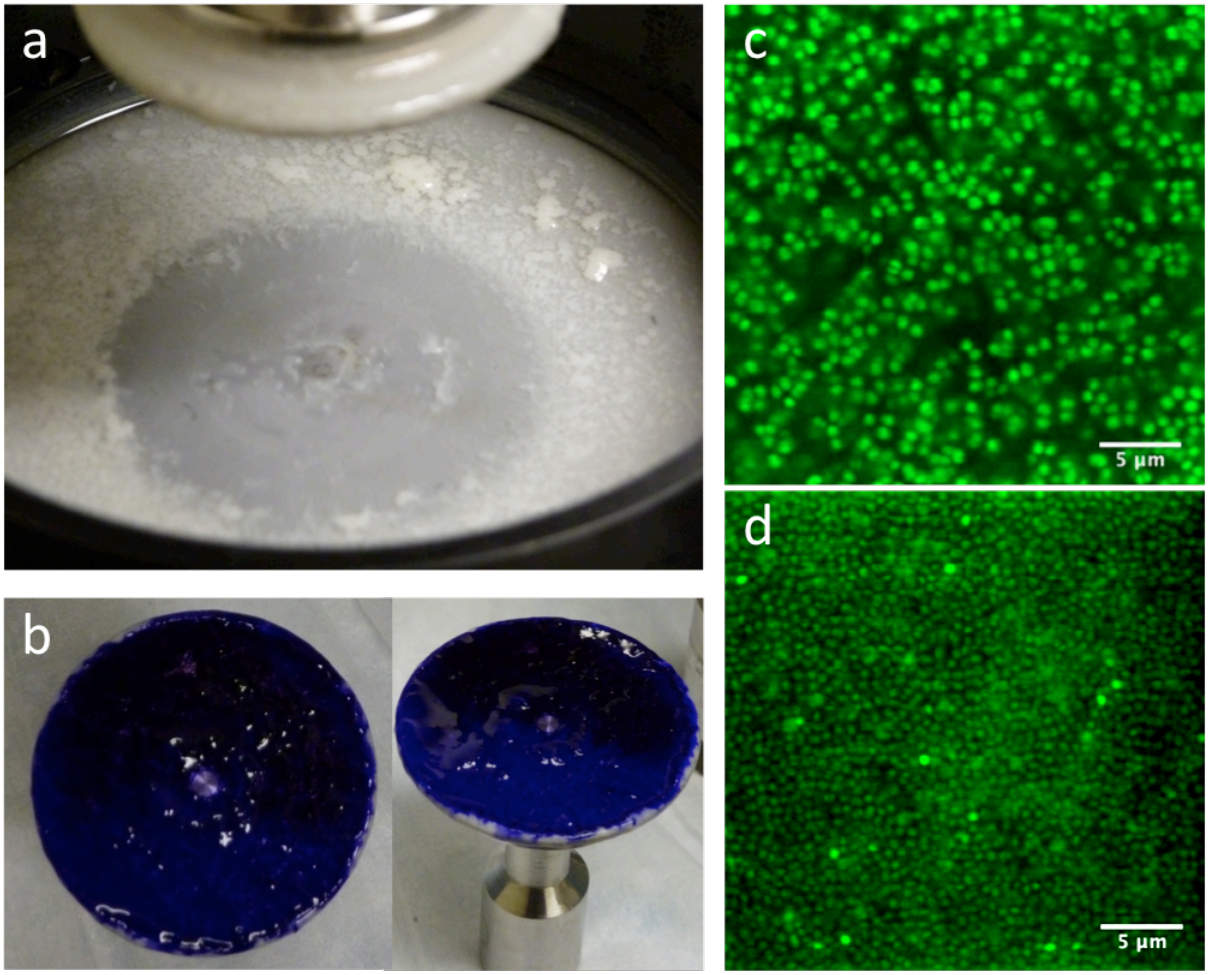

Figure 2.3. Growth of biofilm on the rheometer. (a) Base of rheometer immediately after draining media and lifting the parallel plate. (b) 40mm diameter parallel plate stained with Gram crystal violet depicting full coverage of biofilm. (c-d) CLSM images of various areas of the biofilm after rheological testing, showing similar morphology throughout. Figure reproduced from Pavlovsky *et al.*[1]

Rheological characterization

Small-amplitude oscillatory rheology

After the attachment phase, we determined the linear viscoelasticity of the biofilm by small-amplitude oscillatory deformation over the frequency range of 0.005 – 10 Hz (0.0314 – 62.83 rad/s) and strain amplitude of 0.13 (approximately 10% of the maximum strain within the linear viscoelastic limit). The measurements were conducted at gap heights of 300 and 250 µm,

under compression and tension. The variation in gap was used to check for hysteresis in gap height.

Creep rheology

We measured the creep compliance, $J(t, s_o)$, of a number of specimens to extend the regime of linear rheological characterization to long times (low frequencies) and to determine the non-linear rheological response of the biofilms, including their yield stress. These tests were performed immediately after the small-amplitude oscillatory rheology measurements. The experiments were conducted for duration of 20 minutes. The measurements were performed at the following applied stresses: 0.1 Pa, 0.2 Pa, 0.5 Pa, 1.0 Pa, and then up to 100 Pa in increments of 5 Pa.

Temperature dependent rheology

The effect of temperature on the linear viscoelasticity of the biofilms was studied by means of small-amplitude oscillatory rheology. Initial tests on attached biofilms were conducted at 37°C. Then, the specimen temperature was decreased to 5°C and linear viscoelasticity measured. This procedure was repeated at temperatures from 5°C to 60°C in increments of 5°C. To evaluate hysteresis, measurements were then performed from 60°C to 10°C, with temperature decreased in increments of 5°C. Temperature changes were rapidly induced by the Peltier component of the rheometer.

Sensitivity analysis of small-amplitude rheology

We found that bacterial biofilms displayed greater specimen-to-specimen variability in their rheology than synthetic materials, such as polymer melts or colloidal suspensions. To address this variability, we performed statistical analyses standard in the biological sciences to

evaluate for differences in rheology between different biofilm growth conditions. To examine the impact of such experimental conditions on the G'-frequency and G"-frequency relationships, a linear mixed effects regression approach was used as implemented in the *lme* function in the statistical package R 2.13.2. Frequency, NaCl concentration, the gap height, and whether measurements were taken before or after a compressive strain were considered as fixed effects. Individual biofilms were considered as a random effect. For analysis of G', modeling was performed with log transforms of G' and angular frequency. For G", similar modeling was performed but included also polynomial fitting of the G"-frequency curve. Between-model comparisons were performed using *anova.lme* in the same package.

Results and Discussion

Small-amplitude oscillatory rheology of *S. epidermidis*

Small-amplitude oscillatory rheology was used to determine the frequency dependence of the elastic and viscous moduli of *S. epidermidis* biofilms (Figure 2.4). The elastic modulus, G', was approximately 10 Pa and exhibited a power-law increase at increasing angular frequency while the viscous modulus G" was on the order of 1 Pa and deviated from power-law behavior at increasing angular frequency. For comparison, soft living tissues have the following elastic moduli: swine brain (260-490 Pa), human liver (640 Pa), human breast tumor (4 kPa), rat skeletal muscle (100 kPa), and bovine cartilage (950 kPa).[28-32] As G' is greater than G" at all frequencies studied, the material is elastic and solid-like. Unfortunately, due to the small frequency range, and the lack of applicability of time-temperature superposition (as discussed in a later section), this technique does not reveal much about the material rheology other than confirming that biofilms are soft, viscoelastic materials. The non-linear rheological characterization by creep will

provide a better indication of the mechanical properties of the biofilm. We can, however, conclude from the linear rheology that the longest viscoelastic relaxation time of the biofilm must be greater than ~10^2 seconds because no terminal region was observed within the frequency range of the measurements. This conclusion is consistent with the findings of Shaw *et al.* for the case of *S. aureus*, *Pseudomonas aeruginosa,* and natural pond biofilms.[2]

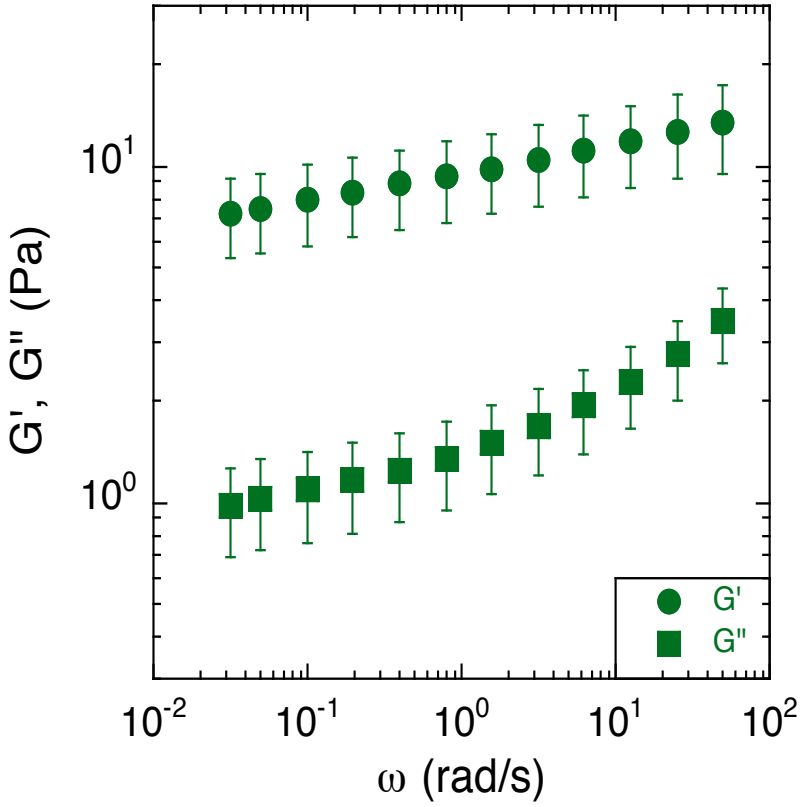

Figure 2.4. Elastic and viscous moduli of *S. epidermidis* biofilms grown in TSB with 86 mM NaCl. This data includes 6 replicates, with each comprised of an average modulus of the experiments conducted at 300 and 250 μm under both compression and tension. Error bars represent the standard error of the mean. Figure reproduced from Pavlovsky *et al.*[1]

More specifically, the *S. epidermidis* elastic and viscous moduli resemble those of soft glassy materials at frequencies above the onset of the plateau region and at temperatures below the glass transition.[33] At that point, the elastic modulus exhibits the same power-law increase as that of the biofilm while the viscous modulus exhibits a greater rate of increase after passing a

local minimum. Other soft glassy materials with analogous properties include jammed emulsions, colloidal glasses and colloidal gels.[34-36]

However, as compared to previous findings, the moduli from the small-amplitude rheology of *S. epidermidis* are at least an order of magnitude less than previously reported for *S. epidermidis* biofilms.[14, 17-20] A possible origin of this large variability could be the sensitivity of biofilm elasticity to measurement strategies and environmental conditions. For example, measurements conducted under shear deformation instead of tensile deformation can result in properties for gels and pastes that vary by a factor of 50.[37] Moreover, the *in situ* growth protocol could also play a role: By providing a continuous source of nutrients and fluids, as is present in the natural environment of *S. epidermidis*, mechanical properties potentially avoid a regime of extremely high moduli more commonly seen in a dry-growth environment. (Recall that biofilms themselves are ~ 80% water, so properties could be very sensitive to degree of hydration[38]) Additionally, in this work, by removing the need to transport the biofilm, we avoid the risk of altering or compacting it. Such a transport step could lead to a collapse of the microstructure of water channels known to exist in biofilms, and thereby increase the overall concentration of cells and polymer per volume of the biofilm and with it, the modulus. [39, 40]

Creep compliance of *S. epidermidis*

To study the non-linear rheology of the *S. epidermidis* biofilms, the creep compliance of the biofilm was measured as a function of time (Figure 2.5). A number of interesting features of the creep compliance are apparent from this measurement.

First, at low applied stress, there is a region of linear viscoelastic behavior. The compliance displayed a nearly instantaneous step response followed by a plateau region and then

a small, progressive increase in compliance at long times. These observations are consistent with the behavior of a viscoelastic solid with long-term creep.

Second, a transition from solid- to liquid-like behavior is evident in the graph at 15 Pa of applied stress. At the intermediate stress of 15 Pa, there is an upturn after the instantaneous step response, which illustrates a transition from solid-like deformation to viscous-like flow in the material.

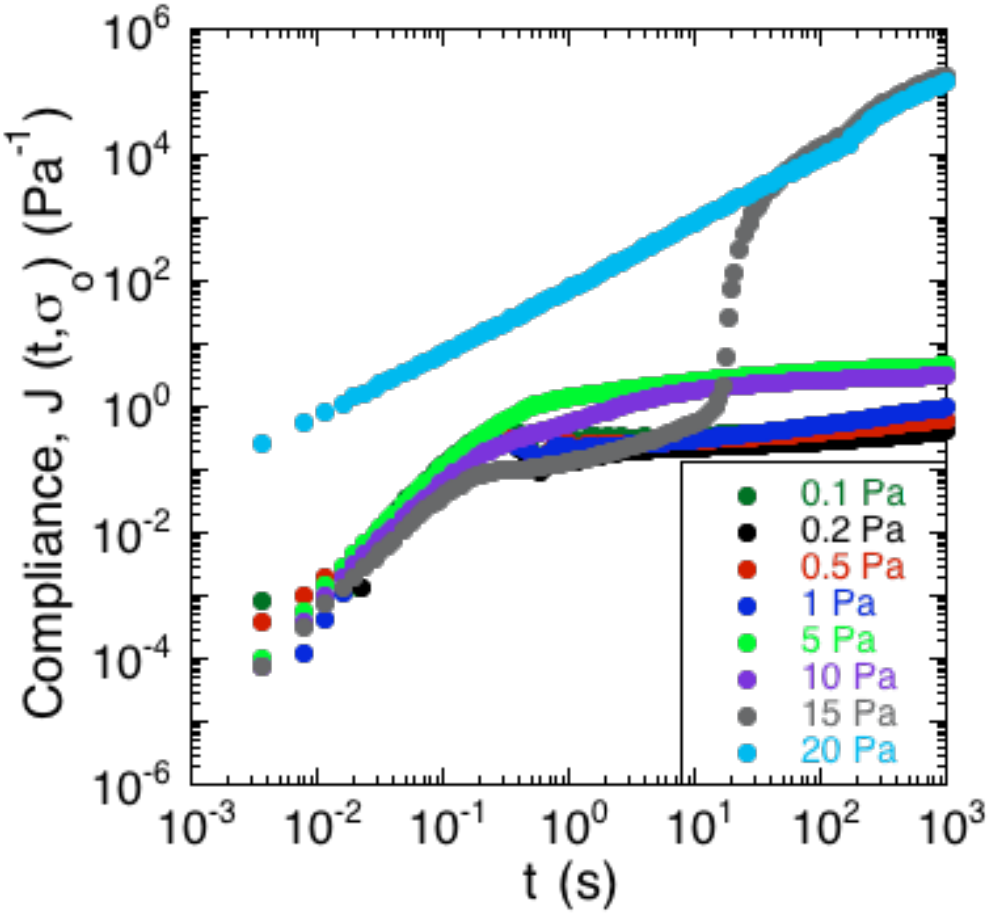

Figure 2.5. Creep of *S. epidermidis* grown in TSB with 86mM NaCl. A constant stress was applied at t = 0 and the material compliance measured over 20 minutes. Data shown from 1 experiment for purposes of clarity. Figure reproduced from Pavlovsky *et al.*[1]

Third, at applied stresses above 15 Pa, the creep compliance increased linearly as a function of time, as is characteristic of a viscous liquid with a viscosity of approximately 8.3 mPa·s.

The behavior in Figure 2.5 is consistent with a soft glassy rheological response for the biofilm, as has been reported for gels, pastes and nanocomposites.[41-43] The solid regime is characterized by a finite compliance being achieved at relatively low applied stresses, followed by very slow creep indicative of a very high viscosity. Upon greater applied stresses, this critical deformation is surpassed and the material flows like a liquid. The transition is consistent with a yield stress for the biofilm.[42] Although this value varies from sample to sample, Figure 2.5 illustrates the characteristic trend that was observed. This generic behavior has previously been reported in gels of polymers and pastes of particle suspensions.[41] The average yield stress of the 3 samples was approximately 20 Pa.

Additionally, we characterized the creep compliance response through modeling. In previous work, Towler *et al.* fit a linear viscoelastic Burgers model for the creep-stress relaxation spectrum of a mixed culture of biofilms.[15] We fit the *S. epidermidis* biofilms with three different viscoelastic solid models to capture the linear behavior of the material prior to yielding: the Burgers model, the Kelvin-Voigt model, and the Jeffreys model.[15, 44-46] In order to capture the short-time behavior and creep ringing seen in our experiments, an inertial term was required for each model. This inertial term represents the inertia of the mobile part of the apparatus, which in our case is the rheometer spindle and the parallel plate geometry.[45] We found that the additional complexity in the Burgers model of a finite jump to compliance was not needed, therefore we only modeled the linear creep data with the Kelvin-Voigt and Jeffreys models. These models and their respective equations can be seen in Table 2.1.

Kelvin-Voigt

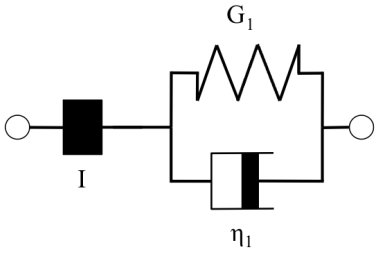

$$J(t,\sigma_o) = \frac{1}{G_1}\left\{1 - e^{-At}\left[\cos(\omega t) + \frac{A}{\omega}\sin(\omega t)\right]\right\}$$

$$A = \frac{\eta_1 b}{2I} \qquad \omega = \sqrt{\frac{G_1 b}{I} - A^2}$$

G_1 = 5.2 Pa $\qquad$ η_1 = 0.095 Pa·s

Jeffreys

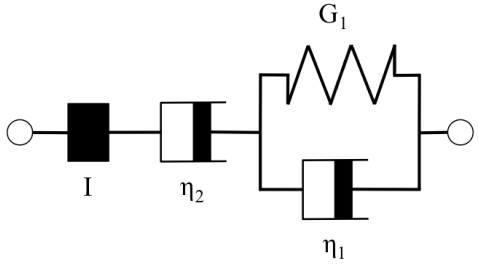

$$J(t,\sigma_o) = \frac{t}{\eta_2} - B + e^{-At}\left\{B\cos(\omega t) + \frac{A}{\omega}\left[B - \frac{1}{\eta_2 A}\right]\sin(\omega t)\right\}$$

$$A = \frac{G_1 + \eta_1\eta_2 b/I}{2(\eta_1 + \eta_2)} \qquad \omega = \sqrt{\frac{G_1 b}{I}\frac{\eta_2}{(\eta_1 + \eta_2)} - A^2} \qquad B = \frac{\eta_1 + \eta_2}{G_1\eta_2}\left(\frac{2AI}{\eta_2 b} - 1\right)$$

G_1 = 4.0 Pa $\qquad$ η_1 = 0.095 Pa·s $\qquad$ η_2 = 3000 Pa·s

Table 2.1. Viscoelastic models and equations. The Kelvin-Voigt and Jeffreys models and their corresponding mathematical equations composed of springs (G_1), dashpots(η_1 and η_2), and inertial terms (I) that were used to capture the linear creep behavior of *S. epidermidis*. The values of the parameters determined to be a good fit by visual inspection are listed. The models were adapted from Baravian and Quemada, and Ewoldt and McKinley.[42, 43] Table adapted from Pavlovsky *et al.*[1]

* $I = I_{instrument} + I_{geometry}$

**b (cone and plate) = $2\pi R^3 / (3\tan\theta)$

***b (parallel plate) = $\pi R^4/(2h)$

Both the Kelvin-Voigt and the Jeffreys models incorporate a short-time viscosity (η_1), an elastic modulus (G_1), and an inertial term (I). The difference between these models lies in the addition of a linear creep viscosity (η_2) in the Jeffreys model. The reported fit parameters (η_1, η_2, and G_1) for both models generate a good agreement between the models and the data, as is apparent by inspection of Figure 2.6. As seen in that Figure, the lack of a linear creep viscosity term in the Kelvin-Voigt model does not allow it to capture the long-time behavior of the material; thus the Jeffreys model is preferred for modeling the linear viscoelasticity of the *S. epidermidis* biofilms.

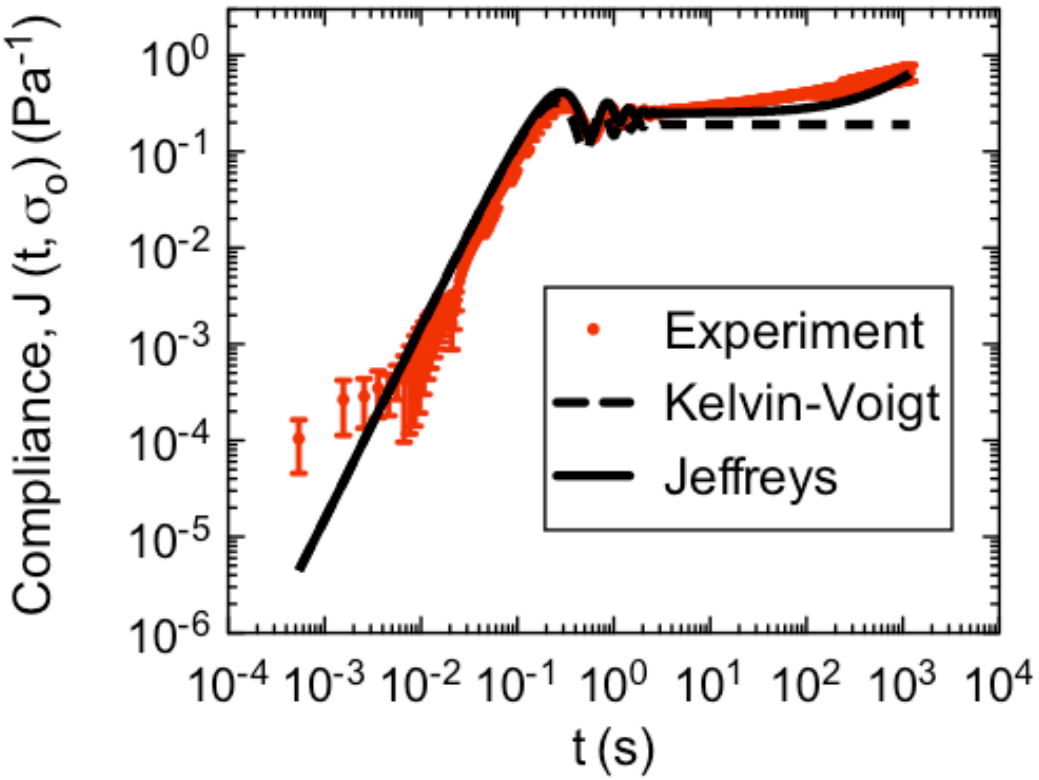

Figure 2.6. Fitting of creep testing results. Linear region of creep of *S. epidermidis* (stress of 0.1 – 1 Pa) fit with Kelvin-Voigt and Jeffreys models. The error bars are standard error of the mean. Figure reproduced from Pavlovsky *et al.*[1]

Thus, the Jeffreys model successfully predicts the creep response of the *S. epidermidis* biofilm in all of previously described regions. In optimizing the Jeffreys model, we noticed that the η_1 term accounts for the magnitude of the creep ringing, the η_2 term dictates the long-term creep viscosity, and the G_1 term is responsible for the overall magnitude of the compliance. The viscous terms were found to be approximately 0.095 Pa·s and 3000 Pa·s for η_1 and η_2, respectively. This is particularly interesting when compared to the viscosity of 8.3 mPa·s after the biofilm yields. The comparison shows how significantly the material is affected by the imposed stress and how viscous the material is at long times. The modulus was found to be approximately 4 Pa. The relaxation times of the biofilm are approximately 750 seconds, and were calculated as follows: $\lambda_1 = (\eta_1 + \eta_2) / G_1$ and $\lambda_2 = \eta_2 / G_1$. This is consistent with the relaxation time spectrum found by Shaw *et al.* (350 - 2600 seconds) for a variety of naturally occurring biofilms.[2] Additionally, our relaxation time was much greater than that found by Hohne *et al*. (13.8 seconds) in compression.[14]

Effects of osmotic stress on the rheological properties

Elevated osmotic pressure of growth media is a known bacterial metabolic stressor that prompts a number of defensive changes by *S. epidermidis,* including increased export of EPS-related polysaccharides.[47, 48] To probe the effects of osmotic stress on biofilm mechanical properties, the biofilms were grown in media of three different NaCl concentrations: 86 mM, 135 mM and 770 mM. By conducting small-amplitude oscillatory rheology, we determined that the concentration of NaCl affects the biofilm material properties. This is summarized in Figure 2.7. The values of the moduli at a frequency of 1 Hz (6.283 rad/s) are displayed in Table 2.2 with the respective standard error of the mean.

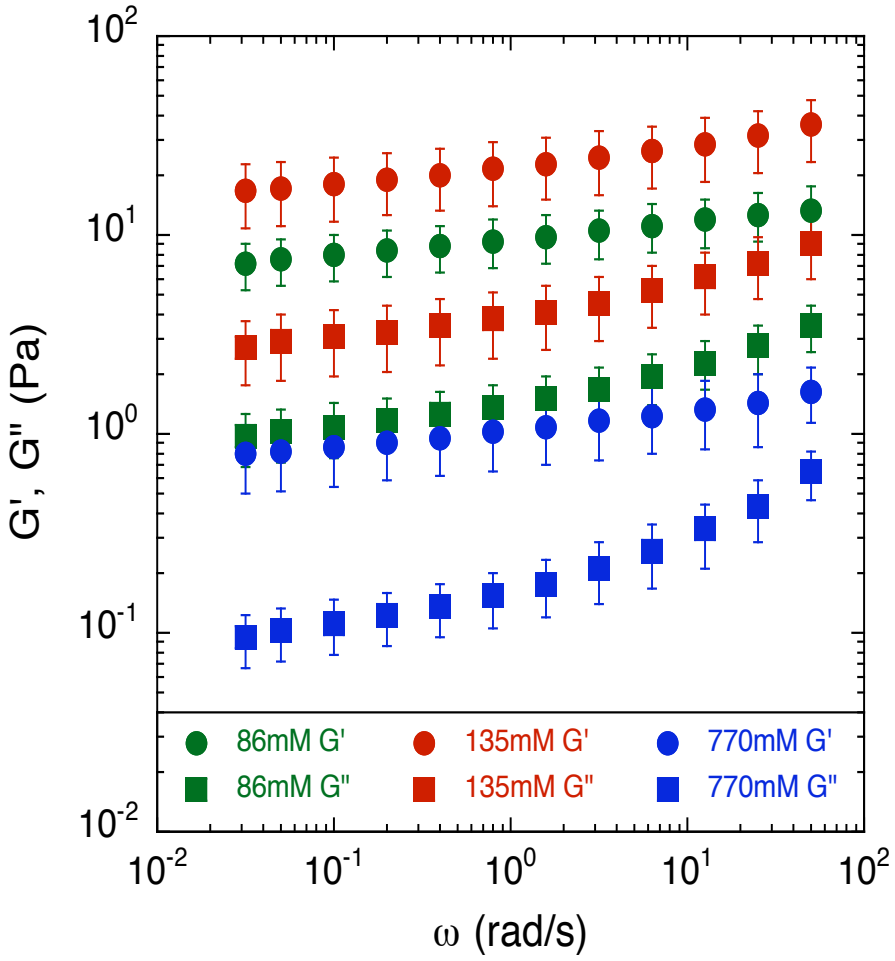

Figure 2.7. Effect of [NaCl] on the elastic and viscous modulus of *S. epidermidis* biofilms. Error bars were plotted as the standard error of the mean, which includes 6 replicates of the physiological condition, 5 replicates of the no-salt-added condition, and 3 replicates of the high salt condition. Figure reproduced from Pavlovsky *et al.*[1]

	86 mM	135 mM	770 mM
G’	11.1 ± 3.0 Pa	26.3 ± 9.1 Pa	1.2 ± 0.5 Pa
G”	1.9 ± 0.5 Pa	5.2 ± 1.8 Pa	0.3 ± 0.1 Pa

Table 2.2. Effect of [NaCl] on moduli of *S. epidermidis* biofilm at 1 Hz. Values extracted from points in Figure 2.7. Table reproduced from Pavlovsky *et al.*[1]

At a frequency of 1Hz, (selected for attention because of its biologically relevance as the fundamental frequency of human circulation) the biofilms grown with 86 mM NaCl had storage and loss moduli of 11.1 Pa and 1.9 Pa, respectively. However, high salt concentrations resulted in biofilms with significantly lower moduli, 1.2 Pa and 0.3 Pa for the elastic and viscous modulus, while human physiological salt conditions (corresponding to 135mM in the figure and table) exhibited the highest moduli, 26.3 Pa and 5.8 Pa for the elastic and viscous modulus, respectively. Hence, there is a non-monotonic relationship between the magnitude of the moduli and the concentration of salt in the media.

We believe this trend can be explained by a combination of effects. The initial increase of moduli from the base condition to the human physiological condition may be due to increased amounts of EPS, as salt is known to up-regulate genes responsible for EPS production.[47, 48] This up-regulation would suggest that with higher salt concentrations, EPS concentrations continue to increase or level off after reaching a maximum rate of production. However, this effect cannot be the only one observed, because the moduli for the highest salt condition are significantly lower than the other conditions. Therefore, we suggest that after a certain concentration of salt is exceeded, an additional effect dominates.[49] One possible effect would be the screening of intermolecular Coulombic interactions that leads to destabilization of the biofilm matrix.[50] For example, sodium cation and chloride anion concentrations can disrupt interactions between the negatively charged *S. epidermidis* cells and the positively charged polymers, potentially causing them to dissociate or otherwise alter their configuration, thereby making the biofilm less elastic.

In order to ensure that our results were statistically significant and showed definitive changes between conditions, we conducted statistical analysis. We used mixed effects linear regression to determine if there was a relation between the values of the moduli to the various

factors including: frequency, NaCl concentration, gap height, and whether measurements were done under tension or compression. The results are summarized in Table 2.3. Consistent with the prior discussion, the analysis suggested strong statistical associations between the modulus and the NaCl concentration (non-monotonic, with the highest values seen at concentrations mimicking human blood). Moreover, the analysis also found a statistically significance correlation of G' and G" with gap height (higher modulus at lower gap height), and deformation history (higher modulus after compression) of the sample. The dependence on gap height and deformation history may be a signature that the biofilm experiences some irreversible change upon compression. Such irreversibility would be consistent with the behavior seen in creep testing, such as the yielding transition. This result would indicate that both the degree of pre-compression of the biofilm, as well as the imposed pre-shear stress should be considered (and reported) when determining the mechanical properties of bacterial biofilms.

Elastic Modulus		
Feature	Fold Change in G'	P value
[NaCl] 135 mM vs 86 mM	2.2 (1.4, 3.4)	0.105
[NaCl] 770 mM vs 86 mM	0.1 (0.1, 0.2)	0.002
Gap 250 μm vs 300 μm	0.9 (0.8, 0.9)	0.036
Tension vs compression	1.2 (1.1, 1.2)	0.023
Viscous Modulus		
Feature	Fold Change in G"	P value
[NaCl] 135 mM vs 86 mM	2.5 (1.6, 3.8)	0.051
[NaCl] 770 mM vs 86 mM	0.1 (0.1, 0.2)	0.002
Gap 250 μm vs 300 μm	0.7 (0.7, 0.7)	$< 10^{-4}$
Tension vs compression	1.0 (1.0, 1.0)	0.102

Table 2.3. Statistical analysis of the effect of [NaCl], gap height, and deformation history on the moduli of *S. epidermidis* biofilm. Table reproduced from Pavlovsky *et al.*[1]
* Estimate (Estimate – SE, Estimate + SE)

Temperature dependence of the rheological properties

To determine the effects of temperature on the linear rheological properties, we conducted small-amplitude oscillatory rheology at temperatures ranging from 5°C to 60°C. Here, temperature was increased and then decreased while the moduli were measured on a frequency range of 0.005-10 Hz. A number of conclusions can be drawn from the temperature dependence of the biofilm rheology.

First, the results show that time-temperature superposition is not valid for this material. The results are not consistent with the validity of time-temperature superposition in this material because the modulus does not display a monotonic dependence on temperature. Thus, measurements at a certain temperature and frequency cannot be uniquely shifted to match measurements at a lower temperature and frequency (data not shown). Consequently, the frequency range of the Figure 2.4 viscoelastic moduli cannot be extended by means of this method.

Second, although time-temperature superposition is not valid, the results do display a very interesting hysteresis of the viscoelastic moduli with temperature. This effect is clearly apparent when plotted in Figure 2.8 for both G' and G". Here, the elastic and viscous moduli were plotted at the constant frequency of 1 Hz and plotted as function of temperature. The biofilm rheology is a strong function of temperature. The moduli reach a local maximum at around 45°C and then drop when the temperature is increased further toward 60°C. More importantly, the modulus does not return to its previous condition upon cooling. This behavior shows that the environment it was previously exposed to affects the biofilm and its mechanical properties. We believe that the hysteresis can be due to the denaturing of linking molecules within the biofilm matrix at higher temperatures, thereby breaking EPS-cell associations or

associations within the EPS itself. Rupture of these associations would act to reduce the modulus of the biofilm. An example of linking molecules would be denaturable proteins. These structures denature at higher temperatures and cannot return to their original shape after being cooled back down. Hence, the modulus would be irreversibly decreased after the biofilm undergoes a heating cycle.

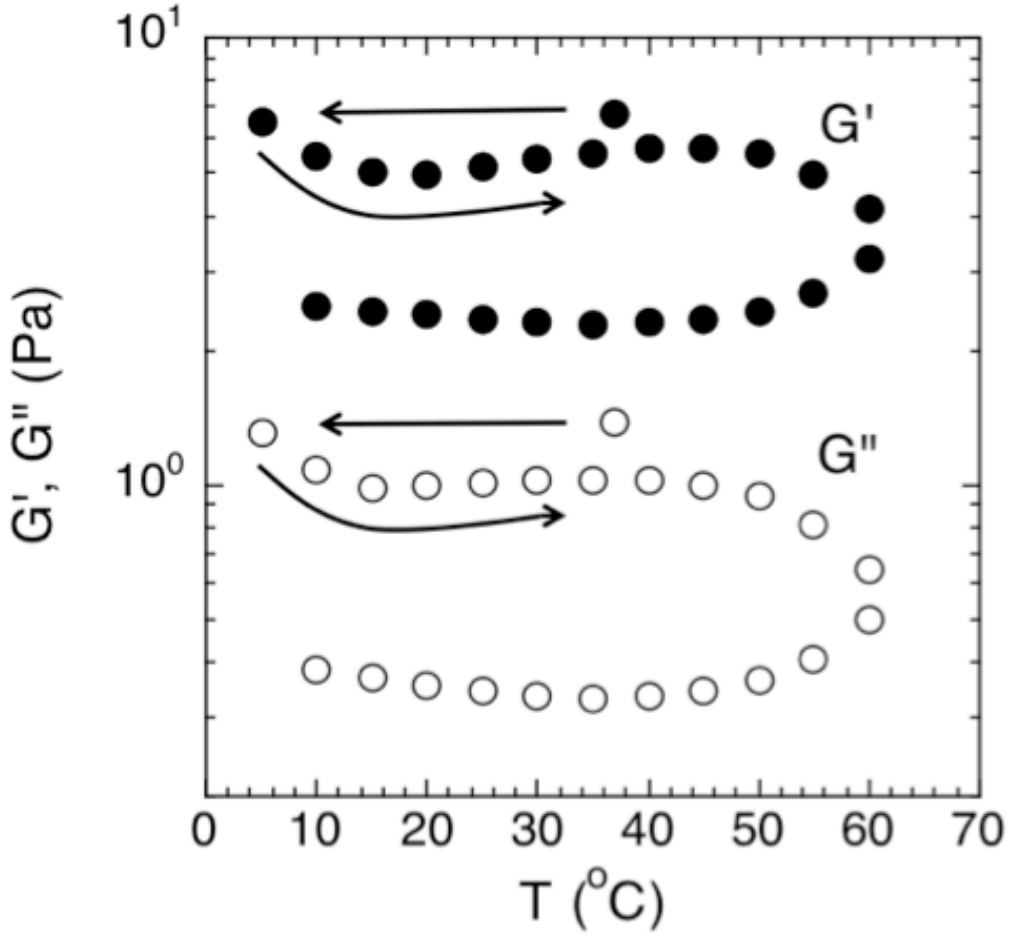

Figure 2.8. Effect of temperature on the elastic and viscous moduli of *S. epidermidis* biofilms at a constant frequency of 1 Hz. Points were extracted from experiments conducted over a frequency range of 0.005-10 Hz. Order of experimentation was 37°C, then 5°C to 60°C increasing at increments of 5, followed by decreasing from 60°C to 10°C in increments of 5. Data shown from 1 experiment for purposes of clarity. Figure reproduced from Pavlovsky *et al.*[1]

Conclusion

We applied a range of rheological methods to interrogate *S. epidermidis* biofilms submerged in media. By adapting the rheometer to house a continuous-flow bioreactor, we eliminated the need to transport the biofilm from the growth environment and gained the ability to perform *in situ* rheology. This allowed us to study small-amplitude oscillatory rheology and creep rheology on materials that were previously inaccessible due to the fact that they had to be deformed or grown in non-physiological conditions. Using this method, we determined that *S. epidermidis* biofilms are soft, viscoelastic solids under linear deformation, but yield and show rheology that is similar to soft glassy materials and pastes upon non-linear deformation. The linear creep compliance was well modeled by the Jeffreys model because it incorporates a creep viscosity at long times. Additionally, we found that the biofilms display a non-monotonic trend upon an increase in osmotic stress and undergo hysteresis under changing temperatures. We believe that the critical temperature responsible for the onset of hysteresis should be examined further, because this hysteresis may reveal features of temperature-dependent physical chemical interactions of the biofilm cells and matrix. The method reported in this paper can be simply adapted to for other species and environmental conditions, thereby allowing *in situ* study that will lead to a more complete characterization of the rheological properties of these complex biomaterials.

Acknowledgments

We thank Ashley Satorius for the biochemical assessments of our bioreactor and Mahesh Ganesan for his advice on modeling. This work was supported by the NSF CDI Program (grant PHYS-0941227), the NIGMS (grant GM-069438), and a University of Michigan Rackham Merit Fellowship (to L.P.).

References

1. L. Pavlovsky, J. G. Younger and M. J. Solomon, *Soft Matter*, 2013, **9**, 122-131.

2. T. Shaw, M. Winston, C. J. Rupp, I. Klapper and P. Stoodley, *Phys. Rev. Lett.*, 2004, **93**, 4.

3. R. M. Donlan and J. W. Costerton, *Clin. Microbiol. Rev.*, 2002, **15**, 167-193.

4. B. Rasmussen, *Nature*, 2000, **405**, 676-679.

5. L. Hall-Stoodley, J. W. Costerton and P. Stoodley, *Nature Reviews Microbiology*, 2004, **2**, 95-108.

6. K. K. Jefferson, *FEMS Microbiol. Lett.*, 2004, **236**, 163-173.

7. J. W. Costerton, P. S. Stewart and E. P. Greenberg, *Science*, 1999, **284**, 1318-1322.

8. H.-C. Flemming and J. Wingender, *Nat Rev Micro*, 2010, **8**, 623-633.

9. K. Cooksey and B. Wigglesworth-Cooksey, *Aquat. Microb. Ecol.*, 1995, **09**, 87-96.

10. W. G. Characklis, *Biotechnol. Bioeng.*, 1981, **23**, 1923-1960.

11. M. Otto, *Nature Reviews Microbiology*, 2009, **7**, 555-567.

12. H. M. Chung, M. M. Cartwright, D. M. Bortz, T. L. Jackson and J. G. Younger, *Shock*, 2008, **30**, 518-526.

13. M. M. Thornton, H. M. Chung-Esaki, C. B. Irvin, D. M. Bortz, M. J. Solomon and J. G. Younger, *J. Infect. Dis.*, 2012, **206**, 588-595.

14. D. N. Hohne, J. G. Younger and M. J. Solomon, *Langmuir*, 2009, **25**, 7743-7751.

15. B. W. Towler, C. J. Rupp, A. B. Cunningham and P. Stoodley, *Biofouling*, 2003, **19**, 279-285.

16. J. N. Wilking, T. E. Angelini, A. Seminara, M. P. Brenner and D. A. Weitz, *MRS Bull.*, 2011, **36**, 385-391.

17. S. Aggarwal, E. H. Poppele and R. M. Hozalski, *Biotechnol. Bioeng.*, 2010, **105**, 924-934.

18. W. L. Jones, M. P. Sutton, L. McKittrick and P. S. Stewart, *Biofouling*, 2011, **27**, 207-215.

19. A. Di Stefano, E. D'Aurizio, O. Trubiani, R. Grande, E. Di Campli, M. Di Giulio, S. Di Bartolomeo, P. Sozio, A. Iannitelli, A. Nostro and L. Cellini, *Microbial Biotechnology*, 2009, **2**, 634-641.

20. S. Aggarwal and R. M. Hozalski, *Langmuir*, 2012, **28**, 2812-2816.

21. S. S. Branda, Å. Vik, L. Friedman and R. Kolter, *Trends Microbiol.*, 2005, **13**, 20-26.

22. R. L. Fournier, *Basic Transport Phenomena in Biomedical Engineering*, Second edn., Taylor & Francis Group, New York, 2007.

23. K. M. Conlon, H. Humphreys and J. P. O'Gara, *J. Bacteriol.*, 2002, **184**, 4400-4408.

24. J. J. Boelens, J. Dankert, J. L. Murk, J. J. Weening, T. van der Poll, K. P. Dingemans, L. Koole, J. D. Laman and S. A. J. Zaat, *J. Infect. Dis.*, 2000, **181**, 1337-1349.

25. S. M. Finegold and E. E. Sweeney, *J. Bacteriol.*, 1961, **81**, 636-641.

26. J. Loscalzo and A. I. Schafer, *Thrombosis and hemorrhage*, Williams & Wilkins, Baltimore, 1998.

27. S. P. Dzul, M. M. Thornton, D. N. Hohne, E. J. Stewart, A. A. Shah, D. M. Bortz, M. J. Solomon and J. G. Younger, *Appl. Environ. Microbiol.*, 2011, **77**, 1777-1782.

28. K. Miller, K. Chinzei, G. Orssengo and P. Bednarz, *J. Biomech.*, 2000, **33**, 1369-1376.

29. W.-C. Yeh, P.-C. Li, Y.-M. Jeng, H.-C. Hsu, P.-L. Kuo, M.-L. Li, P.-M. Yang and P. H. Lee, *Ultrasound Med. Biol.*, 2002, **28**, 467-474.

30. M. J. Paszek, N. Zahir, K. R. Johnson, J. N. Lakins, G. I. Rozenberg, A. Gefen, C. A. Reinhart-King, S. S. Margulies, M. Dembo, D. Boettiger, D. A. Hammer and V. M. Weaver, *Cancer Cell*, 2005, **8**, 241-254.

31. E. Linder-Ganz and A. Gefen, *J. Appl. Physiol.*, 2004, **96**, 2034-2049.

32. L. E. Freed, R. Langer, I. Martin, N. R. Pellis and G. Vunjak-Novakovic, *Proceedings of the National Academy of Sciences*, 1997, **94**, 13885-13890.

33. D. Bonn, P. Coussot, H. T. Huynh, F. Bertrand and G. Debrégeas, *EPL (Europhysics Letters)*, 2002, **59**, 786.

34. T. G. Mason and D. A. Weitz, *Phys. Rev. Lett.*, 1995, **74**, 1250.

35. G. Yin and M. J. Solomon, *J. Rheol.*, 2008, **52**, 785-800.

36. N. Koumakis and G. Petekidis, *Soft Matter*, 2011, **7**, 2456-2470.

37. G. M. Channell and C. F. Zukoski, *AICHE J.*, 1997, **43**, 1700-1708.

38. T. D. Brock and M. T. Madigan, *Biology of Microorganisms*, 6 edn., Prentice Hall, Englewood Cliffs, NJ, 1991.

39. J. W. Costerton, Z. Lewandowski, D. E. Caldwell, D. R. Korber and H. M. Lappin-Scott, *Annu. Rev. Microbiol.*, 1995, **49**, 711-745.

40. P. Stoodley, K. Sauer, D. G. Davies and J. W. Costerton, *Annu. Rev. Microbiol.*, 2002, **56**, 187-209.

41. P. H. T. Uhlherr, J. Guo, C. Tiu, X. M. Zhang, J. Z. Q. Zhou and T. N. Fang, *Journal of Non-Newtonian Fluid Mechanics*, 2005, **125**, 101-119.

42. P. Coussot, *Soft Matter*, 2007, **3**, 528-540.

43. P. Coussot, H. Tabuteau, X. Chateau, L. Tocquer and G. Ovarlez, *J. Rheol.*, 2006, **50**, 975-994.

44. R. H. Ewoldt and G. H. McKinley, *Rheology Bulletin*, 2007, **76**, 4-6, 22-24.

45. C. Baravian and D. Quemada, *Rheol. Acta*, 1998, **37**, 223-233.

46. H. A. Barnes, J. F. Hutton and K. Walters, *An Introduction to Rheology*, Elsevier Science B. V., New York, 1989.

47. S. Rachid, K. Ohlsen, W. Witte, J. Hacker and W. Ziebuhr, *Antimicrob. Agents Chemother.*, 2000, **44**, 3357-3363.

48. Y. Lim, M. Jana, T. T. Luong and C. Y. Lee, *J. Bacteriol.*, 2004, **186**, 722-729.

49. P. C. Hiemenz and R. Rajagopalan, *Principles of Colloid and Surface Chemistry*, Taylor & Francis Group, New York, 1997.

50. H.-C. Flemming, J. Wingender, C. Mayer, V. Körstgens and W. Borchard, eds. D. G. Allison, P. Gilbert, H. M. Lappin-Scott and M. Wilson, Cambridge University Press, Editon edn., 2000, pp. 87-106.

CHAPTER III

Effects of Temperature on the Morphological, Polymeric, and Mechanical Properties of *Staphylococcus epidermidis* Bacterial Biofilms[‡]

Abstract

Changes in temperature were found to affect the morphology, cell viability, and mechanical properties of *Staphylococcus epidermidis* bacterial biofilms. *S. epidermidis* biofilms are commonly associated with hospital-acquired medical device infections. We observed the effect of heat treatment on three physical properties of the biofilms: the bacterial cell morphology and viability, the polymeric properties of the extracellular biofilm substance (EPS), and the rheological properties of the bulk biofilm. After application of a one hour heat treatment at 45°C, cell reproduction had ceased and, at 60°C, cell viability was significantly reduced. Size exclusion chromatography was used to fractionate the extracellular polymeric substance (EPS) based on size. Chemical analysis of each fraction showed that the relative concentration of the polysaccharide, protein, and eDNA components of the EPS was unchanged by the heat treatment at 45°C and 60°C. The results suggest that the EPS molecular constituents are not significantly degraded by the temperature treatment. However, some aggregation on the scale of 100 nm was found by dynamic light scattering at 60°C. Finally, relative to control biofilms maintained at 37°C, we observe an order of magnitude reduction in the biofilm yield stress after 60°C temperature treatment. No such difference was found for treatment at 45°C. From these results,

[‡] Quantitative growth culture was performed by Rachael Sturtevant.

we conclude that yield stress of bacterial biofilms is temperature sensitive and that this sensitivity is correlated with cell viability. The observed significant decrease in yield stress with temperature suggests a means to weaken the mechanical integrity of *S. epidermidis* biofilms with applications in areas such as the treatment of biofilm infected medical devices.

Introduction

Bacterial biofilms are multicellular communities enclosed within a matrix of extracellular polymeric substance (EPS) that can colonize a variety of water-rich environments.[1, 2] These environments range from natural hot springs and riverbeds to man-made industrial pipelines and medical devices. In these and other environments, flowing fluids impose shear stresses on the biofilms.[1-4] The EPS, composed of polysaccharides, proteins, and DNA, is synthesized by the bacterial cells. The EPS has multiple attributes and functions, one of which is to enable the biofilm to withstand applied shear forces.[5] Another is to slow the diffusion of antimicrobial agents, allowing the bacteria to genetically build resistance.[6-9]

One such biofilm-forming bacterium of medical significance is *Staphylococcus epidermidis*. *S. epidermidis* is a normal member of the human skin flora. However, this organism is prevalent in medical device infections. *S. epidermidis* is among the most common hospital acquired bloodstream infections in the United States. The species is present in approximately 70% of all catheter-related infections.[10, 11] Current antibiotic treatments to eradicate biofilms are not fully effective, because antibiotics are not able to penetrate the EPS to sessile and slow-metabolizing bacteria deep within it.[6, 8, 12-16] Hence, infections often prompt the surgical removal and subsequent replacement of affected devices.[6, 17, 18] Immune-compromised patients, who have a higher risk associated with surgery, exhibit especially high mortality rates (greater than 30%)

from *S. epidermidis* infections.[19] In order to avoid replacement of infected medical devices, the physical and mechanical properties of the biofilms should therefore be interrogated.

Previous work has determined mechanical properties of *S. epidermidis* biofilms. The elastic moduli (G') of these biofilms, found through mechanical rheometry, varies widely, from 1 Pa to 8 kPa, depending on factors such as growth conditions and analytical methods.[20-27] In conditions that most resemble the aqueous environment in which *S. epidermidis* biofilms are endemic, Pavlovsky *et al*. determined that G' is approximately 10 Pa. In the same study a yield stress of approximately 20 Pa was reported for these biofilms.[28] Size exclusion chromatography characterization of the polysaccharide constituent of the *S. epidermidis* EPS, called polysaccharide intercellular adhesion, found a weight average molar mass of $2.01 \times 10^5 \pm 1200$ g/mol. The radius of gyration of the polysaccharide was 29.2 ± 1.2 nm.[29]

Structure and mechanical properties of *S. epidermidis* biofilms depend on environmental conditions. Stewart *et al.* showed, via confocal laser scanning microscopy (CLSM), that *S. epidermidis* biofilms adopt different density phenotypes depending on the concentration of NaCl of the growth media.[30] NaCl concentration and temperature impact the elastic modulus of these biofilms in an analogous way.[28] Moreover, a temperature cycle from 5°C to 60°C was found to decrease the elastic modulus of these biofilms by a factor of three.[28]

This reported effect of temperature on the mechanical properties of biofilms is of particular interest because of its therapeutic potential. Specifically, in seeking to avoid surgical replacement of implantable devices, altering the elasticity and yield stress of a biofilm might allow for its mechanical removal from the infection site without requiring device replacement. Because temperature can be varied within the body non-invasively, this variable's effect on biofilms physical properties should be more comprehensively investigated. Such temperature

modulation, for example, has proven effective as an adjuvant therapy for cancer.[31, 32] Hence, in this paper, we investigate the effect of temperature treatment on cell viability and morphology, as well as the polymeric and mechanical properties of *S. epidermidis* bacterial biofilms. We hypothesize that, by exposing the biofilm to a temperature treatment, we can alter the biofilm morphology, the properties of its EPS, and the mechanical properties of the biofilm. By comparing results for these three different classes of physical properties, conclusions as to the correlation between cell morphology, EPS polymeric properties, and biofilm mechanical properties can be made.

To study the morphology and viability of bacterial cells, we use two forms of microscopy: scanning electron microscopy and confocal laser scanning microscopy. With scanning electron microscopy, we observe the size and surface characteristics of individual bacterial cells. Via confocal microscopy, we distinguish viable and dead cells by differential staining with fluorescent dyes.[33] We determine the weight average molecular weight and the hydrodynamic radius of components in the EPS using size exclusion chromatography and dynamic light scattering, respectively. Finally, we use parallel plate rheometry to study the temperature dependence of the rheological properties of the biofilm *in situ*. The rheological properties studied are the yield stress and the elastic modulus.

Methods and Materials

Rheometry

Biofilm growth and heat treatment

A biofilm-forming clinical isolate of *S. epidermidis*, strain RP62A, was obtained from the American Type Culture Collection (culture 35984). The bacteria were incubated at 37°C on

tryptic soy agar (TSA) overnight. An individual colony forming unit was used to inoculate approximately 30 mL of tryptic soy broth (TSB) media supplemented with 1% D-(+)-glucose. This culture was grown overnight on a shaker table (Innova 2000 Platform Shaker, New Brunswick Scientific) at 200 RPM and 37°C. The next day, 2 mL of the culture was used to inoculate glucose-supplemented TSB on a mechanical stress-controlled rheometer (AR-G2, TA Instruments), with the Peltier plate maintained at 37°C, as per the procedure described by Pavlovsky *et al*.[28] Briefly, at these conditions, the shear stress for growth was 0.1 Pa and the media flow rate was approximately 0.5 mL/min.

After the growth phase, the temperature in the Peltier plate was immediately changed to a higher temperature to thermally stress the biofilm. The temperatures used were 37°C, 45°C, and 60°C, which correspond to the control, the maximum temperature safely applicable in the human body, and the high temperature case in which an irreversible decrease of biofilm elastic modulus was previously observed, respectively.[28, 34] The biofilm was exposed to these temperatures for an hour, a common duration used in hyperthermic cancer treatment, during which time the rheometer fixture was held stationary.[31, 32]

Rheological characterization of the yield stress

Directly following the hour treatment, an oscillatory strain sweep was conducted to determine the elastic modulus (G') and yield stress of the biofilm. The strain sweep was performed at a constant oscillatory frequency of 1 Hz (6.283 rad/s) over the range of 0.01 – 100 dimensionless strain units. This oscillatory frequency was selected because it approximates the fundamental frequency for the human circulatory system.[35] The elastic component of the stress, $\tau_{Elastic}$, equal to G' × strain, was plotted. The point at which $\tau_{Elastic}$ is a maximum is a well known measure of the yield stress and strain.[36]

Cell morphology and viability

Confocal laser scanning microscopy

In order to investigate cell viability after temperature treatment, we used confocal laser scanning microscopy (CLSM). Directly following the oscillatory strain sweep on the rheometer, biofilm samples were removed from the Peltier plate and deposited on a glass slide. The biofilm was then stained using a fluorescent staining kit (LIVE/DEAD *Bac*Light Bacterial Viability Kit, Molecular Probes) with the dye ratios of SYTO 9 to propidium iodide to filter-sterilized deionized water of 3 μL:3 μL:1ml.[24, 33, 37] This mixture has a SYTO 9 to propidium iodide ratio of 1:6 by concentration, with approximately 3 μL of each dye pre-mixed required per mL of bacteria to be stained. After applying the appropriate amount of the diluted dye mixture, the sample was incubated at room temperature for 20 minutes, away from light. After incubation, the dye was gently rinsed with filter-sterilized deionized water covered with a cover glass.

The sample was imaged (A1RSi Confocal Laser Scanning Microscope, Nikon) using two-channel imaging with laser wavelengths of 488 nm and 561 nm, consistent with the excitation spectra of the live and dead bacterial cell dyes, respectively. These channels used FITC and Texas Red filters to capture the emission spectra for the live and dead cell dyes of 525 nm and 595 nm, respectively. The image size was 31.7 × 31.7 × 10.0 μm^3, where the voxel size was 0.062 × 0.062 × 0.062 μm^3. Image analysis was performed using custom codes that make use of the Crocker and Grier algorithm to determine the ratios of live to dead cells in a given sample.[37, 38]

Scanning electron microscopy

Scanning electron microscopy (SEM) was conducted to observe the morphology of the biofilms after heat treatment. Following the oscillatory strain sweep on the rheometer, biofilm

samples were removed from the Peltier plate, deposited on a glass cover slip, and submerged in 4% glutaraldehyde (Electron Microscope Systems) in order to fix the cells and prevent further growth.[12, 39] After a minimum of 1 hour, the sample was the washed and serially dehydrated in increasing concentrations of ethanol, from 50% to 100%. The biofilm sample was then mounted on an SEM stub, sputter-coated with gold, and imaged (AMRAY 1910 Field Emission Scanning Electron Microscope, Amray Inc).

Quantitative growth culture

S. epidermidis colony forming units were isolated overnight on TSA plates. An individual colony was then used to inoculate 5 mL cultures of glucose-supplemented TSB. The cultures were grown for approximately 4 hours at 37°C until they exhibited mid-log growth, as determined through UV/Vis spectrophotometry (Ultrospec 2100 Pro, GE Healthcare). Then, the cultures were washed by the addition of 15-20 mL of 0.9% by weight NaCl in water. Centrifugation (Alegra X-14R Centrifuge, Beckman Coulter) was then conducted at 2000 RPM for 5 minutes. The supernatant was discarded and the pellet resuspended in fresh 0.9% NaCl solution to a final $OD_{600\ nm}$ of 0.1. After washing, 10 μL of culture was added to 1 mL TSB. Samples were incubated in a dry bath incubator (Isotemp 125D, Fisher Scientific) at the desired temperature (37°C, 45°C, or 60°C) for one hour and then quantitatively cultured.

The quantitative culture included three 10-fold serial dilutions of 10 μL each prepared sample using TSB. The dilutions (1:10, 1:100, and 1:1000) as well as an undiluted culture were plated on TSA plates and incubated overnight. Colonies were counted at the dilution that produced in the range of 50-100 colonies, when possible. The density of colony forming units was calculated using the following formula: (count × dilution factor) / 0.01 mL.

Polymer properties

EPS purification

After incubating *S. epidermidis* on TSA overnight, an individual colony was isolated and used to inoculate 50 mL of TSB + 1% glucose media in a 50 mL conical tube. This culture was grown for approximately 15 hours on a shaker table at 60 RPM and 37°C. The sample was then scraped from the tube, taking care to extract all of the biofilm, and placed in 1 L of TSB + 1% glucose media for 24 hours of growth at 60 RPM and 37°C. After this step, a series of washing and centrifugal concentrating steps (3900 g, 3 × 25 min, 4°C) were followed as described by Ganesan *et al*.[29] The remaining pellet was then resuspended in 20 mL deionized water, on which sonication was performed (8 × 30 s cycles, 60% amplitude) using a point sonicator (Model 120 Sonic Dismembrator, Fisher Scientific) to release the polymers from the bacterial cells.[29] Centrifugation (9000 g, 30 min, 12°C) was performed to separate the polymers (supernatant) from the cells (pellet), after which the supernatant was further clarified (12000 g, 10 min). The clarified polymer was then filter sterilized and concentrated using centrifugal filters with a 10kDa cut-off membrane (Amicon Ultra-15, Millipore). Temperature treatment was applied using a dry bath for one hour.

Size exclusion chromatography

Size exclusion chromatography (SEC) was conducted using multiple columns in series (Waters Utlrahydrogel 2000 and 250, Waters Corp.). Approximately 100 μL of sample was injected (Rheodyne) into an aqueous mobile phase of 0.1 M $NaNO_3$ and 0.05% (w/w) NaN_3, flowing at a rate of 0.45 mL/min. The outlet of the column was connected to a multi-angle laser light scattering unit (MALLS; DAWN EOS, Wyatt Technology) and a concentration detector (RI; Optilab DSP Interferometric Refractometer, Wyatt Technology). The chemical complexity

of the sample did not allow for the the angle dependent scattering intensity in be resolved as a distribution of molecular weight (Mw) and z-average radius of gyration (R_g).[40, 41] However, the SEC experiments do yield the mass concentration of the polymers present in each fraction eluting from the column. Chemical analysis of each fraction yielded information about any change in the relative concentration of its constituents.

Chemical analysis

In order to determine if the mass concentration of polysaccharide, protein, or extracellular DNA components of each fraction eluting from the SEC was changing due to the heat treatment, samples that had been fractionated by SEC were collected and three chemical assays were conducted. The Smith-Gilkerson assay was used to determine the presence of N-acetyl-glucosamine, a major component of the polysaccharide intercellular adhesion of the biofilm.[29, 42] Similarly, a bicinchoninic acid assay (BCA) was used to determine the concentration of protein, and a microvolume spectrophotometric assay (Thermo Scientific NanoDrop 2000 Spectrophotometer) was used to determine the concentrations of nucleic acid as well as protein.[43-45]

Dynamic light scattering

Dynamic light scattering (DLS) was performed on the specimens following heat treatment to measure the distribution of hydrodynamic radii (R_h) of species present (ALV CGS-3 Compact Goniometer System). The samples were diluted, if necessary, to a total volume of approximately 0.8 mL. A helium-neon laser source (JDS Uniphase Corporation) with a wavelength $\lambda = 633$ nm was used, with the DLS detectors at a fixed angle $\theta = 90°$. Experiments were conducted in triplicate, recording the time-dependent intensity of the scattered light for 4-minute intervals after the treated biofilms had returned to room. The fluctuations of the scattering

intensity due to particle motion are processed with an ALV multiple–tau digital correlator (ALV–7004), giving an intensity autocorrelation function. The correlation of scattered light is then fit using a non-linear fitting method (constrained regularization) to obtain the DLS relaxation rate which is proportional to the scattering vector $q = 4\pi n_0 / \lambda \sin(\theta/2)$, where n_0 is the solvent refractive index) via the particle diffusivity, D.[46, 47] Using the Stokes-Einstein relation ($D = k_B T / 6\pi\eta R_h$, where k_B is Boltzmann's constant, T is temperature, and η is the viscosity) the probability distribution of effective hydrodynamic radii of the scattering specimen is then obtained.[48] Here, the refractive index and viscosity is that of water at the temperature of the measurement. The output of the measurement is the distribution function of the hydrodynamic radius of the specimen.

Results and Discussion

Morphology and viability of bacterial cells

Figures 3.1a-c report scanning electron micrographs of the bacterial cells following temperature treatment for one hour at 37°C, 45°C, and 60°C, respectively. Differences in the degree of cell reproduction and features of the cells' exterior morphology were apparent. In the untreated case, the normally spherical *Staphylococci* contained a large portion of cells that appeared ellipsoidal, as seen in Figure 3.1a. Upon further investigation, we see that there is a plane between the two halves of the ellipsoid. This is a dividing plane, indicating that those bacteria were in the process of growth and reproduction.[49] Figure 3.1a, the 37°C control case, is indicative of a healthy biofilm, as expected for the natural growth temperature of this strain.

As temperature is increased to 45°C, as shown in Figure 3.1b, significantly fewer dividing cell pairs are apparent. This decrease indicates that conditions at this temperature are

unfavorable for *S. epidermidis* reproduction. Additionally, the exterior morphology of many cells appears dimpled. We believe that these cells are in the process of cell lysis.

For the 60°C treatment, shown in Figure 3.1c, we observe that there are no longer dividing pairs present. Cells that have persisted are coated in a dense layer of material. We believe this residue to be remnants of cells that have lysed due to the temperature treatment.

To corroborate the SEM observations of temperature effects on cell morphology, Figures 3.1d-f show CLSM imaging of the biofilms at the same three conditions. In this case, live-dead staining directly yields information about cell viability. Imaging was accomplished using two different fluorescent nucleic acid stains: SYTO 9, which penetrates both intact (i.e., live, green) and damaged (i.e., dead, red) cell membranes, and propidium iodide, which can only penetrate damaged cell membranes and displaces any present SYTO 9. By comparing Figure 3.1d and Figure 3.1e, we cannot distinguish a difference in the proportions of live to dead cells at these two lower treatment temperatures. However, at 60°C, the majority of the cells (> 70%) are dead. The complete SEM and CLSM results are summarized in Table 3.1.

Figure 3.1g confirms this trend. Here, quantitative growth culture was performed via serial dilutions of treated biofilms and the colony-forming units (CFU) were counted. The 37°C and 45°C treatments had almost identical amounts of CFU: 4.31 ± 1.58 ($\times 10^5$) CFU and 4.28 ± 1.63 ($\times 10^5$) CFU, respectively. However, there was greater than a 100-fold decrease in the number of colonies present after a 60°C treatment: 1.43 ± 0.43 ($\times 10^3$) CFU.

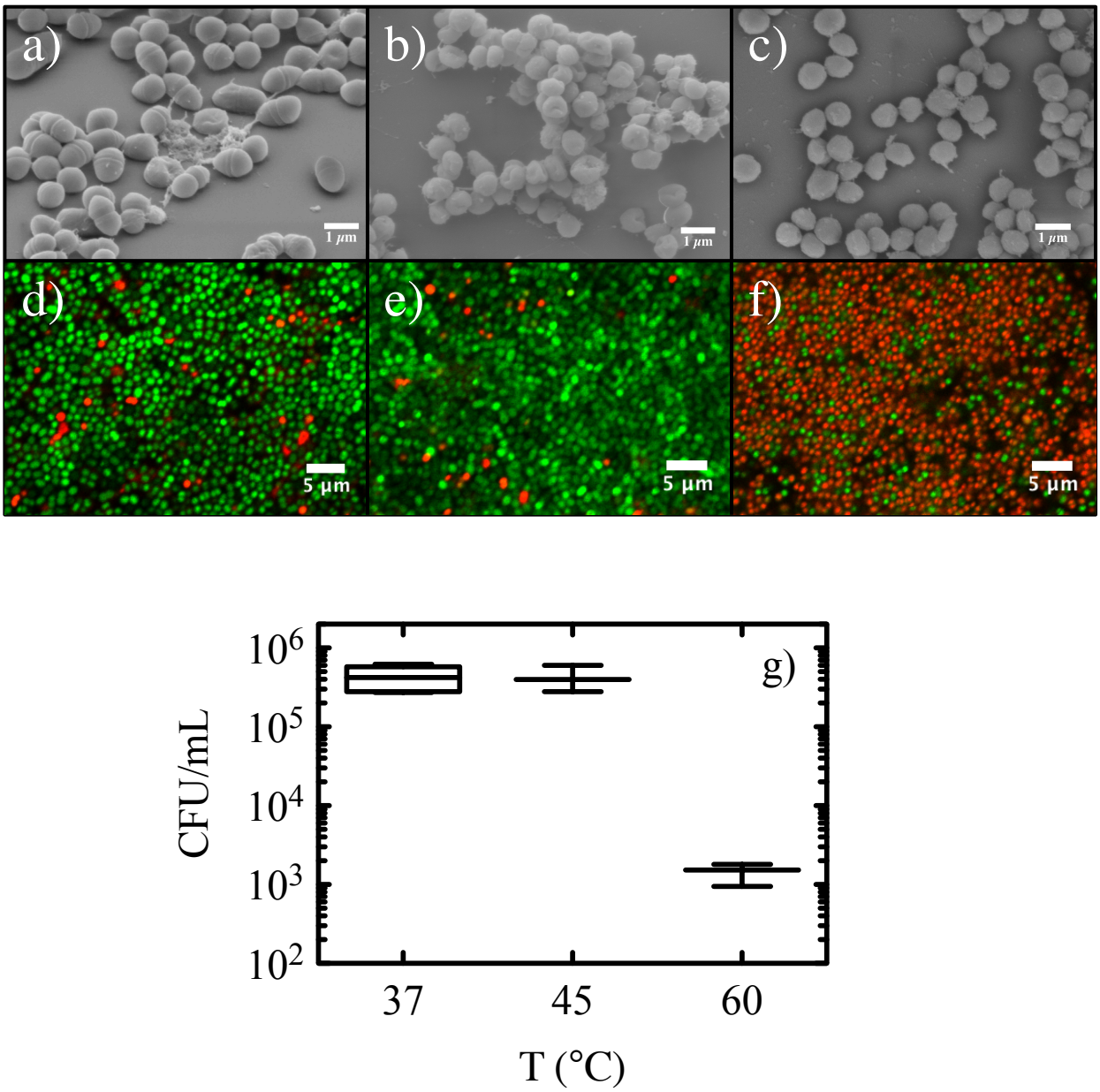

Figure 3.1. Morphology and viability of *Staphylococcus epidermidis* bacterial cells after temperature treatment. Scanning electron microscopy micrographs show the external contours of individual cells after treatments of a) 37°C, b) 45°C, and c) 60°C. Confocal laser scanning microscopy shows the ratio of live (green) to dead (red) cells after treatments of d) 37°C, e) 45°C, and f) 60°C. g) Quantitative growth cultures show the density of colony-forming units present, per mL of media following the three different temperature treatments. Each sample was tested in triplicate and error bars represent the standard error of the mean.

Temperature (°C)	% Single Cells (SEM)	% Dividing Pairs (SEM)	% Dead Cells (CLSM)
37	42.7 ± 2.3	57.3 ± 2.3	11.0 ± 3.5
45	97.2 ± 0.3	2.8 ± 0.3	10.4 ± 1.1
60	100 ± 0.0	0.0 ± 0.0	73.0 ± 3.4

Table 3.1. Reproductive health and viability of bacterial cells found via SEM and CLSM. The percent single cells and dividing pairs are from three SEM images per temperature treatment and represent the cells with and without a dividing plane, respectively. The percentage of dead cells from the total cells present was determined using CLSM from three 3-dimensional volumes of biofilm per sample condition. Each result is displayed with the standard error of the mean.

Polymeric properties of EPS

In Figure 3.2, we report the results of the refractive index (RI) detector of the size exclusion chromatography (SEC) of EPS produced by *S. epidermidis* biofilms. The RI detector signal is proportional to the mass of solute eluting from the SEC. Following EPS purification (c.f. Methods), SEC was conducted on the heat-treated EPS samples. In SEC, the elution time is inversely proportional to the size and molecular weight of the sample; smaller species have longer elution times. The signal in this case is proportional to the solute concentration passing through the SEC. The concentration profile of material eluting from the SEC does not vary for the different temperature treatments. Hence, the mass fraction of different sized species in the EPS is nearly independent of temperature. Any changes in mass fraction are smaller than can be detected by the RI instruments of the SEC system.

Four peaks in the RI signal with elution volume are apparent in Figure 3.2. These peaks reflect the chemical heterogeneity of the EPS. Chemical analysis of these elution fractions, as

discussed subsequently, suggest that from the left to right, the first two peaks are N-acetyle-glucosamine, while the third and fourth peaks contain both nucleic acid and proteins.

Figure 3.3a-c shows the SEC elution times of the three major chemical species of the biofilm. Fractions from the SEC were collected and assayed for presence of N-acetyl-glucosamine (a), nucleic acid (b), and proteins (c) as a function of elution time from the SEC and the particular temperature treatment. The protein results are the average of two different methods, so as to address the known deficiency of such assays; the difference between the assays was at most approximately 97% from the average.[50] From these chemical assays, we learn that the mass distribution of polysaccharide, protein, and DNA in each SEC elution fraction does not change appreciably because of the temperature treatment. This finding corroborates the results of the SEC RI detector. We therefore conclude that temperature does not play a role in the elution time of these species to a degree that is resolvable by these mass detection assays. The absence of changes in elution time suggest that none of the three molecular species analyzed for – polysaccharide, protein, and eDNA – are undergoing significant degradation due to the temperature treatment. If degradation of one of these species had occurred, we would have expected that its mass fraction would have shifted to later times, because the degraded species, now of lower molar mass, would have eluted from the SEC column more rapidly.

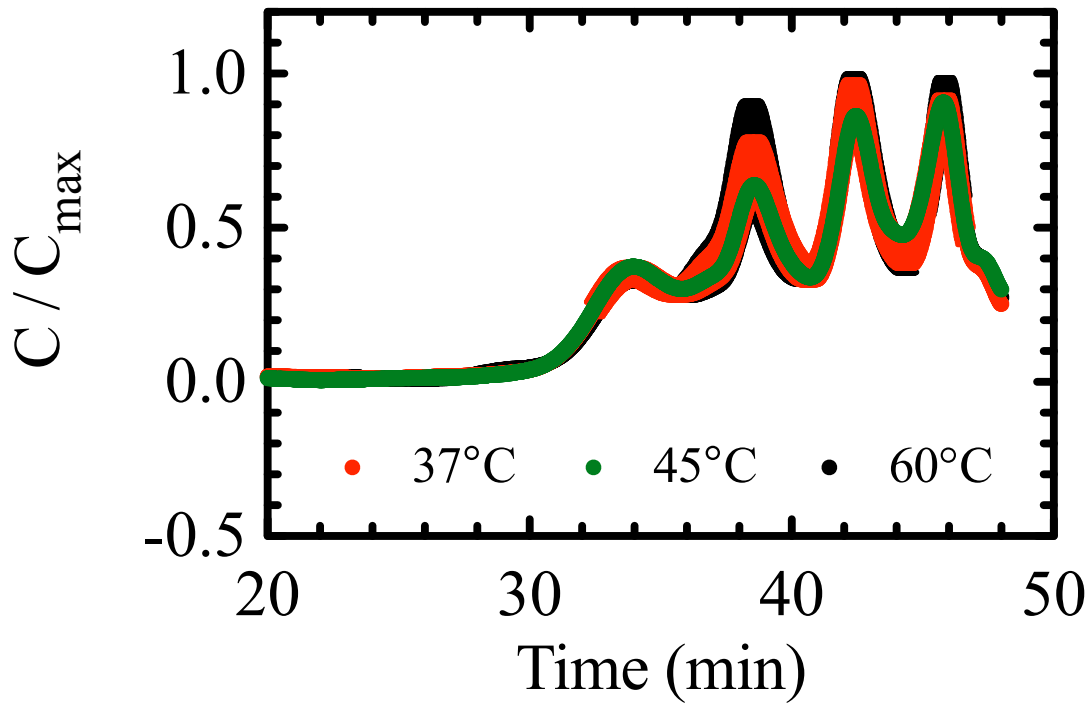

Figure 3.2. Size exclusion chromatography of EPS as a function of temperature. The concentration detector curves for the SEC samples. Each temperature treatment was tested in triplicate, while the 37°C control case consisted of six replicates. The results were normalized for each sample. Error bars represent the standard error of the mean.

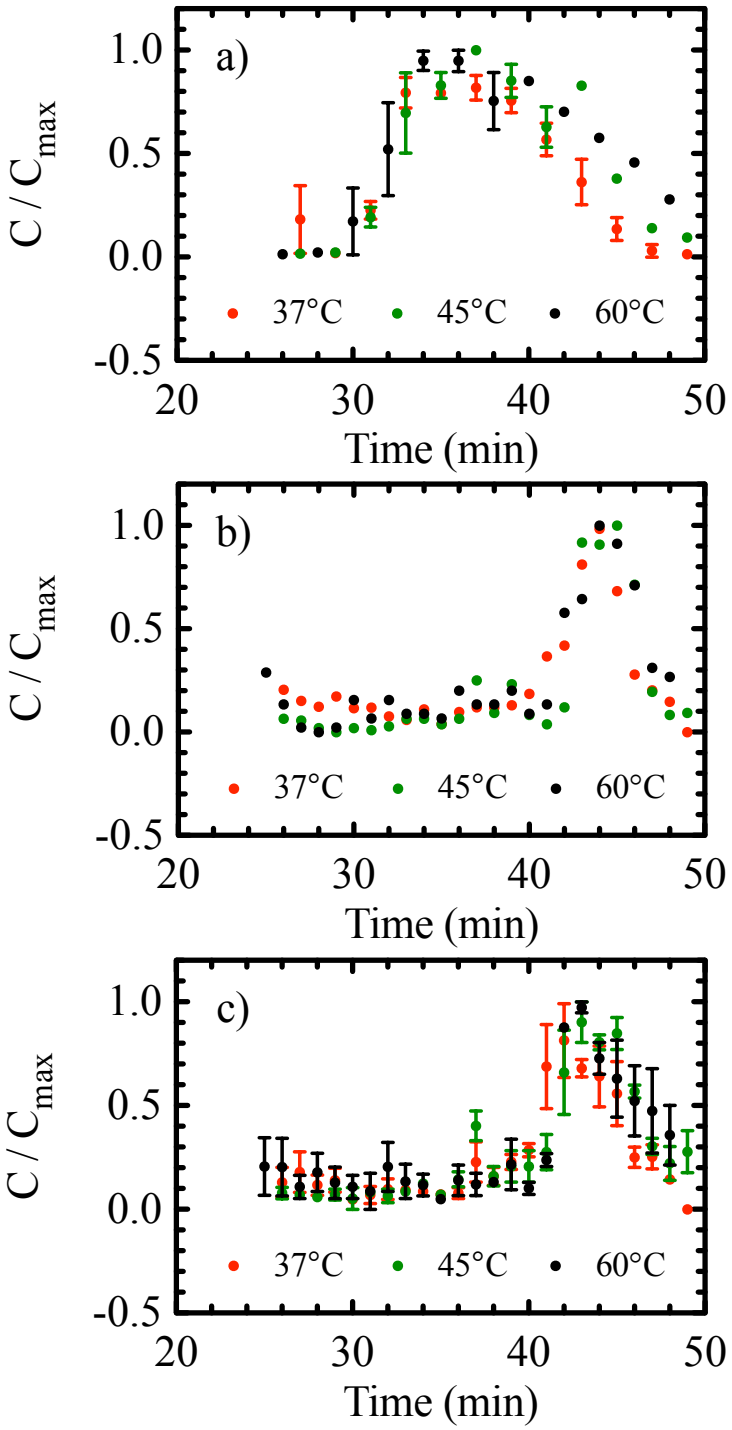

Figure 3.3. The chemical composition of EPS as a function of temperature. The presence of a) N-acetyl-glucosamine, b) nucleic acid, and c) protein in the SEC effluent fractions are shown as a function of temperature, determined by various chemical assays. N-acetyl-glucosamine assays were conducted in triplicate, while the remaining assays were single experiments. The protein is shown as an average concentration of two different assay techniques. The points were normalized for each sample. Error bars represent the standard error of the mean.

Figure 3.4 shows the probability distribution function (PDF) of the hydrodynamic radius of species detected in the purified EPS samples, as quantified by DLS. Without heat treatment (i.e. the 37°C case), a broad distribution of hydrodynamic radii is detected in the EPS, spanning from smaller than 10 nm to greater than 100 nm. A similar trend exists for the 45°C case, with the additional effects of a slight narrowing of the distribution and a shift toward large hydrodynamic radii. For the 60°C case, the hydrodynamic radii has not narrowed considerably, with a pronounced peak at size ~ 100 nm.

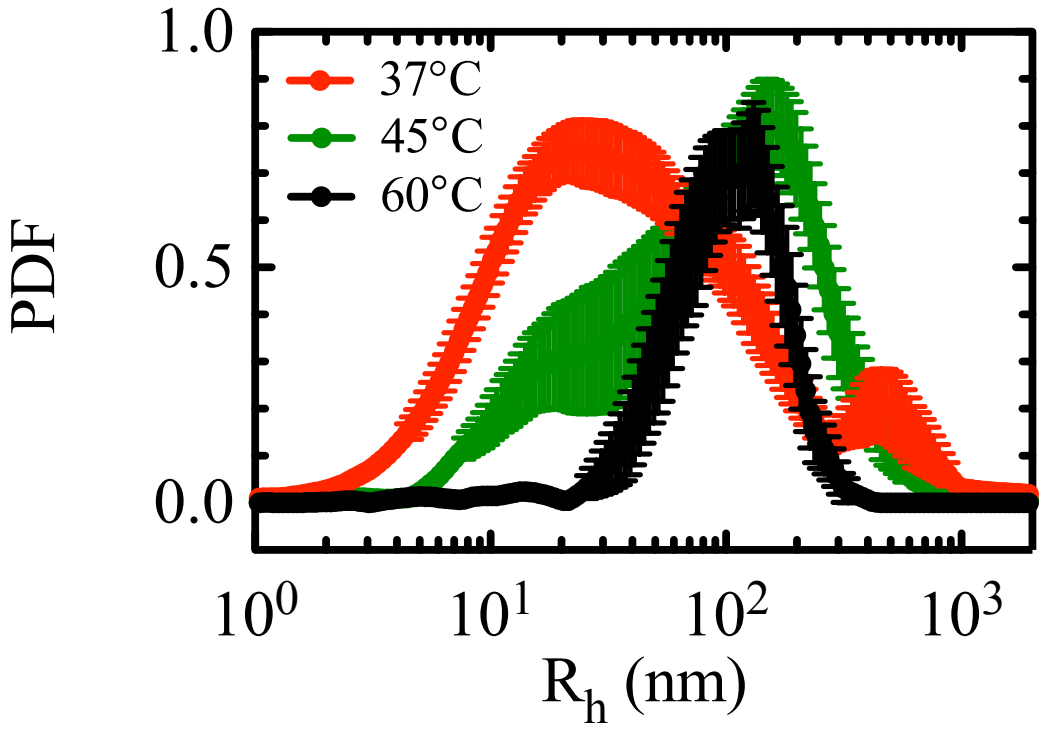

Figure 3.4. The probability distribution of the hydrodynamic radius of the polymers in EPS as a function of temperature, determined via dynamic light scattering. Each temperature treatment was tested in triplicate, while the 37°C control case consisted of six replicates. Results were normalized for each sample. Error bars represent the standard error of the mean.

The 100 nm length scale that is the dominant peak detected by DLS at 60°C is both larger than the expected size of the molecular species (e.g. PIA ~ 30 nm in size[29]) and smaller than the size of individual cells (e.g. *S. epidermidis* radius is ~ 500 nm[29, 51]). A number of potential explanations for the prominent characteristic size of 100 nm in the 60°C sample are available; however, we do not have sufficient information available to select among them. The potential explanations are: (i) aggregation; (ii) cellular debris. Aggregation of the smaller components of the biofilm may be occurring as the presence of materials with R_h < 30 nm disappear following the 60°C treatment. Also, the absence of particles with R_h > 300 nm, which are prevalent in the lower temperature cases, may indicate cell lysis, as was shown via SEM in Figure 3.1. In this case, the cellular debris would be smaller than the radius of the cell and may account for increased presence of particles with R_h ~ 100 nm

Yield stress of *S. epidermidis* biofilms

Figure 3.5 reports the measurement used to determine the yield stress of the *S. epidermidis* biofilms as a function of treatment temperature. An oscillatory strain sweep was conducted to measure the strain dependent, nonlinear elastic modulus. Figure 3.5a shows the elastic component of the stress ($\tau_{Elastic}$ = G' × strain) plotted as a function of applied strain amplitude for the three different temperature conditions. Previous work has found that the stress maximum is a measure of the yield stress.[36] By this method, the yield stress was found to be 23.3 ± 4.4 Pa for our control case of 37°C. This value agrees with the yield stress found in earlier study by a different method – non-linear biofilm creep compliance testing. The value found in that study was 18.3 ± 6.0 Pa, a difference of 27%, thereby validating the method used in the present study.[28]

The biofilm treated at 45°C exhibited a yield stress of 19.2 ± 6.2 Pa. This yield stress is not statistically different than the control case of T = 37°C ($p = 0.60$). However, the yield stress of the biofilm treated at 60°C was significantly lower than the control case: 3.9 ± 1.0 Pa ($p = 0.006$). This same trend is apparent in the measurements of the small strain (linear) G'. The linear elastic modulus and yield stress results are summarized in Fig. 3.5b and 3.5c, respectively. Thus, following a 60°C temperature treatment, the *S. epidermidis* biofilm yield occurs at a stress that is an order of magnitude smaller than in the untreated, control case. The integrity of the biofilm is therefore significantly weakened by temperature treatment.

Lastly, we consider how the individual biofilm components, as quantified in Figures 3.1 – 3.4, might be correlated with the observed changes in mechanical properties. First, the morphology measurements indicate that cell reproduction stops by 45°C and cell death has occurred by 60°C. Second, there is little change in the mass distribution of EPS constituents as a consequence of the different temperature treatments, with the exception of the appearance of a component of size 100 nm after temperature treatment at 60°C.

Thus, cellular death and the production of an EPS species of size 100 nm, are correlated with the observed decrease in biofilm yield stress at 60°C. Furthermore, we conclude that the halt of cell replication at 45°C is not associated with a change in yield stress, because the 45°C treated yield stress was not significantly different than the control case. Finally, the yield stress of a mature biofilm can change without being accompanied by significant degradation of the polysaccharide, protein, and DNA components of the EPS.

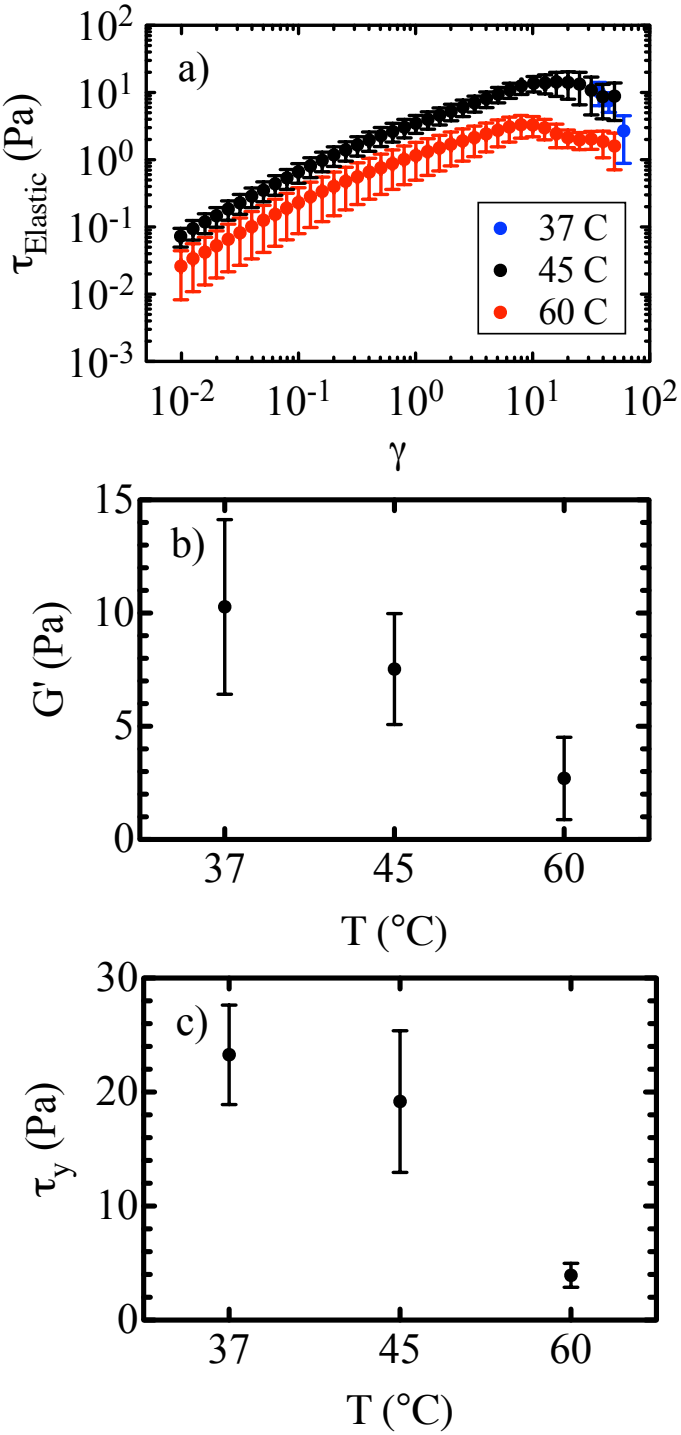

Figure 3.5. Rheological characterization of *Staphylococcus epidermidis* biofilms as a function of temperature through parallel plate rheometry. a) The shear stress ($\tau_{Elastic}$ = G' × strain) as a function of the strain over the three temperatures of interest. The maximum point of each curve was taken as the yield stress. b) The small strain elastic modulus of the biofilms at 37°C, 45°C, and 60°C. c) The yield stress (τ_y) of the biofilms at 37°C, 45°C, and 60°C. Each measurement was done in triplicate and error bars represent the standard error of the mean.

Conclusions

The effects of antibiotics and antimicrobial agents on bacterial biofilm infections have received significant attention in the literature.[4, 6, 15, 52] However, little attention has been paid to the potential role of physical methods for biofilm treatment. The physical methods that have received attention are magnetic fields, ultrasound, and pulsed electrical fields.[53-56] However, heat has been used successfully to treat certain types of cancer. Therefore, it could potentially play a role in fighting medical device infections by bacterial biofilms. To establish the scope for such a role, we have investigated the impact of heat treatment on the two main microscopic structural components of the biofilm matrix: the bacterial cells and the extracellular polymeric substance. In our experiments, we found that the application of heat caused morphological changes in the bacterial cells present in the biofilm, including a drastic decrease in cell viability when the biofilms were exposed to a treatment of 1 hour at 60°C. Additionally, a new component of size ~ 100 nm was formed in the EPS after heat treatment at 60°C. Species of this size were largely absent from the control biofilms and from the biofilms treated at 45°C. This ~ 100 nm species was the only change in the EPS: chemical analysis of fractionated samples designed to monitor for chemical degradation of polysaccharide, protein, and eDNA constituents of the EPS were unchanged by the temperature treatments at 45°C and 60°C.

Bulk rheological characterization correlated strongly with the ratio of live to dead cells in the bacterial biofilm. A 60°C temperature treatment resulted in a significant decrease of the yield stress and small strain elastic modulus of the biofilm. Thus, the effect of temperature on cell viability is implicated in the observed weakening of bacterial biofilms upon temperature treatment.

We have therefore shown that by exposing the biofilm to a local temperature treatment, we can weaken the integrity of the biofilm. This reduction of the yield stress supports the idea that biofilms are mechanically weakened by short bursts at high temperature, and suggests that possibility that a temperature-treated biofilm might be more easily sheared off an infected device. If validated by future work, this finding would open the door to the treatment of biofilm infections via external means, such as heat-enhanced ultrasonic vibration, and thereby ameliorate the need for surgical intervention in treatment of biofilm infections on medical devices.

Acknowledgements

We thank Mahesh Ganesan for his assistance with size exclusion chromatography and dynamic light scattering as well as Lilian Hsiao for her assistance with multi-channel confocal imaging. This work was supported by the NSF CDI Program (grant PHYS-0941227), the NIGMS (grant GM-069438), and a University of Michigan Rackham Merit Fellowship (to L.P.).

References

1. T. Shaw, M. Winston, C. J. Rupp, I. Klapper and P. Stoodley, *Physical Review Letters*, 2004, **93**, 4.

2. R. M. Donlan and J. W. Costerton, *Clinical Microbiology Reviews*, 2002, **15**, 167-193.

3. B. Rasmussen, *Nature*, 2000, **405**, 676-679.

4. L. Hall-Stoodley, J. W. Costerton and P. Stoodley, *Nature Reviews Microbiology*, 2004, **2**, 95-108.

5. J. N. Wilking, *MRS bulletin*, 2011, **36**, 385-391.

6. J. W. Costerton, P. S. Stewart and E. P. Greenberg, *Science*, 1999, **284**, 1318-1322.

7. L. Hall-Stoodley and P. Stoodley, *Cellular Microbiology*, 2009, **11**, 1034-1043.

8. M. S. Cheema, J. E. Rassing and C. Marriott, *Journal of Pharmacy and Pharmacology*, 1986, **38**, 53P-53P.

9. K. K. Jefferson, D. A. Goldmann and G. B. Pier, *Antimicrobial Agents and Chemotherapy*, 2005, **49**, 2467-2473.

10. H. M. Chung, M. M. Cartwright, D. M. Bortz, T. L. Jackson and J. G. Younger, *Shock*, 2008, **30**, 518-526.

11. J. P. O'Gara and H. Humphreys, *Journal of Medical Microbiology*, 2001, **50**, 582-587.

12. T. J. Marrie, J. Nelligan and J. W. Costerton, *Circulation*, 1982, **66**, 1339-1341.

13. J. C. Nickel, I. Ruseska, J. B. Wright and J. W. Costerton, *Antimicrobial Agents and Chemotherapy*, 1985, **27**, 619-624.

14. M. R. W. Brown, D. G. Allison and P. Gilbert, *Journal of Antimicrobial Chemotherapy*, 1988, **22**, 777-780.

15. T.-F. C. Mah and G. A. O'Toole, *Trends in Microbiology*, 2001, **9**, 34-39.

16. C. A. Fux, J. W. Costerton, P. S. Stewart and P. Stoodley, *Trends in Microbiology*, 2005, **13**, 34-40.

17. J. W. Costerton, Z. Lewandowski, D. E. Caldwell, D. R. Korber and H. M. Lappin-Scott, *Annual Review of Microbiology*, 1995, **49**, 711-745.

18. R. Wolcott and S. Dowd, *Plastic and Reconstructive Surgery*, 2011, **127**, 28S-35S.

19. M. Otto, *Nature Reviews Microbiology*, 2009, **7**, 555-567.

20. A. Di Stefano, E. D'Aurizio, O. Trubiani, R. Grande, E. Di Campli, M. Di Giulio, S. Di Bartolomeo, P. Sozio, A. Iannitelli, A. Nostro and L. Cellini, *Microbial Biotechnology*, 2009, **2**, 634-641.

21. S. Aggarwal, E. H. Poppele and R. M. Hozalski, *Biotechnology and Bioengineering*, 2010, **105**, 924-934.

22. S. Aggarwal and R. M. Hozalski, *Langmuir*, 2012, **28**, 2812-2816.

23. W. L. Jones, M. P. Sutton, L. McKittrick and P. S. Stewart, *Biofouling*, 2011, **27**, 207-215.

24. D. N. Hohne, J. G. Younger and M. J. Solomon, *Langmuir*, 2009, **25**, 7743-7751.

25. A. M. Vinogradov, M. Winston, C. J. Rupp and P. Stoodley, *Biofilms*, 2004, **1**, 49-56.

26. I. Klapper, C. J. Rupp, R. Cargo, B. Purvedorj and P. Stoodley, *Biotechnology and Bioengineering*, 2002, **80**, 289-296.

27. C. J. Rupp, C. A. Fux and P. Stoodley, *Applied and Environmental Microbiology*, 2005, **71**, 2175-2178.

28. L. Pavlovsky, J. G. Younger and M. J. Solomon, *Soft Matter*, 2013, **9**, 122-131.

29. M. Ganesan, E. J. Stewart, J. Szafranski, A. E. Satorius, J. G. Younger and M. J. Solomon, *Biomacromolecules*, 2013, **14**, 1474-1481.

30. E. J. Stewart, A. E. Satorius, J. G. Younger and M. J. Solomon, *Langmuir*, 2013, **29**, 7017-7024.

31. W. Rao, Z.-S. Deng and J. Liu, *Crit Rev Biomed Eng.*, 2010, **38**, 101-116.

32. R. D. Issels, L. H. Lindner, J. Verweij, P. Wust, P. Reichardt, B.-C. Schem, S. Abdel-Rahman, S. Daugaard, C. Salat, C.-M. Wendtner, Z. Vujaskovic, R. d. Wessalowski, K.-W. Jauch, H. R. Dürr, F. Ploner, A. Baur-Melnyk, U. Mansmann, W. Hiddemann, J.-Y. Blay and P. Hohenberger, *The Lancet Oncology*, 2010, **11**, 561-570.

33. P. S. Stewart, S. A. Rani, E. Gjersing, S. L. Codd, Z. Zheng and B. Pitts, *Letters in Applied Microbiology*, 2007, **44**, 454-457.

34. K. L. O'Neill, D. W. Fairbairn, M. J. Smith and B. S. Poe, *Apoptosis*, 1998, **3**, 369-375.

35. E. A. Zerhouni, D. M. Parish, W. J. Rogers, A. Yang and E. P. Shapiro, *Radiology*, 1988, **169**, 59-63.

36. M.-C. Yang, L. E. Scriven and C. W. Macosko, *Journal of Rheology (1978-present)*, 1986, **30**, 1015-1029.

37. S. P. Dzul, M. M. Thornton, D. N. Hohne, E. J. Stewart, A. A. Shah, D. M. Bortz, M. J. Solomon and J. G. Younger, *Applied and Environmental Microbiology*, 2011, **77**, 1777-1782.

38. J. C. Crocker and D. G. Grier, *Journal of Colloid and Interface Science*, 1996, **179**, 298-310.

39. T. J. Marrie and J. W. Costerton, *Journal of Clinical Microbiology*, 1984, **19**, 687-693.

40. G. C. Berry, *The Journal of Chemical Physics*, 1966, **44**, 4550-4564.

41. C. E. Ioan, T. Aberle and W. Burchard, *Macromolecules*, 1999, **32**, 7444-7453.

42. R. L. Smith and E. Gilkerson, *Analytical Biochemistry*, 1979, **98**, 478-480.

43. P. K. Smith, R. I. Krohn, G. T. Hermanson, A. K. Mallia, F. H. Gartner, M. D. Provenzano, E. K. Fujimoto, N. M. Goeke, B. J. Olson and D. C. Klenk, *Analytical Biochemistry*, 1985, **150**, 76-85.

44. P. R. Desjardins and D. S. Conklin, in *Current Protocols in Molecular Biology*, John Wiley & Sons, Inc., Editon edn., 2011.

45. P. Desjardins and D. Conklin, *Journal of Visualized Experiments*, 2010, e2565.

46. S. W. Provencher, *Computer Physics Communications*, 1982, **27**, 213-227.

47. Q. Lu and M. J. Solomon, *Physical Review E*, 2002, **66**, 061504.

48. A. M. Shetty and M. J. Solomon, *Polymer*, 2009, **50**, 261-270.

49. A. Touhami, M. H. Jericho and T. J. Beveridge, *Journal of Bacteriology*, 2004, **186**, 3286-3295.

50. C. V. Sapan, R. L. Lundblad and N. C. Price, *Biotechnology and Applied Biochemistry*, 1999, **29**, 99-108.

51. G. D. Christensen, W. A. Simpson, A. L. Bisno and E. H. Beachey, *Infection and Immunity*, 1982, **37**, 318-326.

52. D. Davies, *Nat Rev Drug Discov*, 2003, **2**, 114-122.

53. C. G. Kumar and S. K. Anand, *International Journal of Food Microbiology*, 1998, **42**, 9-27.

54. Z. Qian, R. Sagers and W. Pitt, *Annals of Biomedical Engineering*, 1997, **25**, 69-76.

55. K. Okuno, K. Tuchiya, T. Ano and M. Shoda, *Journal of Fermentation and Bioengineering*, 1993, **75**, 103-106.

56. U. R. Pothakamury, H. Vega, Q. Zhang, G. V. Barbosa-Canovas and B. G. Swanson, *Journal of Food Protection*, 1996, **59**, 1167-1171.

CHAPTER IV

Elasticity of Microscale Volumes of Viscoelastic Soft Matter by Cavitation Rheometry[§]

Abstract

Measurement of the elastic modulus of soft, viscoelastic liquids with cavitation rheometry is demonstrated for specimens as small as 1 microliter by application of elasticity theory and experiments on semi-dilute polymer solutions. Cavitation rheometry is the extraction of the elastic modulus of a material, E, by measuring the pressure necessary to create a cavity within it [J. A. Zimberlin *et al*., Soft Matter **3**, 763-767 (2007)]. This paper extends cavitation rheometry in three ways. First, we show that viscoelastic samples can be approximated with the neo-Hookean model provided that the time scale of the cavity formation is measured. Second, we extend the cavitation rheometry method to accommodate cases in which the sample size is no longer large relative to the cavity dimension. Finally, we implement cavitation rheometry to show that the new theory accurately measures the elastic modulus of viscoelastic samples with volumes ranging from 4 mL to as low as 1 μL.

Introduction

The linear elastic modulus of a soft material is a characteristic mechanical property measurable by a broad range of techniques spanning from mechanical rheometry to

[§] Mahesh Ganesan performed the theoretical derivation presented in this work, which are described in detail in Appendix B. He is the second author in this work.

microrheometry to atomic force microscopy (AFM).[1, 2] Needs for both *in vivo* characterization of linear elasticity (such as in tissue viability), as well as rapid measurement (such as in quality control applications), have driven recent methods development.[3-5] Mechanical rheometry typically requires approximately milliliter sample volumes and, if sample loading and testing durations are considered, requires as much as five minutes to test one specimen at one deformation frequency. Passive microrheology is a widely used technique to study the mechanical properties of small volumes (between ~ 3 and 50 μL) of soft matter. One method of microrheology – which uses the multiple scattering technique of diffusing wave spectroscopy – requires as much as an hour of measurement time. This method can probe elastic moduli up to ~ 2000 Pa.[1, 6, 7] Microrheology measurements can also be impacted by the stability of the dispersed probes and the heterogeneity of the material studied.[8, 9] AFM can also be used to characterize the elastic modulus of very small volumes (< 1 μL) of material; however, this technique requires long durations for measurements and sample preparation time.[3, 10] The duration of these techniques makes them challenging for high throughput applications, while the lack of portability of the equipment and the ideal testing environments necessary complicate the scope for *in vivo* diagnostics with these techniques.

Cavitation rheometry, as introduced by Zimberlin *et al*., is a technique to characterize the linear elastic modulus of soft matter with Young's modulus in the range 0.12 kPa < E < 40 kPa.[11, 12] It is an inexpensive, fast, and portable method that estimates the elastic modulus of a material by measurement of the critical pressure (P_c) required for internal cavitation. The cavitation is typically induced by air pumped through a needle that has been inserted into the sample. The measured critical pressure predicts the elastic modulus, E, through the theory of cavitation in an incompressible hyperelastic material.[11] A hyperelastic material is described by a

rate independent constitutive model that relates the stress to a strain energy density function, which depends on strain invariants and material properties.[13] Using a neo-Hookean strain energy function, the inflation pressure (P), cavity expansion ratio (λ), and the elastic modulus (E) are related by [14]

$$\frac{P}{E} = \frac{5 - 4\lambda^{-1} - \lambda^{-4}}{6}. \quad (4.1)$$

The cavity expansion ratio is the ratio of the radius of the bubble (R_c) formed to the inner diameter of the needle (R_i), $\lambda = R_c/R_i$.[11] The critical pressure, P_c, is the maximum inflation pressure, which is achieved as λ approaches infinity. If the surface tension (γ) of the material is taken into account, the critical pressure is [11, 15]

$$P_c = \frac{5E}{6} + \frac{2\gamma}{R_i}. \quad (4.2)$$

A linear fit of experimentally measured P_c versus $2/R_i$ therefore yields the elastic modulus of the sample as an intercept.

Two key limitations of equations (4.1) and (4.2) restrict the scope of this method. The first limitation is that because the analysis assumes a neo-Hookean strain energy function, cavitation rheometry has been used to characterize elastic solids, such as triblock co-polymers, PVA hydrogels, and biological tissues, in which all can effectively be described as neo-Hookean elastic solids.[11, 12, 16-18] In other instances, the neo-Hookean strain energy function has been widely used to model the linear elasticity of soft, cross-linked polymers such as rubber.[19] In order to extend this method to viscoelastic materials, the assumption of neo-Hookean mechanics must be examined relative to their rheological behavior.

The second key limitation of the analysis is that equations (4.1) and (4.2) are valid only in the case of a sample volume whose dimension is large relative to the radius of the expanding

cavity. This assumption is termed the "thick shell" or "thick-wall" case.[14] In order to extend the scope of cavitation rheometry to smaller volumes, the analysis should be generalized to the case of cavitation in materials of arbitrary thickness or finite volumes.

In this paper, we examine these two limitations by theoretical analysis, numerical simulation, and experimental validation. We find instances in which the assumptions that underlie both limitations can be relaxed, allowing the extension of the cavitation rheometry method for characterization of both viscoelastic liquids and small sample volumes. These extensions significantly broaden the scope to apply cavitation rheometry to a greater set of materials and a broader range of conditions.

Experimental Methods and Hypotheses

Mechanical rheometery was performed using a stress-controlled rheometer (AR-G2, TA Instruments) to determine the linear elastic and viscous moduli of our viscoelastic fluid. We use semi-dilute solutions of high molar mass poly(ethylene oxide) (PEO, Polysciences Inc., 1 x 10^6 g/mol) at 3.0, 4.0, 6.0 and 8.0 % (w/w) in water as model materials. The solutions were gently rolled from one to five days allow the PEO to dissolve. Cone-and-plate rheometry was performed using a 6 cm diameter cone with a 2° angle. An oscillatory frequency sweep was conducted at constant strain amplitude, γ, of 0.3. In the linear regime, the frequency dependent shear elastic ($G'(\omega)$) and viscous ($G''(\omega)$) moduli of these test fluids are plotted in Fig. 4.1a. The elastic and viscous moduli span from a characteristic liquid-like regime at low frequency, where $G' \alpha \omega^2$ and $G'' \alpha \omega$, and approach a plateau value at high frequency. Because these solutions are incompressible liquids, the Poisson's ratio is approximately 0.5 and hence the elastic and shear

elastic moduli are related as E' = 3G'.[20] The dynamic viscosity can be extrapolated to a zero shear viscosity, which is used to estimate the viscosity of PEO for our simulations (Fig. 4.1b).

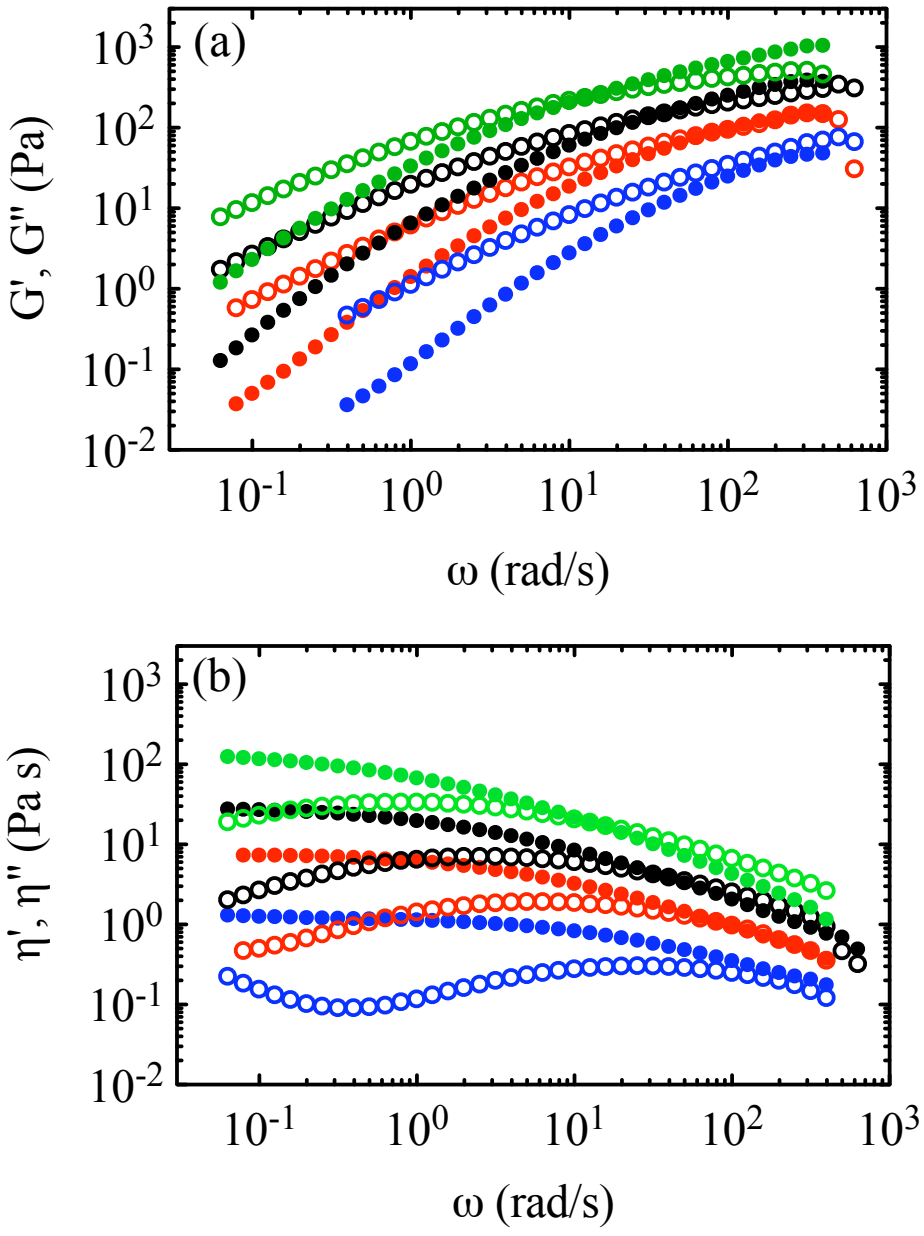

Figure 4.1. Mechanical rheometry data from oscillatory frequency sweeps of aqueous solutions of PEO (1 x 10^6 g/mol). The concentrations presented are: 3.0% (blue), 4.0% (red), 6.0% (black), and 8.0% (green) (w/w). The material properties, measured over a span of approximately four decades, include: (a) the G'(ω) (filled circles) and G"(ω) (open circles) as well as (b) the dynamic viscosity, η' (filled circles), and elastic portion of the complex viscosity, η" (open circles).

The PEO mechanical rheology (Fig. 4.1) differs from the behavior of the neo-Hookean constitutive equation in two critical ways: First, a neo-Hookean material is purely elastic, while the polymer solutions display a finite viscous modulus, G". Second, in hyperelastic models, the stress-strain relationship is independent of deformation path, strain rate and deformation history.[19] Therefore, the neo-Hookean model describes a frequency independent elastic modulus while the polymer solution rheology exhibits frequency dependent elasticity. We hypothesize that neither of these differences is critical to the application of cavitation rheometry. In the first case, we will show that the viscous contribution to the cavitation event does not affect the data analysis of equations (4.1) and (4.2), as demonstrated by measurements on viscous solutions. In the second case, we show, via imaging, that cavitation occurs at a high frequency in which G' > G". In this limit, the estimate of G' through cavitation rheometry is found to be in good agreement with mechanical rheometry.

The second limitation, the cavitation length scale, must be addressed to extend the technique to small, microliter volumes. The analysis used to produce equations (4.1) and (4.2) assumes that the cavitation deformation occurs in a region that is small relative to the overall volume of the elastic body. Because the cavitation region scales on the needle radius, the sample volume must be significantly larger than ~ 0.2 μL, which is the minimum volume of material necessary when commercially available needles are used to generate the cavity. We hypothesize that, as the sample volume decreases into the microliter range, the thick-wall assumption must be relaxed and equations (4.1) and (4.2) must be modified to account for the effect of material volume, relative to the size of the needle, on the cavitation pressure. To verify this second hypothesis, we formulate the generalized form of equations (4.1) and (4.2) for specimens of

arbitrary volume and subsequently validate the formulation by means of numerical simulations and cavitation rheometry experiments in samples of small volume.

Large Volume Cavitation Rheometry

The cavitation pressure of the four test fluids was measured with air as the cavitating agent, as delivered by syringe pump at a rate of 0.4 mL/min (Fisher Scientific). In order to differentiate the viscoelastic response from that of a purely viscous fluid, experiments were also performed on glycerol. Cavitation was induced with five different needle radii ranging from 0.084 mm to 0.419 mm (Hamilton). The volume of specimen used in all cases was greater than 1 mL, a limit in which equation (4.2) applies. Each permutation of needle size and solution was tested in triplicate. The typical time for the onset of cavitation was approximately 10 s after the start of airflow. Once initiated, the time for the formation of the cavity was very rapid, typically faster than 80 ms. The cavitation pressure was taken as the maximum pressure observed.

Equation (4.2) suggests a linear dependence of the cavitation pressure on the ratio $2/R_i$. This analysis, plotted in Fig. 4.2a, yields the shear elastic modulus from the intercept of the least-squared fit (i.e., it is 2/5 of the intercept) and the surface tension from the slope. For comparison, the cavitation of glycerol (gray) results in a shear elastic modulus of zero, within error. (A zero intercept in Fig. 4.2a indicates zero elasticity, as per equation (4.2).) This result demonstrates that a fluid with a vanishing elastic modulus, such as the Newtonian liquid glycerol, can be identified as such by the technique. The error on the glycerol measurement also provides a lower bound on the elasticity of a material that can be resolved by the cavitation rheometry. Specifically, the ~ 50 Pa error in the intercept for the glycerol indicates that a shear elastic

modulus of this magnitude or lower cannot be resolved by the cavitation rheometry method. These measured values and their standard errors of the mean are reported in Table 4.1.

Table 4.1 furthermore shows that the elastic modulus, as characterized by the cavitation rheometry measurement, increases with concentration. To assess the performance of the neo-Hookean based cavitation rheometry technique, we compare these moduli to those determined from mechanical rheometry in the following way. First, we performed high speed imaging of the cavity formation dynamics (Fig. 4.2b). From these images we estimate a characteristic strain rate for cavitation; it is at this strain rate that the mechanical and the cavitation rheometry are compared. We recorded cavitation events using a 120 frames per second CCD camera (Pulnix Progressive Scan TM-6710) attached to a stereoscope (Zeiss Stemi 2000-C) imaging at approximately 20x magnification. From the imaging, which can be seen frame-by-frame for a 4% PEO solution in Fig. 4.2b, we measured the radius of the bubble for each step of the cavity growth with the use of image processing software (ImageJ). The local strain, ε_L, and the strain rate, $\dot{\varepsilon}$, were determined at each frame as $\varepsilon_L = \left(R_j - R_{j-1}\right)/R_{j-1}$ and $\dot{\varepsilon} = \varepsilon_L/t_c$, where t_c is the time between frames j and j-1. The point of maximum strain rate was designated the critical condition for cavitation. The total strain, ε, was was determined from the beginning of the experiment to the point of cavitation as $\varepsilon = \left(R_{j,critical} - R_i\right)/R_i$. The cavitation rate varied from 74 s^{-1} (8% PEO) to 270 s^{-1} (4% PEO) for the cavitation pressures and surface tensions listed in Table 4.1. (The cavitation rate for the 3% PEO sample could not be evaluated because of a limitation of the camera frame rate.) By means of the Cox-Merz rule, we compare the elastic modulus at the cavitation rate to the G'(ω) at the equivalent frequency from the mecanical rheology.[21]

Test Material	Rheometry G' (Pa)	Cavitation G' (Pa)	Correction Factor, k	Total Strain, ε	Characteristic Strain Rate, $\dot{\varepsilon}$ (s^{-1})	Surface Tension (N/m)
3% PEO	-	91 ± 33	-	-	-	0.066 ± 0.006
4% PEO	140	205 ± 31	0.70 ± 0.11	1.80	270	0.071 ± 0.006
6% PEO	290	255 ± 20	1.1 ± 0.09	0.65	130	0.077 ± 0.004
8% PEO	590	305 ± 47	1.0 ± 0. 03	0.21	74	0.088 ± 0.008
Glycerol	-	-8 ± 48	-	-	-	0.069 ± 0.009

Table 4.1. The shear elastic modulus and surface tension determined by cavitation of four different concentrations of $1x10^6$ g/mol PEO. This is directly compared to the shear elastic modulus determined from mechanical rheometry at a strain rate estimated from high-speed imaging. The total strain to cavitation is also reported. The rheometry values for the 3% PEO sample were not evaluated due to limitations of the camera frame rate. The correction factor, k, is $k = G'_{Rheo} / G'_{Cav}$. The cavitation properties of the viscous fluid glycerol are presented for comparison. The cavitation G' are from a least-squared error fit of the cavitation pressure vs. $2/R_i$, at five different needle radii. Measurements were performed in triplicate.

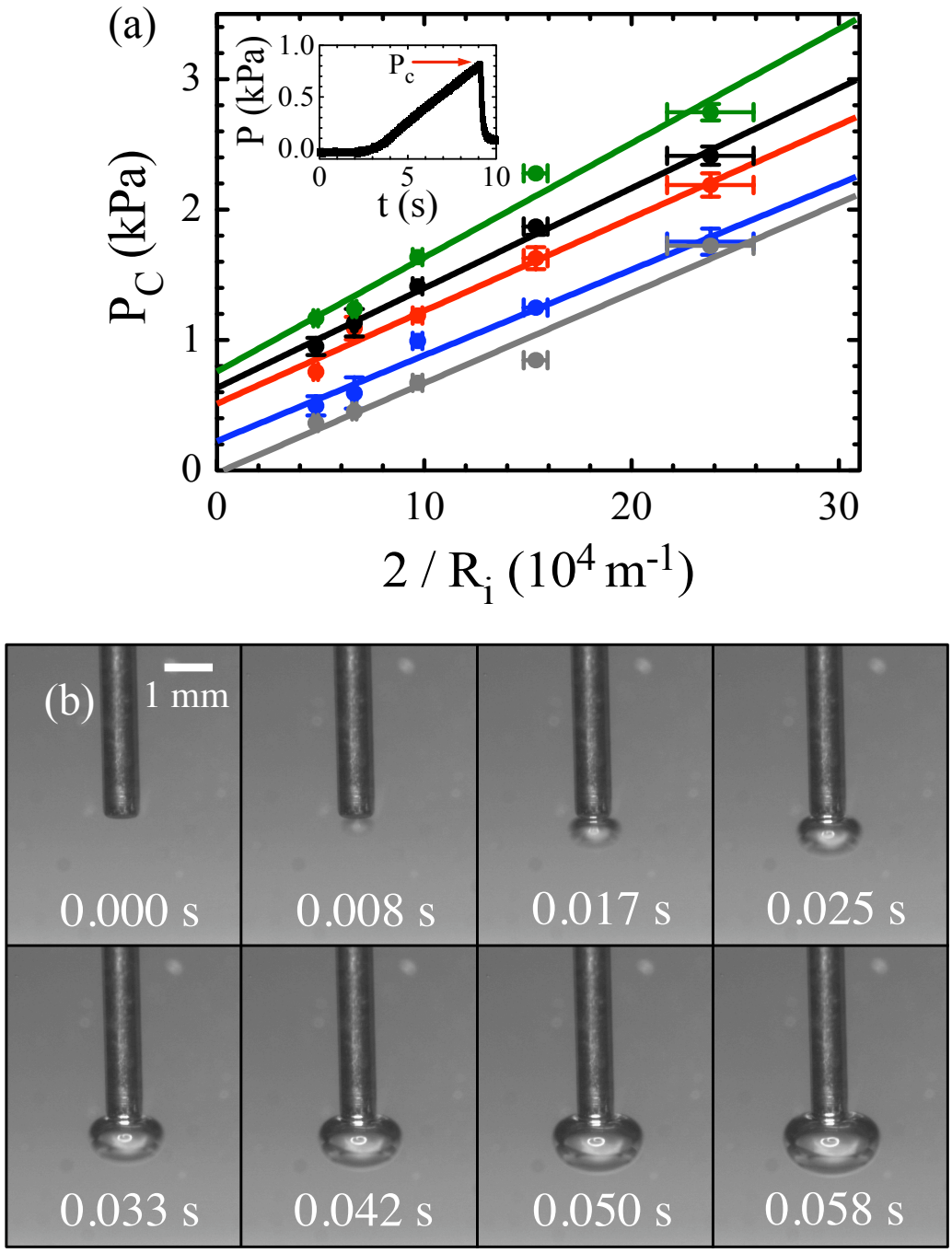

Figure 4.2. Cavitation rheometry of PEO solutions. (a) Critical pressure of 1 x 10^6 g/mol PEO solutions at various concentrations and a viscous fluid, glycerol, as a function of needle size; 3% (blue), 4% (red), 6% (black), 8% (green), and glycerol (grey). Five needle sizes were used (R_i of: 0.084 mm, 0.13 mm, 0.207 mm, 0.302 mm, and 0.419 mm), with 3 replicates of each. The vertical error bars are standard error of the mean and the horizontal error bars are the variability of the needle size based on the manufacturer. Inset: An individual cavitation experiment with 4% PEO and R_i = 0.419 mm, with P_c denoted as the maximum pressure. (b) Frame-by-frame images of a cavitation event in 4% PEO with a needle of 0.084 mm inner radius, captured at 120 fps.

The shear elastic moduli at aformentioned frequencies are in a region at which G' ~ G" and the elasticity of the system is significant. This correlation validates our first hypothesis and therefore, we directly compare the cavitation and mechanical rheometry at these deformation rates.

We establish a correction factor, $k = G'_{Rheo} / G'_{Cav}$ to connect cavitation rheometry and mechanical rheometry. We find that the average correction factor ($k_{avg} = 1.23 \pm 0.17$) results in a cavitation rheometry deviation from the mechanical rheometry modulus that is not in any case more than a factor of two of the true modulus. Although the cavitation and mechanical rheometry agree to within a factor of two and both sets of moduli increase with increasing PEO, the dependence of each displays a different dependence of PEO concentration. This result is likely tied to the sensitivity of the comparison to the strain rate extracted from the imaging; additional experimental and theoretical effort to improve this comparison is warranted. Nevertheless, the cavitation and mechanical rheometry results differ, on average, by less than a factor of two. Although not exact, this accuracy is acceptable for many applications, especially those requiring quick, *in situ* diagnostics or high throughput quality control screening. For example, the difference in elastic modulus between healthy tissue and a cancerous tumor is approximately an order of magnitude or greater.[4] Differences of this scale are certainly resolvable by cavitation rheometry, even if the underlying material is viscoelastic, rather than purely elastic.

Table 4.1 also provides an auxiliary characterization of the surface tension, the values of which can be compared to literature. Table 4.1 indicates that the liquid-air surface tension of the solutions increases modestly with PEO concentration. The surface tension of the PEO solutions should be bounded by the value for PEO, 0.043 N/m [22, 23], and the value for pure water, 0.072 N/m.[24] The cavitation rheometry measurements are closer to the value for pure water. This

proximity can be explained by the rapid and dynamic nature of the test and interface, respectively. At short times, the dynamic surface tension of a freshly created interface in a polymer solution is close to that of the solvent because the polymers in solution have yet to diffuse to the recently created interface.[25, 26] There is also potentially the additional effect of finite viscosity. Although this effect vanishes in the limit used to characterize the elastic modulus, it may affect the surface tension characterization, and thereby be a determinant in of the values and errors discussed.

Viscous Effects on Cavitation Rheometry

Cavitation rheology of a viscous liquid, glycerol, displayed behavior that was distinguishable from materials with elasticity, as reported in Fig. 4.2a. Specifically, the (apparent, fictious) elastic modulus of the viscous fluid computed from an analysis of critical pressures determined at multiple needle radii was indeed found to vanish, within measurement error (c.f. Table 4.1). Instead of appearing in the elastic cavitation analysis, the effect of viscosity adds to the magnitude of actual pressures measured. To assess the magnitude of this additive effect, finite element simulations (COMSOL Multiphysics) of a viscous material of a large volume, $(R_i+H)/R_i = 20$ (where Ri is the needle radius and H is material thickness), were conducted under the assumption of unconstrained radial expansion of the outer boundary of the material. Figure 4.3 shows the dependence of pressure with respect to the size of the cavity, normalized by its initial size, at various viscosities equivalent to the zero-shear viscosities found in Fig. 4.1b. Here, we see that higher viscosity results in a higher pressure. Hence, in a viscoelastic material, the overall pressure, and hence the critical pressure, is larger than expected for a purely elastic material of the same modulus due to a contribution of viscosity. However,

this effect becomes small in the limit analyzed by cavitation rheology to yield the elastic modulus (Figure 4.3).

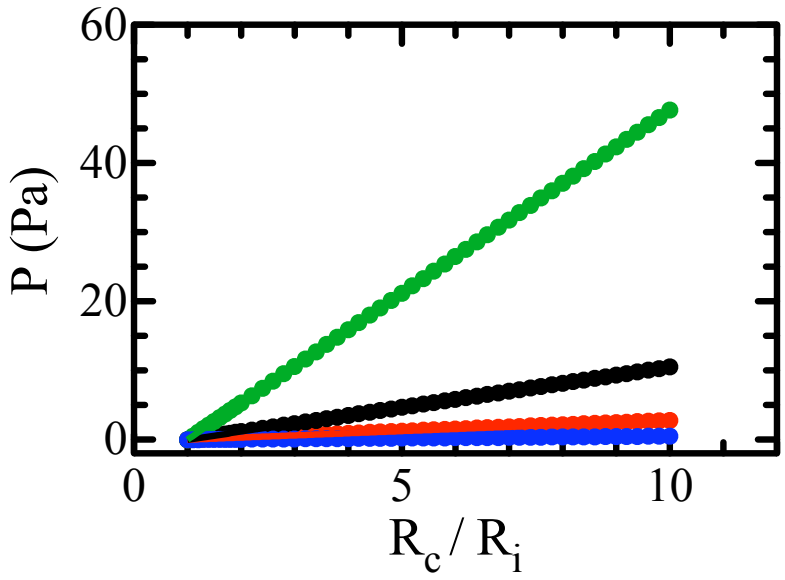

Figure 4.3. COMSOL Multiphysics simulations of the pressure necessary to cause growth of an inclusion, R_c, normalized by its initial size, R_i, in Newtonian fluids of various viscosities. The viscosities are equivalent to the zero-shear viscosities of 3% (blue), 4% (red), 6% (black), and 8% (green) PEO at a constant $(R_i+H)/R_i$ ratio of 20.

Cavitation Rheometry of Small Volumes

We now address the second, volumetric, limitation of cavitation rheometry. The 'thick-shell' assumption in equation (4.1) and (4.2) takes the deformation due to cavitation to be local and contained within an infinitesimal volume surrounding the needle.[27] The outer boundary of the specimen is sufficiently far from the needle and therefore unperturbed by the cavitation deformation. However, with decreasing sample volume, the outer boundary approaches the radius of the expanding cavity, which creates a deformation field extending to the outer boundary. Hence, the mechanics of the cavity expansion in a neo-Hookean material in this case must be explored.

Simulation

To study these mechanics, we performed a finite element simulation of cavitation in a finite volume of a neo-Hookean material with internal loading and unconstrained radial expansion of the outer boundary of the material.[28] We modeled the pressure-stretch relation and displacement gradient of individual regions in materials of varying thickness using COMSOL Multiphysics. The governing equation is the equilibrium momentum balance [26]

$$\nabla \cdot \tau = 0, \quad (4.3)$$

where the Cauchy stress tensor, τ, is

$$\tau = J^{-1} F S F^{T}. \quad (4.4)$$

F is the deformation gradient, which has diagonal components of λ, λ, and λ^{-2}, and $\lambda = R_c/R_i$. J is the determinant of F, equal to 1 for incompressible materials. S is the strain energy derivative [10, 25], given as

$$S = \frac{\partial U_{NH}}{\partial \varepsilon}, \quad (4.5)$$

where

$$U_{NH} = \frac{1}{6} E (\bar{I}_1 - 3) + \frac{1}{2} \kappa (J - 1)^2. \quad (4.6)$$

Here, U_{NH} is the neo-Hookean strain energy density function, ε is the strain tensor, I_1 is the first principal strain invariant, κ is the bulk modulus, and E is the Young's modulus. If we assume incompressibility, equation (4.6) becomes

$$U_{NH} = \frac{1}{6} E (\bar{I}_1 - 3). \quad (4.7)$$

To solve the momentum balance, we defined a hollow spherical geometry with a constant inner radius, R_i = 0.3 mm. The volume was varied by changing the radius of material present, H, which is the radial distance between R_i and the outer wall of the material, to generate ratios of

$(R_i+H)/R_i$ of 1.1, 1.5, 2, 5, 10, 15, and 20. The simulation was conducted over an applied stretch (R_c/R_i) range of 0-10. The material was assumed to have E = 615 Pa, equal to the shear modulus of cavitation of 4% PEO. Because of the problem's symmetry, a hemisphere of the cavitation phenomenon was simulated. The outer radius was an unconstrained, free boundary. Loading was at the inner radius boundary by specification of a pressure.

The mesh was scaled by adaptive mesh refinement to resolve the deformation near the inner radius of the material while still simulating to the specimen outer boundary (a standard fine mesh was used for the complete simulation space, with a refined mesh 2 mm radially from the origin). An example of the simulations at small and large volumes, with (Ri+H)/Ri ratios of 1.5 and 20, respectively, is in Fig. 4.4. Here, the heat map indicates stretch (λ) experienced by the material during a cavitation event from high (red; λ_{thin}= 0.24 mm, λ_{thick} = 0.25 mm) to low (blue; λ_{thin} = 0.16 mm, λ_{thick} = 0.00 mm).

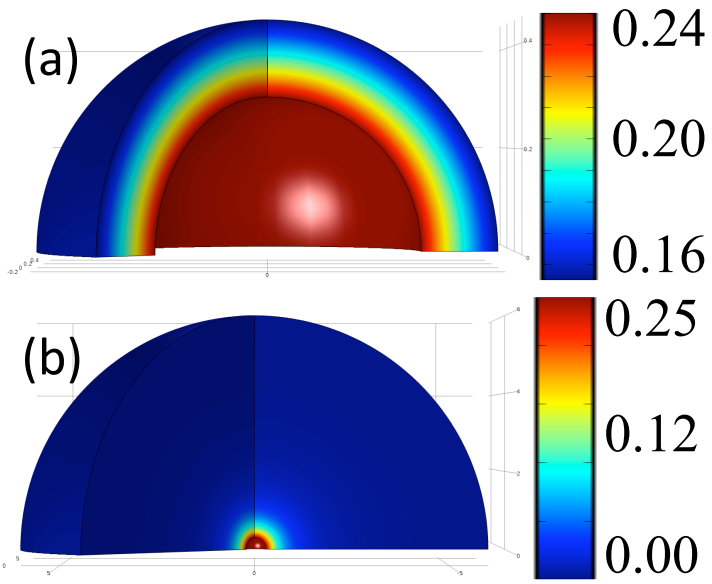

Figure 4.4. COMSOL Multiphysics simulations of the growth of an inclusion in a thin (a) and thick (b) elastic shell. The $(R_i+H)/R_i$ ratios 1.5 and 20, for the thin and thick shell respectively, assume a neo-Hookean material and no forces opposing expansion at the outer boundary. The heat map indicaties areas of large (red) and small material displacement (blue) within the elastic shell during cavitation. Dimensions are in mm. These simulations were run assuming an elastic modulus of 1 Pa to obtain a critical pressure of 5/6 at large volume.

Results of these simulations are scaled on the ratio P/E, normalizing the relation to all values of G, as well as $(R_i+H)/R_i$, which characterizes the radius of the specimen (R_i+H) to the initial radius of the cavity (R_i). Results of the simulation are rendered in Fig. 4.4 for $(R_i+H)/ R_i$ ratios of 1.5 and 20, which correspond to thin and thick shells, respectively.[14] For the thin shell (Fig 4.4a) case, the deformation of the most distant material during cavitation is significant, whereas in the thick shell case (Fig. 4.4b), deformation at the outer boundary is negligible.

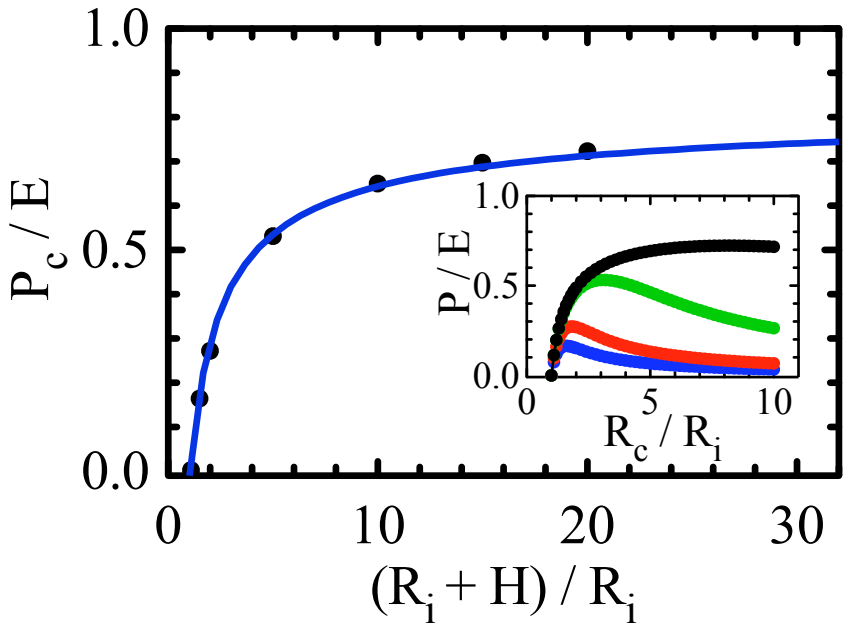

Figure 4.5. The dependence of critical pressure, normalized by the elastic modulus, on the volume ratio of material as determined through finite element analysis and theoretical calculations. The finite elemental analysis (COMSOL Multiphysics; black circles) and theoretical calculations (blue line, points omitted) were fit with equation (4.11) to determine that the parameters a and b are -0.8558 and -0.6574, respecitvely. Inset: Simulation and theoretical calculations of the pressure, P, scaled by the elastic modulus, E, as a function of the radius of the cavity, R_c, normalized by the radius of the needle, R_i, during cavity inflation. Each curve represents a different volume of material, characterized as a radius, H, scaled by the radius of the needle (i.e. $[R_i+H]/R_i$). The volume ratios shown are 1.5 (blue), 2.0 (red), 5.0 (green), and 20.0 (black). The maximum P/E value in each curve represents the critical pressure, P_c, at that particular material volume. Theory and simulation curves overlay exactly in the inset.

The pressure curves found from simulation (Fig. 4.5 Inset) are plotted as the change in pressure, normalized by the elastic modulus, as a function of the radius of the cavity (R_c; $R_c = R_i$ at t = 0), normalized by the initial cavity radius. We notice that the response is dependent on the amount of material initially present (i.e. $(R_i+H)/R_i$). At small material volumes ($(R_i+H)/R_i \leq 5$), we find that, after reaching its critical value, the pressure decreases significantly with increasing cavity expansion. This effect is well-known in the elacticity of incompressible materials; physically it would be manifested as an unbounded expansion at this critical pressure.[13] For $(R_i+H)/R_i > 5$, we find that the critical pressure increases and occurs at increasingly larger values of R_c/R_i. At large volumes, such as at $(R_i+H)/R_i = 20$, the pressure reaches an asymptotic limit of ~ 5E/6 with increase in cavity size, consistent with equation (4.2). The critical pressure for cavitation is significantly lower for finite volumes (i.e. P_c ~ 0.5E and ~ 0.2E at $(R_i+H)/R_i$ equal to 5 and 1.5, respectively). This substantial difference indicates that applying equation (4.2), valid only in a large volume limit, in this regime of finite volume would yield an incorrect characterization of the elastic modulus.

Cavitation theory

We analyzed the mechanics of cavity deformation in a neo-Hookean material. The material is defined as a hollow spherical system having an internal radius, R_i, and an external radius, R_i+H, which is free to expand. Assuming the material to be incompressible, the application of a pressure at the inner wall generates equibiaxial extension.[27] The principal Cauchy stress tensors, τ_{rr} and $\tau_{\theta\theta} = \tau_{\phi\phi}$, are obtained from the first derivative of the neo-Hookean strain energy density function with respect to the principal stretches (c.f. Appendix B). The equilibrium momentum balance [29], in terms of the deformation variable, λ, is

$$\frac{d\tau_{rr}}{d\lambda} + \frac{2\lambda^{-1}}{\lambda^3 - 1}(\tau_{rr} - \tau_{\theta\theta}) = 0, \quad (4.8)$$

We solve equation (4.8) subject to the boundary conditions of internal loading (τ_{rr} = -P at $\lambda = R_c/R_i$) and an unbounded surface ($\tau_{rr} = 0$ at $\lambda = \lambda_b$), where

$$\lambda_b = \left[(\lambda^3 - 1)\left(\frac{R_i + H}{R_i}\right)^{-3} + 1\right]^{1/3}. \quad (4.9)$$

We find that the applied pressure, P, and deformation, λ, are related as

$$P = \frac{E}{6{\lambda_b}^4} + \frac{2E}{3\lambda_b} - \frac{E}{3}\left(\frac{1}{2\lambda^4} + \frac{2}{\lambda}\right), \quad (4.10)$$

Here, λ is the spatially varying stretch ratio of the cavity and λ_b is the stretch ratio of the material at any point within the elastic shell. Additional details are in Appendix B. By numerically solving equation (4.10) and plotting the result along with the simulation results, we find that our theoretical equation overlays exactly with the simulation results (Fig. 4.5 Inset).

We lack an analytical expression for P_c, defined as the first derivative maxima of P with respect to λ. Thus, we numerically generate pressure-stretch curves to determine P_c at many dimensionless sample thicknesses (results not shown). From these calculated values, we obtain the modified cavitation equation by fitting the results (Fig. 4.5) to

$$P_c = \frac{5E}{6}\left[\frac{6a}{5}\left(\frac{R_i + H}{R_i}\right)^b + 1\right], \quad (4.11)$$

where a and b are fitting parameters, equal to -0.8558 and -0.6547, respectively. Under the limit of infinite material volume ($(R_i+H)/R_i \rightarrow \infty$), equation (4.11) approaches equation (4.2) monotonically, thus validating our fit. This equation is valid for all $H > 0$, as $R_i+H > R_i$.

Small volume experiments

Equation (4.11) predicts that the cavitation pressure in finite volumes is a function of the elastic modulus and the geometric parameter $(R_i+H)/R_i$. To test this equation in the finite volume limit, 4% PEO droplets of varying volume were dispensed on a glass slide. To cause the PEO droplet to bead, the glass slide was coated with a hydrophobic layer (Rain-X). The droplet dimensions were measured with a stereoscope equipped with a CCD camera (PCO Pixelfly QE). The overall volume of our PEO droplets were approximately 1 μL. An example experiment is shown in Fig. 4.6a.

Cavitation was induced in the small volume drops by pressurization of the syringe. The measured cavitation pressures, after subtracting the surface tension term as determined by large volume cavitation ($2\gamma/R_i$), are plotted for a range of drop dimensions in Fig. 4.6b. The trend between the small volume experiments (circles) and the large volume experiments (squares) is consistent with both the simulation and theory reported earlier. The small volume experiments were fit with equation (4.11), which yielded an elastic modulus of 840 Pa. The large volume experiments, from Table 1, found E = 615 Pa, a discrepency of 35%. Moreover, the large volume data fell within the 95% confidence interval of our small volume fitting, further indicating the applicability of equation (4.11).

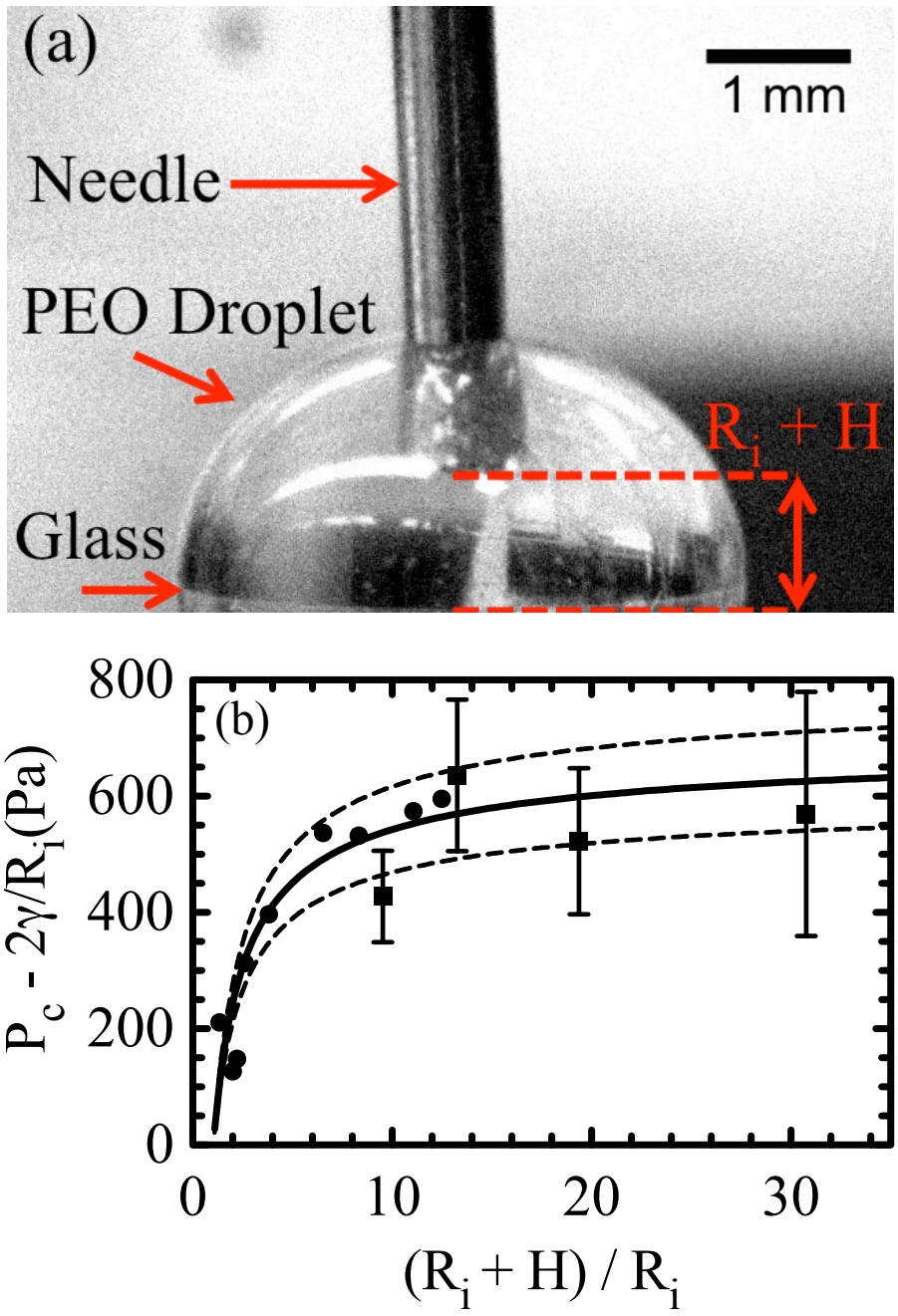

Figure 4.6. Small volume cavitation rheometry of 4% PEO. (a) Example image from a small volume cavitation experiment of 4% PEO. Pictured is ~1 μL droplet on a glass slide with a hydrophobic coating used to cause the droplet to bead. The needle is inserted in the sample and a characteristic dimension, R_i+H, is established. The critical pressure, with the surface tension contribution subtracted, is plotted for a range of drop dimensions in (b). Small (circles) and large (squares) volume cavitation experiements are plotted and fit (solid line) with the modified cavitation equation (4.11). The 95% confidence interval (dotted lines) are shown. The fit yields an estimate of the elastic modulus of 840 Pa, as compared to 615 Pa determined from large volume experiments alone. The relative error is between the large and small volume measurements is 35%.

In conclusion, cavitation rheometry has been succesfully extended to estimate the elastic modulus of viscoelastic fluids in the limit of large volumes. This method, pioneered by Zimberlin *et al.* for elastic materials, works well provided that sample dimensions are > 20X R_i. When seeking to apply cavitation rheometry using commercially available needles to specimen volumes less than about 0.1 ml, additional analysis is required. Using simulations and theoretical calculations, the decrease in cavitation pressure in this small specimen case is successfully modeled, and this analysis agrees well with experiments. Areas for future attention include viscoelastic modeling of the cavitation experiment; this step would allow correspondence between this technique and other methods for elongation deformation, and their accompanying instabilities, to be better assessed.[30, 31] We develop an equation that can be used to predict the shear modulus of material for specimen volumes as small as 1 μL. The extension of cavitation rheometry to both viscoelastic materials and to small specimen volumes improves the scope for this method's new application in a range of areas, including the diagnostic characterization of the mechanical properties of tissues and the high throughput rheological characterization of materials in formulation and manufacturing.

Acknowledgments

This work was supported by the NSF CDI Program (grant PHYS-0941227), the NIGMS (grant GM-069438), and a University of Michigan Rackham Merit Fellowship (to L.P.). We thank Prof. M.A. Burns for use of the high-speed camera.

References

1. P. Cicuta and A. M. Donald, *Soft Matter*, 2007, **3**, 1449-1455.

2. N. Gavara and R. Chadwick, *Nature Nanotechnology*, 2012, **7**, 733-736.

3. M. Balooch, I. C. Wu-Magidi, A. Balazs, A. S. Lundkvist, S. J. Marshall, G. W. Marshall, W. J. Siekhaus and J. H. Kinney, *Journal of Biomedical Materials Research*, 1998, **40**, 539-544.

4. W.-C. Yeh, P.-C. Li, Y.-M. Jeng, H.-C. Hsu, P.-L. Kuo, M.-L. Li, P.-M. Yang and P. H. Lee, *Ultrasound in Medicine & Biology*, 2002, **28**, 467-474.

5. L. Pavlovsky, J. G. Younger and M. J. Solomon, *Soft Matter*, 2013, **9**, 122-131.

6. T. G. Mason and D. A. Weitz, *Physical Review Letters*, 1995, **74**, 1250.

7. Q. Lu and M. J. Solomon, *Physical Review E*, 2002, **66**, 061504.

8. T. M. Squires and T. G. Mason, *Annual Review of Fluid Mechanics*, 2010, **42**, 413-438.

9. T. Savin and P. S. Doyle, *Biophysical Journal*, 2005, **88**, 623-638.

10. N. Jalili and K. Laxminarayana, *Mechatronics*, 2004, **14**, 907-945.

11. J. A. Zimberlin, N. Sanabria-DeLong, G. N. Tew and A. J. Crosby, *Soft Matter*, 2007, **3**, 763-767.

12. J. A. Zimberlin, J. J. McManus and A. J. Crosby, *Soft Matter*, 2010, **6**, 3632-3635.

13. R. W. Ogden, *Non-linear Elastic Deformations*, Halsted Press, New York, 1984.

14. A. N. Gent, *International Journal of Non-Linear Mechanics*, 2005, **40**, 165-175.

15. A. N. Gent and D. A. Tompkins, *J. Appl. Phys.*, 1969, **40**, 2520-&.

16. J. A. Zimberlin and A. J. Crosby, *Journal of Polymer Science Part B-Polymer Physics*, 2010, **48**, 1423-1427.

17. A. Delbos, J. Cui, S. Fakhouri and A. J. Crosby, *Soft Matter*, 2012, **8**, 8204-8208.

18. S. Kundu and A. J. Crosby, *Soft Matter*, 2009, **5**, 3963-3968.

19. L. R. G. Treloar, *The Physics of Rubber Elasticity*, Third edn., Oxford University Press, New York, 2005.

20. J. D. Ferry, *Viscoelastic Properties of Polymers*, Third edn., John Wiley & Sons, New York, 1980.

21. C. W. Macosko, *Rheology: Prinicples, Measurements, and Applications*, Wiley-VCH, Inc., New York, 1994.

22. R.-J. Roe, *The Journal of Physical Chemistry*, 1968, **72**, 2013-2017.

23. A. K. Rastogi and L. E. St. Pierre, *J. Colloid Interface Sci.*, 1971, **35**, 16-22.

24. J. A. Dean, *Lange's Handbook of Chemistry*, Fifteenth edn., McGraw-Hill Professional, 1998.

25. N. J. Alvarez, L. M. Walker and S. L. Anna, *Langmuir*, 2010, **26**, 13310-13319.

26. J. Eastoe and J. S. Dalton, *Advances in Colloid and Interface Science*, 2000, **85**, 103-144.

27. A. E. Green and W. Zerna, *Theoretical Elasticity*, Second edn., Dover Publications, Inc., Mineola, 2012.

28. G. A. Holzapfel, *Nonlinear Solid Mechanics: A Continuum Approach for Engineering*, John Wiley & Sons, New York, 2000.

29. M. E. Gurtin, *An Introduction to Continuum Mechanics*, Academic Press, Boston, 1981.

30. G. H. McKinley and O. Hassager, *Journal of Rheology (1978-present)*, 1999, **43**, 1195-1212.

31. A. Y. Malkin and C. J. S. Petrie, *Journal of Rheology (1978-present)*, 1997, **41**, 1-25.

CHAPTER V

Conclusions and Future Work

Concluding Remarks

The objective of this thesis was to provide an understanding of the mechanical properties of *Staphylococcus epidermidis* bacterial biofilms. We focused on developing experimental systems that mimic the environments in which the biofilms naturally grow in order to establish a more accurate and clinically relevant assessment of the bulk properties of the biofilms. Our hope was that our research would ultimately be applied to diagnose and increase the efficacy of current clinical treatment strategies of infections. The use of this particular strain was motivated by its prevalence in hospital-acquired medical device infections.

In Chapter II, we introduced an *in situ* parallel plate bio-rheometer to mimic the native growth conditions of the biofilms. In our device, we were able to control environmental conditions such as the shear stress and temperature at which the biofilms grow while also supplying a constant source of nutrients. By growing the biofilms directly on the rheometer, we were able to mechanically characterize our samples without having to damage the biofilm matrix in transportation. With the use of our system, we were able to determine the elastic modulus of the biofilm and monitor how it changes as a function of NaCl concentration, with blood like NaCl levels resulting in the most elastic biofilms. We were also able to study the non-linear rheology, characterizing the yield stress, and applying viscoelastic models to determine the material's relaxation time. Then, while studying the effects of temperature on the elastic

modulus, we found that a heating cycle up to 60°C irreversibly decreased the elastic modulus. This result motivated the work presented in our following chapter.

In Chapter III, we studied the effect of a temperature treatment on the polymeric, cellular, and bulk rheological properties of the biofilm. We used our previous *in situ* rheometric system to grow and then apply an hour-long heat treatment at 37°C, 45°C, and 60°C. These temperatures represented body temperature, maximum allowable therapeutic temperature, and the temperature at which we began to notice the irreversible decrease in elastic modulus, respectively. With the use of scanning electron microscopy, we determined that both higher temperature treatments essentially eliminated cell reproduction. However, cell viability was only impacted by a 60°C treatment, where approximately 70% of cells were found to be dead based on two-channel fluorescent imaging using confocal laser scanning microscopy. Although dynamic light scattering and chemical assays did not find any distinguishable differences between the treated polymers, it was evident that the 60°C treatment resulted in a drastic decrease in the yield stress of the *Staphylococcus epidermidis* biofilms. These results can be used to enhance current treatment strategies to weaken the integrity of the biofilm and subsequently allow infections to be more easily sheared off of medical devices.

Finally, in Chapter IV, we introduced a technique, cavitation rheometry, which we believe can be used as a means of *in vivo* diagnostics. Cavitation rheometry can rapidly characterize the elastic modulus of purely elastic solids. In order to interrogate bacterial biofilm and other biological soft matter, it was vital to show that this technique can be used on viscoelastic material. Hence, through experimentation, simulation, and theoretical analysis, we extend this technique to a range of materials and microliter volumes. Experimentally, we compared the elastic modulus of various concentrations of 10^6 g/mol viscoelastic poly(ethylene

oxide) determined through standard mechanical rheometry and cavitation rheometry at large volumes to develop a correction factor. Then, we proved the ability of cavitation rheology to rightfully identify Newtonian fluids as having no elastic modulus. Once showing the feasibility of this method on viscoelastic materials, we performed finite element analysis simulations (COMSOL Multiphysics) to determine the effect of finite volume on the measurement of the cavitation modulus. We further constructed a theoretical derivation to compare with our simulation, through which we were able to fit a volume-dependent cavitation equation. Finally, we conducted small volume cavitation experiments of poly(ethylene oxide) with our new equation to prove its validity.

Our findings address multiple areas in biofilm research. First, we have introduced a technique to obtain mechanical information about the biofilm in its natural environment. Then, we investigated a possible treatment method for biofilm infections. Finally, we extended a technique that may be able to incorporate our previous knowledge to give rapid diagnosis of biofilm infections. Overall, the research presented in this thesis allows the construction of biological models that more accurately capture the properties of bacterial biofilm while also making a significant impact in the field of combatting bacterial biofilm bloodstream infections.

Future Work

In order to progress in our study of biofilm rheology, there are a few areas that must be expanded. These areas consist of further developing and improving the cavitation method for use on biofilms, characterizing multi-species biofilms as they appear in infections, and beginning to explore methods to clear infections from medical devices.

In Chapter IV, we used cavitation rheometry to estimate the elastic modulus of a model material: poly(ethylene oxide). In order to bring this finite volume rheometry technique closer to use in medical diagnostics, it must be applied to biological soft matter. Hence, an obvious future goal of this research is to apply cavitation on bacterial biofilms and compare the results to the *in situ* rheometry of Chapter II. Provided the characterization is successful, the speed of this technique would also allow for a rapid cataloguing of the elastic modulus of various biofilms for the purpose of diagnostics.

Additionally, with cavitation rheometry, we used a neo-Hookean model to predict the elastic modulus of a viscoelastic material. This was done to extend an existing technique to formerly untestable volumes. However, from a theoretical standpoint, there is an obvious gap in applying this technique to viscoelastic materials. Although we showed that an estimate was sufficient, it is pertinent to understand the complete physics of cavitation. Hence, the cavitation equation must be constructed based on a viscoelastic liquid model, such as the Lodge elastic model.[1] The Lodge model can model a fluid behavior as that of an elastic material, provided sufficiently fast extension occurs. This is the exact condition we are looking to achieve in cavitation, as we are trying to elastically quantify a viscoelastic liquid. By constructing our theory around this equation, we can better understand if the strain-rate we are generating is sufficient to make the assumption of an elastic material, as well as account for viscous dissipation if our strain is not sufficiently fast. Also, we should consider the Considère criterion, which determines the maximum strain allowable for homogenous extension in a viscoelastic material.[1, 2] If the graph of force versus strain (analogous to Figure 4.5) has a maximum, as ours exhibits, the uniform extension will become unstable and failure, or necking occurs.[2] Hence, as cavitation rheometry induces an extensional flow, failure of the material may be better predicted

by accounting for the Considère criterion in our theory. This way, it would be easier to directly compare material failure from cavitation to other, non-extensional methods.

Secondly, biofilms should be characterized as they appear in clinical infections in order to develop a meaningful understanding of their *in vivo* mechanics. Although *Staphylococcus epidermidis* is one of the most common causes of bloodstream infections in the US, biofilm infections seldom consist of a singular bacterial species.[3, 4] Therefore, to understand the mechanics of biofilms seen in the clinical setting, it is important to study multi-species infections. Multiple species of bacteria are known to coaggregate and grow synergistically to improve biofilm formation and antibiotics resistance.[5-7] As these species have different morphologies (cell size/geometry) and are capable of producing different polymers, the rheology of the overall biofilm may be vary significantly from that of the individual species. Hence, a study of the elastic modulus, yield stress, and overall structure of bacteria that are known to coagggregate and present themselves simultaneously in clinical infections should be conducted. By comparing the structure of mono-culture and multi-species biofilms via confocal microscopy and relating it to their respective rheology, we would enable biological modeling to more accurately predict behaviors of clinical infections.

Finally, as would be the ultimate goal of this research, we must focus on improving possible treatment methods. In Chapter III, we discussed using heat treatment to weaken the structural integrity of the biofilm. To add significance to this result, steps must be made to show how externally applied stresses can easily and safely cause the biofilm to yield from medical devices, such as catheters. This can be accomplished by placing an infected catheter in a flow channel experiencing central venous-like flowrates. Through application of ultrasonic stresses,

the cells and biofilm fragments being sheared from the catheter can be monitored through a flow camera to determine the efficacy of the treatment in clearing an infection from a medical device.

Mechanical rheometry and imaging techniques haven previously used to analyze the structure and property of biofilms. In this thesis, we have built upon this fundamental work to bring new methods and techniques capable of interrogating the biofilms *in situ.* These techniques can be further extended to provide an understanding of clinical biofilm infections, develop more realistic predictive biological models, and to possibly alter current procedures and improve clinical treatment of biofilm infections.

References

1. G. H. McKinley and O. Hassager, *Journal of Rheology*, 1999, **43**, 1195-1212.

2. A. Y. Malkin and C. J. S. Petrie, *Journal of Rheology*, 1997, **41**, 1-25.

3. H. M. Chung, M. M. Cartwright, D. M. Bortz, T. L. Jackson and J. G. Younger, *Shock*, 2008, **30**, 518-526.

4. J. W. Costerton, P. S. Stewart and E. P. Greenberg, *Science*, 1999, **284**, 1318-1322.

5. M. Burmølle, J. S. Webb, D. Rao, L. H. Hansen, S. J. Sørensen and S. Kjelleberg, *Applied and Environmental Microbiology*, 2006, **72**, 3916-3923.

6. D. W. McCormick, M. R. Stevens, B. R. Boles and A. H. Rickard, *Culture*, 2011, **32**, 1-5.

7. A. H. Rickard, P. Gilbert, N. J. High, P. E. Kolenbrander and P. S. Handley, *Trends in Microbiology*, 2003, **11**, 94-100.

APPENDICES

APPENDIX A

Validation of Procedures for *In Situ* Biofilm Rheology[**]

Non-standard Rheometry Procedures

The procedures applied to measure the *in situ* elastic and viscous moduli of *Staphylococcus epidermidis* bacterial biofilms in Chapter II had to be validated prior to testing incorporating biofilm as they are non-standard experiments.

First of all, rheometry of a material is typically performed in a dry state, with only the material of interest present. However, as the biofilms are grown and their moduli evaluated in a submerged state, rheology of a model material must confirm that results are not altered due to the presence of water. Our model material was 4% w/w poly(ethylene oxide) (g/mol PEO, Polysciences Inc., 1 x 10^6 g/mol) in water. In order to determine the effect of submerging the geometry and material in water, analogous to what would be seen with tryptic soy broth in the biofilm, an oscillatory frequency sweep was conducted over three varying operating conditions. The first case, plotted in Fig A.1. as Dry_Dry, refers to instrument inertial mapping being conducted in a dry environment, followed by sample loading and testing, also in a dry environment. This is the standard procedure when conducting rheometric measurements; hence, this is our control case. The second case (Dry_Wet) refers to a dry inertial mapping followed by a submerged measurement and similarly, the last case (Wet_Wet) is a submerged inertial mapping and measurement. The elastic and viscous moduli are plotted for each case in Fig A.1.

[**] Biochemical assays were performed, in part, by Ashley E. Satorius.

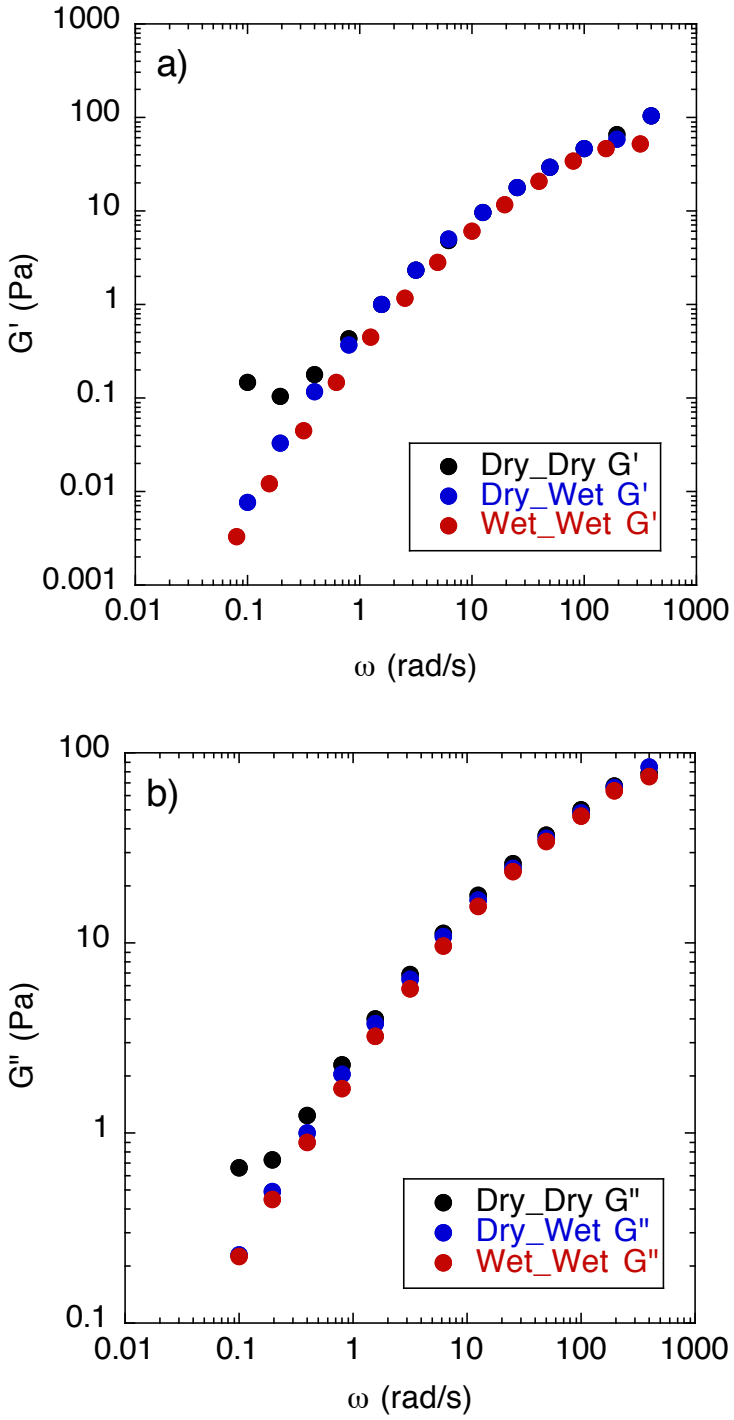

Figure A.1. Submerged rheology of poly(ethylene oxide). The (a) elastic (G') and (b) viscous (G") moduli are plotted from oscillatory frequency sweeps, with instrument mapping and measurement done in standard and submerged conditions. 'Dry' refers to standard rheometry procedures and 'Wet' refers to submerged rheology. These are listed in the order of inertial mapping condition followed by measurement condition.

Here, we can see that the measurements of both the elastic and viscous moduli are the same in each case. This allows us to be confident that the moduli determined from submerged rheology of the biofilm are in fact the true moduli.

Secondly, due to the range of thickness of biofilm reported in literature, it was necessary to establish a lower sensitivity limit of the rheometer gap height. A compression study of our model poly(ethylene oxide) was conducted to determine the resolution limit. In this study, we used standard rheometric procedures to measure the elastic and viscous moduli of our model material using a 40 mm stainless steel parallel plate geometry. We began with a gap height of 500 μm, at which we conducted an oscillatory frequency sweep from 100 – 0.005 s^{-1}. Then, the gap was reduced 50 μm and the test was repeated until we reached a gap height of 150 μm. Our results can be seen in Fig A.2.

As the elastic and viscous moduli are material properties, they should remain constant irrelevant of the gap height. From our results, we notice that the elastic and viscous moduli measured between 250 and 500 μm fairly consistent. However, at gap heights smaller than 250 μm, both the elastic and viscous moduli begin to increase. Due to the consistency of the measurements over the larger gap heights, we can conclude that this increase in moduli is an artifact of the instrument sensitivity, and therefore we are able to determine a lower gap height resolution limit of 250 μm to be incorporated in our biofilm testing.

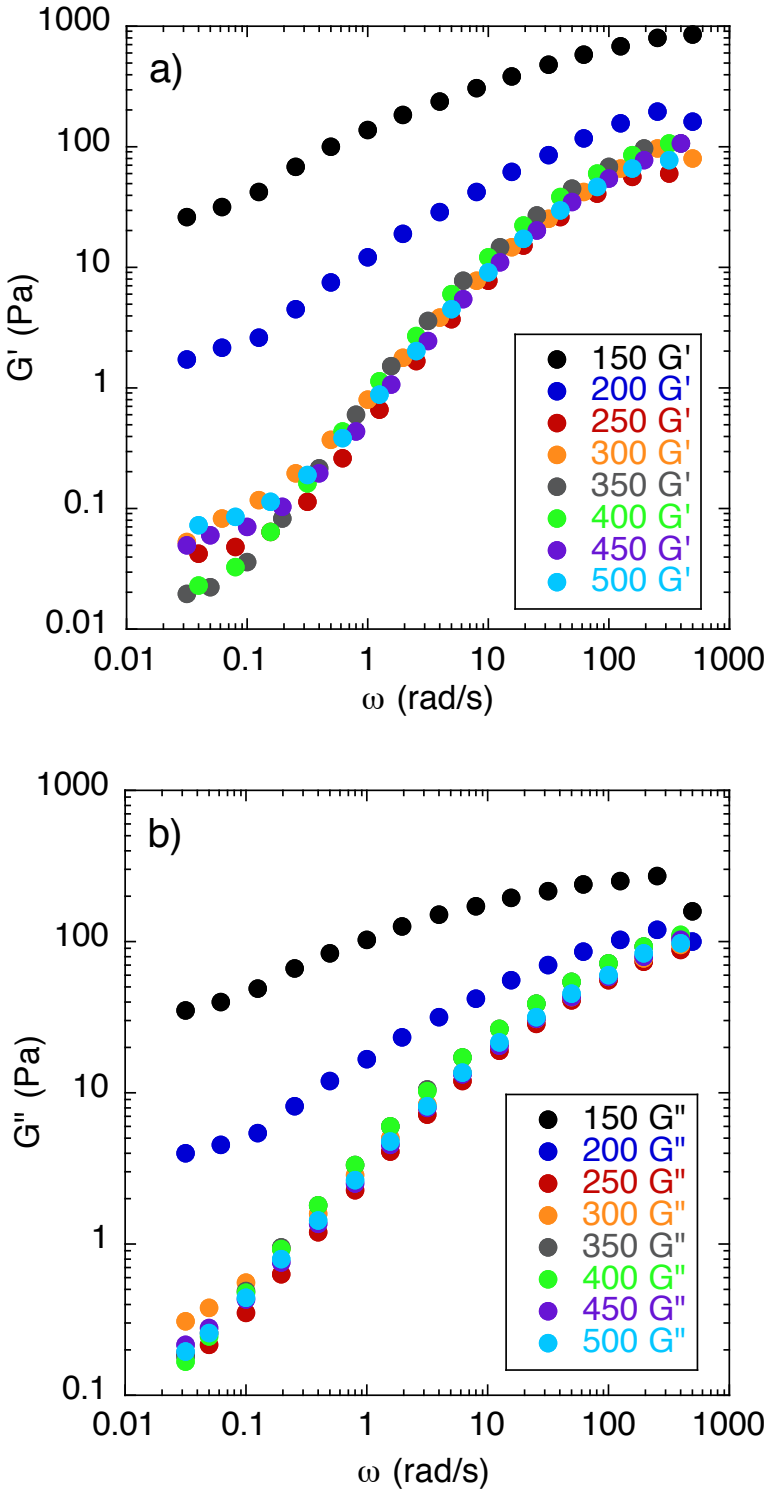

Figure A.2. Gap height resolution testing with poly(ethylene oxide). The (a) elastic (G') and (b) viscous (G") moduli are plotted from oscillatory frequency sweeps conducted at various gap heights.

Refining Rheometry Methods for Biofilm

After confirming that the deviations from standard operating procedures would not alter the results, we can begin validation of our methods with the use of biofilm. First, it is important to note that the system we are working with is the analytical surface of a rheometer, which is open to air. This allows the possibility of contamination in our media from the environment. In order to avoid any possible contaminants, precautions in the form of antibiotics must be used. Specifically, we use cycloheximade and kanamycin, an antifungal and general antibacterial, respectively. However, we must ensure that neither antibiotic has an adverse effect on the growth of *S. epidermidis*. Hence, we ran our antibiotic-free control and compared the effects of individual antibiotic doses on the moduli. The error plotted is the standard error of the mean and, from Figure A.3, we can see that the samples with the antibiotic have moduli within the acceptable range. From this, we can conclude that the use of antibiotic does not adversely affect our system.

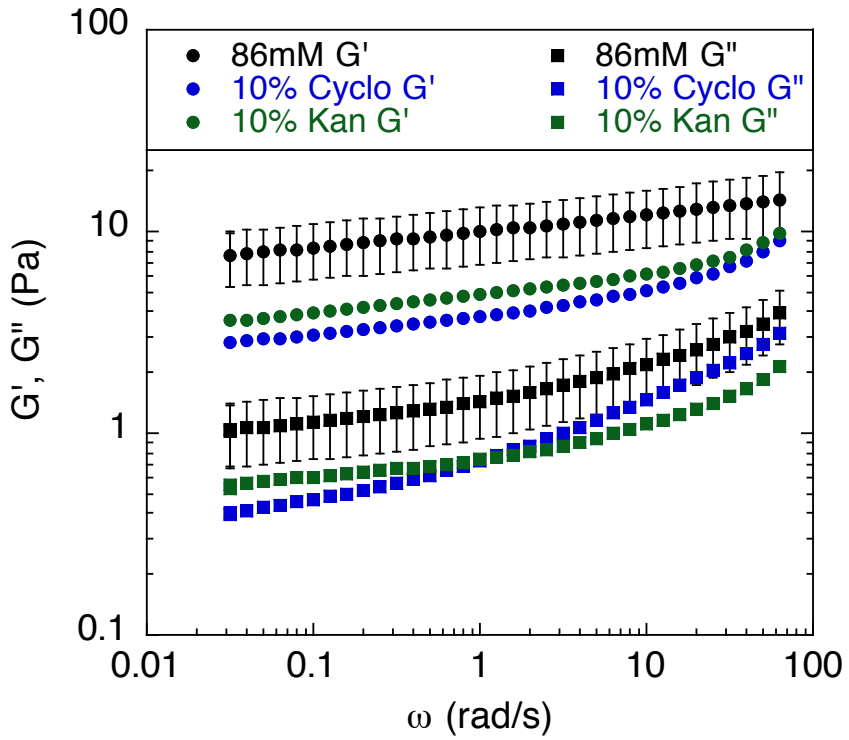

Figure A.3. Effect of antibiotics on the rheology of biofilms. The elastic modulus and viscous modulus of biofilms grown in standard tryptic soy broth (86 mM) without antibiotics are compared with biofilms grown in the standard media with 10% v/v concentration of cycloheximide and kanamycin. The 86 mM results come from triplicate and are shown with their standard error of the mean.

Next, we must ensure that the biofilm has enough time to fuse to the place during the attachment phase. In order to do this, we must determine how long it takes the biofilm to reach its maximum growth rate. The rate of growth of the bacterial cells in the biofilm is related to their metabolism. In order to grow, *S. epidermidis* needs a supply of nutrients, in our case glucose, and oxygen. Hence, we measure the concentration of each present in the media over the course of 7 hours. By conducting an assay for glucose concentration and taking hourly readings from a dissolved oxygen meter, we are able to track these concentrations. Also, we monitor the concentration of lactate present. When the bacteria are operating in an oxygen-deficient environment, they begin to produce lactate. Hence, the presence of lactate indicates that maximum growth rate has been surpassed. From this, we conclude that 7 hours is a sufficient

timeframe to conduct our attachment phase between the biofilm grown on the Peltier plate base and the geometry.

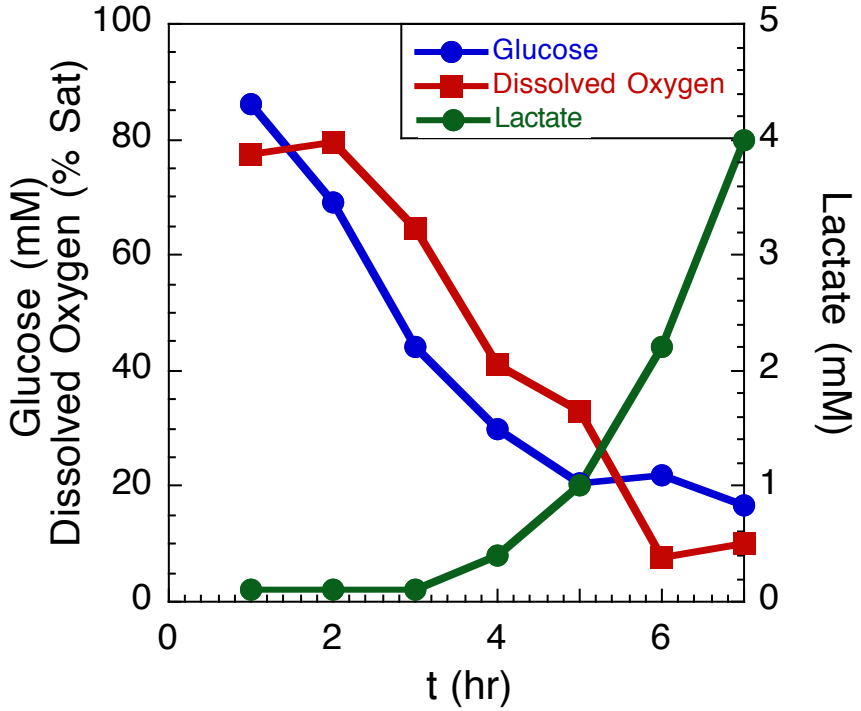

Figure A.4. Nutrient concentration in the media during biofilm growth. The concentrations of the nutrients glucose and dissolved oxygen as well as the concentration of lactic acid secreted during biofilm growth on the rheometer. Lactate and glucose concentrations were obtained by Ashley E. Satorius.

Thirdly, as biofilm is a heterogeneous material and rheology is heavily loading-dependent, we must make sure that variations throughout the biofilm do not significantly affect the bulk modulus measurements. One way to accomplish this is by varying the size of the geometry used. After developing our testing methods, we conducted oscillatory frequency sweeps using our standard 40 mm stainless steel flat plate geometry as well as a larger 60 mm stainless steel flat plate. Specifically, this was done to ensure that the scale of the heterogeneity of the biofilm does not significantly affect the elastic modulus measured with the smaller geometry. The larger geometry, averaging over a larger area, should be able to reduce the affects of any large variations. Our results are seen in Fig. A.5.

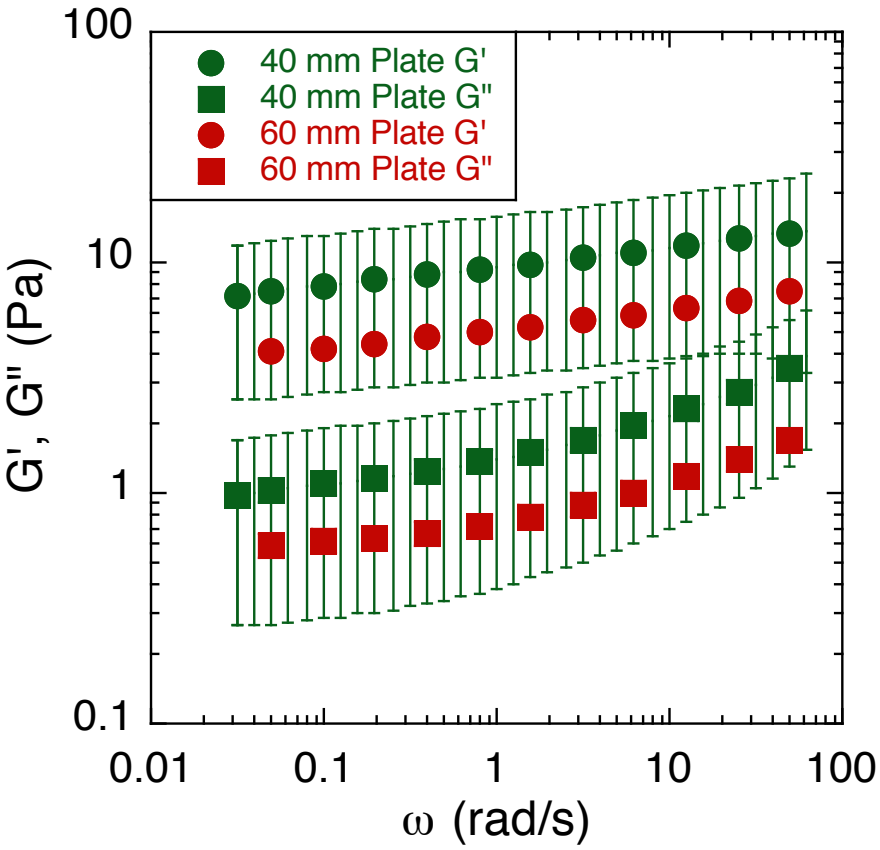

Figure A.5. Geometry dependence of biofilm moduli. Oscillatory frequency sweeps were conducted on *S. epidermidis* using two different geometries: a 40 mm and 60 mm diameter stainless steel flat plate. The 40 mm (green) data and standard deviation are the result of 6 replicates and are the same data set seen in Figure 2.4. The data from the 60 mm plate was only taken once.

From our results, we see that the data set generated with 60 mm flat plate geometry falls well within the standard deviation from the 40 mm flat plate results. This shows that the heterogeneity of the sample is not significantly felt at the length scales on which our bulk rheometry is conducted.

Finally, to further illustrate the instrument sensitivity investigated with the PEO model material and to determine the thickness of our biofilm sample, compression testing was conducted the in the same way it was for PEO. Our results can be seen in Fig. A.6.

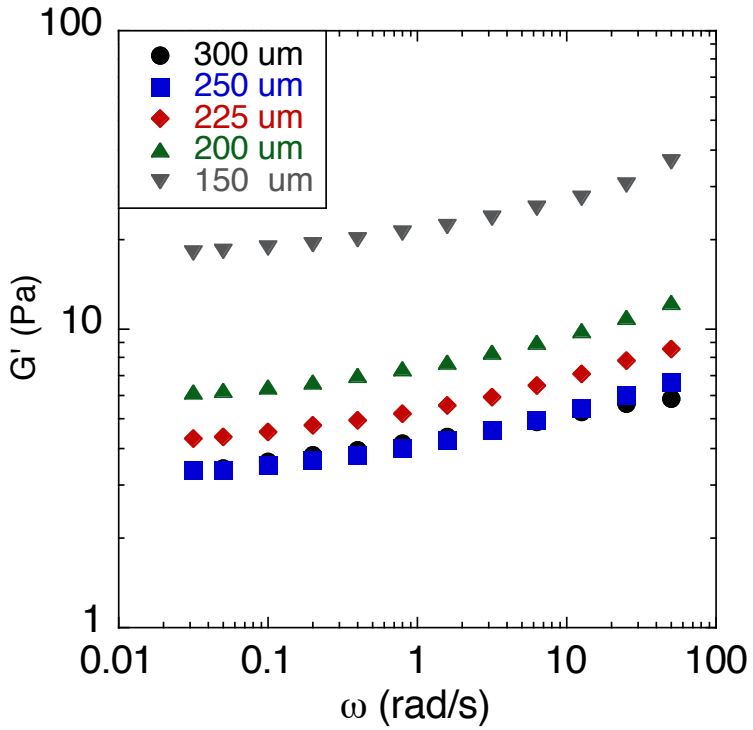

Figure A.6. Gap height resolution and biofilm thickness testing. The elastic (G') modulus is plotted from oscillatory frequency sweeps conducted at various gap heights, starting at 300 μm and decreasing to 150 μm. These results are shown from one individual experiment for the purpose of clarity.

Here, we see that the moduli measured at a gap height of 300 μm and 250 μm overlay perfectly. This gives us confidence that what we are measuring is the modulus of the biofilm and is not being influenced by the water content. At a gap height of 225 μm, we already notice an increase in the modulus. This can possibly be coming from two factors: 1) the water may be being squeezed out, concentrating the solids in the biofilm or 2) this is already approximately the lower resolution limit previously determined from PEO testing. Either way, the measurements below a gap height of 250 μm are thrown out and the biofilm thickness is determined to be approximately 300 μm.

Appendix B

Theory of Cavitation in Neo-Hookean Solids[††]

The relationship between the inflation pressure P and the deformation field λ for the symmetric inflation of a spherical cavity in an incompressible neo-Hookean material of finite volume and elastic modulus E is derived. The material is treated in spherical coordinates of initially undeformed radius, R where $R_i \leq R \leq R_i+H$. Upon inflation due to *P* at the inner wall, the material expands symmetrically to a material of deformed radius *r* where [1]

$$r^3 = \left(1 + \frac{{R_c}^3 - {R_i}^3}{R^3}\right) R^3 = \lambda^3 R^3. \quad (B.1)$$

Equation (B6) is obtained using the incompressibility and spherical symmetry criterion. The neo-Hookean strain energy function is given by equation (4.7) where, $I_1 = \sum_{i=1}^{3} \lambda_i^2$ and $\lambda_1 = \lambda^{-2}$, $\lambda_2 = \lambda_3 = \lambda$, which are the principal stretch ratios under symmetric expansion.[2] From U_{NH}, the principal components of the Cauchy stress, from equation (4.4), are [1, 3]

$$\tau_{rr} = \frac{E}{4}\lambda^{-4} - p \; ; \; \tau_{\theta\theta} = \tau_{\phi\phi} = \frac{E}{3}\lambda^2 - p, \quad (B.2)$$

where, p is the hydrostatic pressure required to maintain equilibrium in the case of incompressibility. In the absence of any body forces, the relation between inflation pressure P and λ is obtained by solving the equilibrium condition, equation (4.3),

$$\frac{\partial \tau_{rr}}{\partial r} + \frac{2}{r}(\tau_{rr} - \tau_{\theta\theta}) = 0, \quad (B.3)$$

[††] Mahesh Ganesan performed the theoretical derivations presented in this work.

which reduces to [4]

$$\frac{\partial \tau_{rr}}{\partial \lambda} + \frac{2\lambda^{-1}}{\lambda^3 - 1}(\tau_{rr} - \tau_{\theta\theta}) = 0, \quad (B.4)$$

after a change of variables using equation (B.1). Equation (B.4) is solved subject to the boundary conditions $\tau_{rr} = -P$ at $\lambda = R_c/R_i$ and $\tau_{rr} = 0$ at $\lambda = \lambda_b$, where

$$\lambda_b = \left(\left[(\lambda^3 - 1)\left(\frac{R_i + H}{R_i}\right)^{-3}\right] + 1\right)^{1/3}. \quad (B.5)$$

The final equation is obtained as

$$P = \frac{E}{6\lambda_b^4} + \frac{2E}{3\lambda_b} - \frac{E}{3}\left(\frac{1}{2\lambda^4} + \frac{2}{\lambda}\right), \quad (B.6)$$

By numerically solving for critical pressure, taken as the first derivative maxima of P with respect to λ, fitting those results, and adding the surface tension term, we find the cavitation equation modified for finite specimen size

$$P_c = \frac{5E}{6}\left[\frac{6a}{5}\left(\frac{R_i + H}{R_i}\right)^b + 1\right] + \frac{2\gamma}{R_i}, \quad (B.7)$$

where a = -0.8558 and b = -0.6574.

References

1. R. W. Ogden, *Non-linear Elastic Deformations*, Halsted Press, New York, 1984.

2. L. R. G. Treloar, *The Physics of Rubber Elasticity*, Third edn., Oxford University Press, New York, 2005.

3. A. E. Green and W. Zerna, *Theoretical Elasticity*, Second edn., Dover Publications, Inc., Mineola, 2012.

4. M. E. Gurtin, *An Introduction to Continuum Mechanics*, Academic Press, Boston, 1981.